Therapeutic RNA regulation during cardiac remodeling and disease

Marta Vigil García

Therapeutic RNA regulation during cardiac remodeling and disease

ISBN/EAN	978-94-6419-708-2
NUR	923
Illustrations	Adrián de la Cruz García |DROSTE Delacroix | @droste_delacroix
Publisher	Gildeprint proefschrift

The research described in this thesis was performed at the Hubrecht Institute of the Royal Dutch Academy of Arts and Sciences (KNAW), and University Medical Center Utrecht (UMCU) within the framework of Cancer, Stem Cells and Developmental Biology (CSnD) program, which is part of the Graduate School of Life Sciences (Utrecht University).

Financial support by the Dutch Heart Foundation for publication of this thesis is gratefully acknowledged.

Therapeutic RNA regulation during cardiac remodeling and disease

Therapeutische RNA-regulatie tijdens cardiale remodellering en ziekte

(with a summary in English)/
(met een samenvatting in het Nederlands)

Proefschrift

ter verkrijging van de graad van doctor aan de
Universiteit Utrecht
op gezag van de
rector magnificus, prof.dr. H.R.B.M. Kummeling,
ingevolge het besluit van het college voor promoties
in het openbaar te verdedigen op

donderdag 16 februari 2023 des ochtends te 10.15 uur

door

Marta Vigil García

geboren op 15 april 1989
te Porlamar, Venezuela

Promotor:

Prof. dr. E. van Rooij

Beoordelingscommissie:

Prof. dr. ir. J.P.W.M. Bakkers (voorzitter)
Prof. dr. J.P.G. Sluijter
Prof. dr. ir. H.M. den Ruijter
Dr. E.E.J.M. Creemers
Prof. dr. L. de Windt

TABLE OF CONTENTS

CHAPTER 1: INTRODUCTION AND OUTLINE OF THIS THESIS PAGE

CHAPTER 2: GENE EXPRESSION PROFILING OF HYPERTROPHIC CARDIOMYOCYTES IDENTIFIES NEW PLAYERS IN PATHOLOGICAL REMODELING PAGE

CHAPTER 3: GENE EXPRESSION PROFILE OF CARDIOMYOCYTES AFTER EXERCISE PAGE

CHAPTER 4: HYDROGEL-BASED DELIVERY OF ANTIMIR-195 IMPROVES CARDIAC EFFICACY AFTER ISCHEMIC INJURY PAGE

CHAPTER 5: SUMMARIZING DISCUSSION PAGE

ADDENDUM: PAGE
SUMMARY IN ENGLISH
NEDERLANDSE SAMENVATTING
ACKNOWLEDGEMENTS
LIST OF PUBLICATIONS
CURRICULUM VITAE

CHAPTER 1

GENERAL INTRODUCTION & OUTLINE OF THIS THESIS

Marta Vigil-Garcia[1]

[1]Hubrecht Institute, Royal Netherlands Academy of Arts and Sciences (KNAW) and University Medical Center Utrecht (UMCU), The Netherlands.

GENERAL ASPECTS OF HEART DISEASE AND CLINICAL INSIGHTS

Cardiovascular diseases (CVDs) are diseases that affect the heart and blood vessels, including stroke, hypertension, ischemic heart disease (IHD), heart failure (HF), and many others. The prevalence of CVD continues to rise with an aging population, and it contributes to 17.8 million deaths worldwide every year [1]. In Europe, it is the leading cause of death with a mortality rate of 3.9 million, accounting for 45% of all deaths each year. CVD contributes to an average annual direct and indirect estimated cost of €210 billion in the European Union [2,3], leading to a large economic burden.

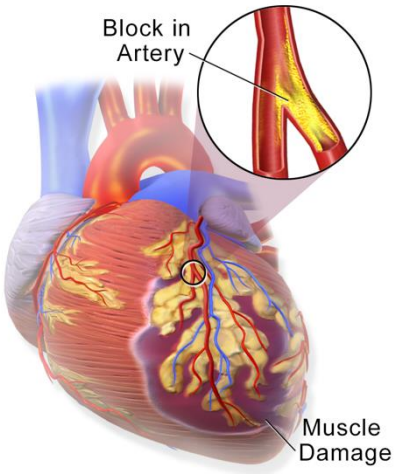

FIGURE 1. REPRESENTATION OF MYOCARDIAL INFARCTION (ADAPTED FROM BLAUSEN MEDICAL COMMUNICATIONS, INC. 2013)

To date, there is no cure for CVD. Current clinical practices include lifestyle changes, exercise-based cardiac rehabilitation, symptom management with medication, surgical intervention to prevent sudden cardiac arrest, or heart transplantation in case of end-stage HF. Research efforts are focused on understanding the molecular mechanisms behind disease progression and identifying relevant targets that could aid the development of novel therapies.

ISCHEMIC HEART DISEASE & HEART FAILURE

IHD is the result of reduced blood flow to the heart muscle that can lead to myocardial infarction (MI), also known as heart attack (Figure 1). MI is the most prevalent form of CVD, with 862,000 deaths a year (19% of all deaths) among men, and 877,000 deaths (20%) among women [3]. Patients who survive an MI are at high risk of a recurrent MI. After an MI, the myocardial cells do not receive oxygen and nutrients, leading to cardiomyocyte (CM) death and necrosis. The heart responds by activating a maladaptive remodeling process, which initially causes hypertrophy of the heart and activation of the fibrotic response, and can ultimately lead to HF [4].

Nowadays, the most effective strategy to prevent maladaptive cardiac remodeling after an MI aims at increasing reperfusion of the ischemic tissue to minimize myocardial damage and preserve as much myocardium as possible. A second strategy is combining re-perfusion with drugs, such as heparin (blood thinner). Follow up treatments consist of neurohormonal blockade (β-blockers) and statins together with aspirin to decrease the risk of a re-occurring MI [5]. These therapies cannot prevent HF.

HF is a complex clinical syndrome in which the heart presents a reduced ability to pump the blood around the circulatory system. It is the consequence of the unstoppable maladaptive remodeling. The prevalence of HF is approximately 1-2% of the population in developed countries and it rises to 10% among >70 years of age [5]. Patients with HF are diagnosed by the presence of structural changes in the

heart, leading to reduced left ventricular systolic or diastolic function, and increased brain natriuretic peptide (BNP) levels in the blood.

Recent research has focused on developing novel strategies to efficiently reverse maladaptive remodeling and prevent HF and has led to new strategies using gene therapy or cell transplantation. For instance, several gene therapy studies are aiming at 1) inducing revascularization by overexpressing the proangiogenic factors VEGF, FGF, IGF-2, or 2) inducing long-term protection by overexpressing survival genes *Bcl-2*, *Akt* or *HGF* [6]. Additionally, with cell transplantation, cells with a proliferative capacity, such as fetal CMs or embryonic stem cells, are injected into the dead myocardium to regenerate the lost tissue. Although *in vivo* studies have shown promising results, clinical trials have shown limited evidence and mixed outcomes. These studies highlight the complex cellular response upon MI and stress the need to identify new targets with relevant mechanisms in cardiac remodeling.

CARDIAC REMODELING

The heart is a dynamic organ exposed to different triggers during life which can lead to transcriptional, structural, electrophysiological and functional changes. On one hand, some triggers, such as exercise or pregnancy, activate beneficial processes that induce **physiological remodeling** of the heart. The heart develops hypertrophy characterized by 1) a reversible and balanced increase in myocardial mass and 2) activation of protective signaling pathways such as angiogenesis or the Akt survival pathway [7]. On the other hand, detrimental triggers can induce **pathological remodeling** of the heart. Detrimental triggers include, among others, MI, hypertension, and insulin resistance. During pathological remodeling, the left ventricle of the heart gradually changes, first, as an adaptive response to restore cardiac output (with compensatory alterations in size, shape, and function) but, when left untreated, the left ventricle starts to suffer from maladaptive alterations. The hallmarks of pathological remodeling are 1) a decline in CM contractility, 2) fibrosis, 3) ventricular dilatation, 4) chronic inflammation and 5) increased cellular apoptosis [8]. The neurohormonal systems renin-angiotensin and β-adrenergic systems are activated, and fibroblasts, vascular smooth muscle cells, immune cells and endothelial cells participate in promoting the pathological remodeling of the heart which can ultimately lead to HF (Figure 2) [8].

One of the main hallmarks of maladaptive remodeling is the activation of the fibrotic program. This is usually an essential, and reversible repairing process in response to tissue damage. Yet in the heart, it is irreversible. During fibrosis, fibroblasts differentiate into myofibroblasts and produce an excessive deposition of extracellular matrix (ECM) which results in the accumulation of fibrous connective tissue and the formation of a scar in the heart [8]. Another hallmark of maladaptive remodeling is hypertrophy. CMs are post-mitotic cells unable to divide and they respond to stress by growing in size

(hypertrophy). Subsequently, the continuous stress drives CMs to become elongated and to lose their contractile properties. Eventually, CMs die, and the loss of muscle tissue is replaced by fibrotic tissue, leading to a compromised contractile function of the heart [8].

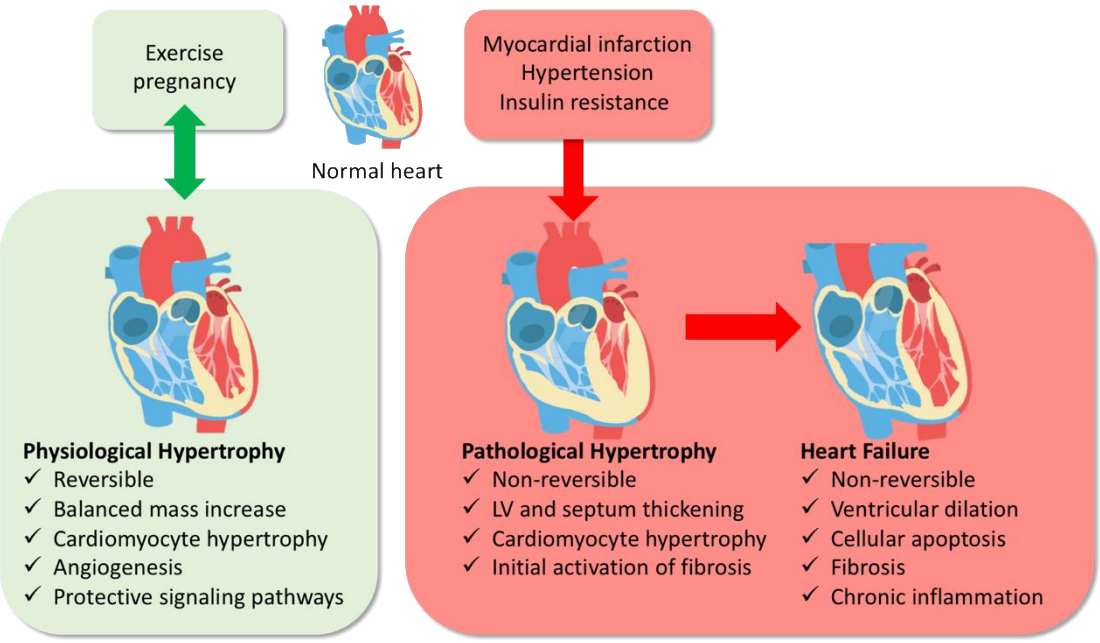

FIGURE 2. CARDIAC REMODELING UPON BENEFICIAL AND DETRIMENTAL TRIGGERS

CARDIOMYOCYTE FUNCTION DURING HEART DISEASE

CMs are the building blocks of the heart. They provide the most important characteristic to the heart, contractility. CMs have unique aspects when compared to other cells, and they function as key determinants of cardiac health and disease [9].

MECHANISMS OF PATHOLOGICAL AND PHYSIOLOGICAL REMODELING IN CARDIOMYOCYTES

During cardiac remodeling, transcriptional profiles in pathological and physiological remodeling are largely distinct, as are the dominant protein regulators of these states. While there are pathways activated in both, the consequences of some of these activated pathways are dramatically different.

Cell-mediated mechano-transduction responses are important regulators of adaptive and maladaptive CM remodeling. Mechanical loading induces the release of factors such as angiotensin II (AngII), endothelin 1 (ET-1) and transforming growth factor β (TGFβ) [10]. The AngII signaling pathway mediates cardiac contractility and is associated with long-term **CM hypertrophy**. AngII signaling links CMs and electrical propagation, and long-term regulation of growth and remodeling. AngII is likely to be produced and released by CMs, under pathological conditions. The AngII type 1 receptors (AT1Rs) start signaling cascades associated with AngII, leading directly to cell growth. In response to stretch, AT1R signaling increases MAPK phosphorylation, JAK–STAT signaling and expression of several

hypertrophic markers [10]. TGFβ signaling in cardiac myocytes is not as well defined. In cultured cardiomyocytes, TGFβ mRNA and protein are upregulated by AngII, and TGFβ itself promotes expression of the fetal gene program associated with CM hypertrophy [11] .

Another common response to hemodynamic or metabolic stress is the activation of **the fetal gene program**. This program is characterized by 1) overexpression of natriuretic peptide genes atrial natriuretic peptide (ANP, Nppa) and brain natriuretic peptide (BNP, Nppb), and 2) sarcomere remodeling induced by a switch in myosin heavy chain (MHC) from alpha-myosin heavy chain (α-MHC, *Myh6*) to beta-myosin heavy chain (β-MHC, *Myh7*).

Plasma levels of natriuretic peptides have proven to be powerful diagnostic and prognostic biomarkers of heart disease. Upon stress, the pro-peptides are released by the heart and the ventricular expression of both Nppa and Nppb is strongly increased in the CMs [12]. Because of this feature, the gene products, especially NT-pro-BNP, serve as reliable molecular markers to assess cardiac disease and heart failure progression. ANP and BNP were found to be the natural ligands for cell membrane-bound guanylyl cyclase receptors that mediate the effects of natriuretic peptides through the generation of intracellular cGMP, which interacts with specific enzymes and ion channels [13].

Sarcomere remodeling occurs during the process of adaptation. Myosin isoform expression will change to maintain an appropriate contractile force. A decrease in the α-MHC isoform and an increase in the β-MHC isoform have been shown in experimental pressure induced cardiac hypertrophy in rats. Although β-MHC is the major isoform throughout life in the human heart, a decrease in α-MHC expression (mRNA) and content (protein), and a relative increase of β-MHC expression has been reported in the left ventricle of patients with cardiomyopathy. While β-MHC expression was also decreased in the failing heart compared with the non-failing heart, the ratio of β-MHC/α-MHC increased because of a greater repression of α-MHC. Indeed, even small decreases in the α-MHC isoform can influence contractility and cardiac output. This **MHC isoform switching** has been shown to be induced by forced glucose uptake both *ex vivo* and *in vivo,* and restricting dietary glucose prevents MHC switching in hearts of rats subjected to pressure overload–induced hypertrophy [14].

A signaling cascade that includes the protein kinase Akt regulates the growth and survival of many cell types. In CMs, phosphatidylinositol-3-kinase (PI3K)-Akt pathway plays a key role in regulating **CM growth and survival**. The Akt1 pathway is necessary for exercise-induced physiological growth and it becomes a cardioprotective pathway in pathological remodeling, where it inhibits hypertrophy [7]. This observation highlights the crosstalk and potential for reciprocal compensation between physiological and pathological cardiac growth. However, initial strategies to improve myocardial repair utilizing AKT where impeded by prolonged AKT activation promoting pathological remodeling and reducing coronary angiogenesis by the downregulation of VEGF and angiopoietin-2 [7].

Under normal conditions, the main pathway for **CM metabolism** is based on the production of ATP by fatty acid (FA) oxidation (FAO), glucose metabolism contributes to a lesser extent. However, under stress conditions, FAO is reduced, and this reduction is compensated by an increased glucose utilization. Inside CMs, glucose is phosphorylated and subsequently goes through multiple metabolic pathways (Figure 3). Pathological alterations of these pathways in cardiac hypertrophy and IHD are associated with impaired signaling transduction, perturbed ion and redox homeostasis, and contractile dysfunction. Intracellular free AMP in the CM is increased when the heart faces pressure overload [15] and as a result, synthesis of fructose 2,6-BP, an activator of phosphofructokinase 1 (PFK1), is upregulated. The increase in glycolysis is, however, accompanied by reduced or normal glucose oxidation, which may lead to an uncoupling between glucose uptake and oxidation [16].

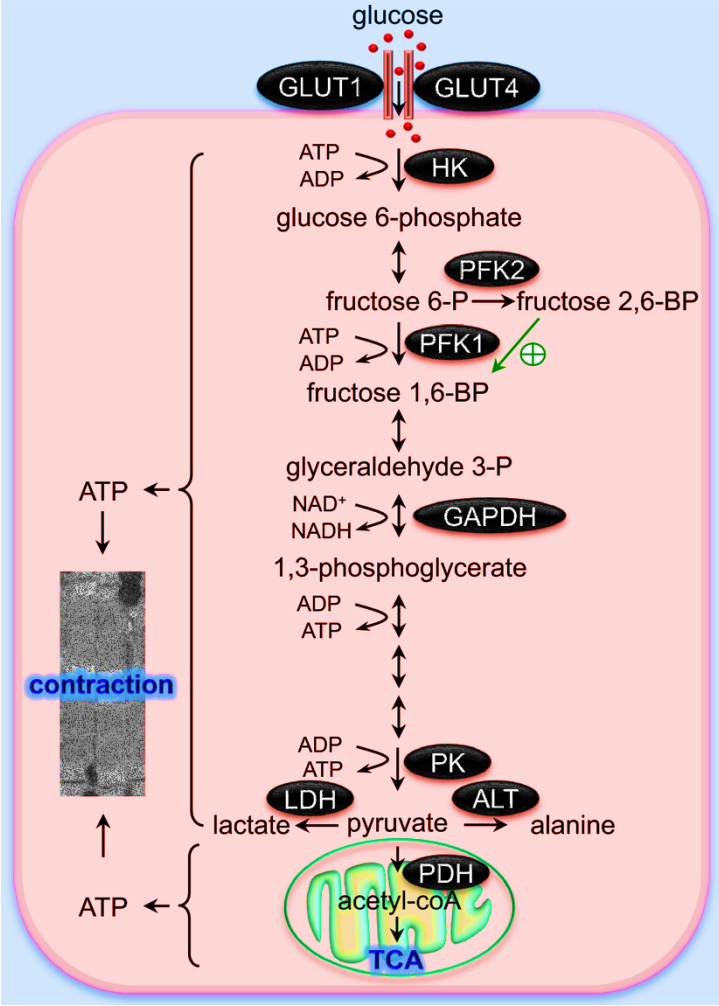

FIGURE 3. GLUCOSE METABOLISM IN A CM (ADAPTED FROM DIEM H. TRAN ET AL, 2019) [17]

Growing evidence indicates that metabolic remodeling precedes most of other pathological alterations and likely plays an essential role in cardiac hypertrophy and HF [17] . A recent study showed that following MI, inducible deletion of pyruvate dehydrogenase kinase 4 (PDK4), to selectively enhance oxidation of glycolytically derived pyruvate in CMs mitochondria, improved left ventricular function and decreased remodeling [18]. Transcription of the PDK4 gene is induced directly by the transcription factors FoxO1, which is repressed by insulin, and peroxisome proliferator-activated receptor (PPAR)-α, which is activated by FA [19]. PPAR-α is also a key factor in the transcriptional regulation of substrate preference in the heart. Peroxisome proliferator-activated receptor gamma coactivator 1-alpha (PGC-1α) promotes mitochondrial biogenesis and the activation of PPAR-α leads to mitochondrial long-chain FA oxidation. The potential success of metabolic remodeling as a therapy

depends on whether the shift from FA towards glucose utilization should be considered beneficial or detrimental. To date, this question remains incompletely resolved.

Accumulating evidence indicate a pivotal role of the **CM cytoskeleton**, including the Z disc complex, in the pathogenesis of cardiomyopathy and HF. Cardiac cytoskeletal proteins participate not only in organization of the cytoskeleton and biomechanical force production but also in the transmission of stress signals leading to changes in cardiac gene expression and function. However, the precise molecular mechanisms by which cytoskeletal proteins modulate transcription are largely unknown [20].

Altogether, the different signaling pathways studied can be targeted to restore CM function partially, reinforcing the need of in-depth research to identify novel factors with key roles in cardiac remodeling and HF.

CARDIOMYOCYTE PROLIFERATION

Adult CMs have a very **limited endogenous proliferative capacity** [21]. More recently, low levels of CM proliferation have been found in adult mammalian hearts, including humans. In addition, genetic manipulations in mice provide evidence that barriers to adult CM proliferation can be circumvented by looking at developmental transitions in CM maturation. Promoting CM proliferation could become clinically relevant with efforts to prevent unrestrained cardiac growth in the long term.

Molecular signals that stimulate CM proliferation include growth factors, intrinsic signaling pathways, microRNAs (miRNAs), and cell cycle regulators [22]. In the developing heart, CM proliferation is regulated by Neuregulin/ErbB/ERK signaling, which is the primary proliferative pathway in the embryonic heart. After mid-gestation, BMP signaling and IGF/PI3K pathways are required for hyperplastic growth of CMs. Throughout development and after birth, the Hippo/Yap pathway is a critical regulator of CM proliferation and organ size [22]. Manipulation of signaling molecules, such as Yap and neuregulin pathway proteins, is important for developmental regulation of CM proliferation. By altering these pathways, one can overcome post-natal cell cycle arrest and promote adult CM proliferation [22]. Inhibition of the Hippo pathway promotes adult CM cell cycle activity, cytoskeletal remodeling, dedifferentiation, and cardio-protection after injury [23]. Moreover, inhibiting FA utilization by PDK4 conditional deletion in CMs resulted in decreased CM size and DNA damage, while CM proliferation was increased in the postnatal heart [18]. Additionally, gene therapy targeting the low-density lipoprotein receptor-related protein 6 (Lrp6) using adeno-associated virus (AAV)9 construct encoding miRNA-Lrp6 promoted the repair of heart injury in mice. Lrp6 is a Wnt co-receptor that is required for embryonic heart development [24].

While we are far from clinical translation, the possibility that resident CM in an injured heart could be stimulated for repair is an exciting new direction to explore.

MICRORNAS IN HEART DISEASE & THERAPEUTIC REGULATION

MiRNAs are short, single-stranded non-coding oligonucleotides that suppress protein formation post-transcriptionally by binding to complementary sequences in the mRNA. MiRNAs are composed of ~21 nucleotides transcribed from intergenic, intronic or polycistronic regions. They arise from primary transcripts of variable sizes that are processed to 70-to 100-nucleotide hairpin-shaped precursors into mature miRNAs. The canonical biogenesis includes Drosha and DiGeorge Syndrome Critical Region 8 (DGCR8) for the cleavage of pri-miRNA to form pre-miRNA. This is exported to the cytoplasm by Exportin5/RanFTP-dependent manner and processed to produce the mature miRNA duplex. Finally, either the 5p or 3p strands of the mature miRNA duplex is loaded into the Argonaute (AGO) family of proteins to form a miRNA-induced silencing complex (miRISC). MiRISC binds to target mRNAs to induce translational inhibition [25].

MiRNAs have been shown to be essential for normal heart development and cardiac function. MiRNAs are involved in the etiology of cardiac disease and the remodeling of hearts, including cardiac hypertrophy, MI, and HF, and the action of miRNAs become stronger during pathology [26]. The expression of miRNAs can be manipulated, triggering enthusiasm for miRNAs as novel therapeutic targets. MiRNA expression can be silenced with miRNA inhibitors, also called antimiRs. AntimiRs are single stranded oligonucleotides directly complementary to the target miRNA which can decrease or even eliminate the expression of this miRNA [25]. On the contrary, **miRNA mimics** can provide miRNA gain-of-function. MiRNA mimics are double stranded oligonucleotides with a sequence motif on its 5'-end that is partially complementary to a mRNA target sequence in the 3'UTR resulting in posttranscriptional repression or translational inhibition of the target gene [27].

MiRNAs can be categorized into different groups, named miRNA families. The families are based on the mature miRNA, or the sequence and/or structure of the pre-miRNA. Families are relevant because they suggest a common sequence or structure configuration in sets of genes that hint to a shared function [28] .

One of the first studies on a genetic deletion of a miRNA was on **miR-208a,** a cardiac-specific miRNA transcribed with α-MHC. MiR-208 plays a key role in the expression of β-MHC in response to cardiac stress with a dominant function in regulating cardiac hypertrophy and remodeling. In response to pressure overload, miR-208a null mice showed virtually no CM hypertrophy, fibrosis, and no upregulation of β-MHC. Systemic delivery of an LNA-modified antimiR showed that therapeutic silencing of miR-208a prevents pathological cardiac remodeling, functional deterioration, and lethality during diastolic heart disease [25].

During the pathological growth of cardiomyocytes, **miR-132** has been identified as a major driver [29]. The first clinical trial with antisense drug in HF patients using miR-132 inhibitor suggests cardiac

improvements, indicating strong clinical potential in HF patients with increased cardiac expression levels of the miR-212/132 cluster [29].

After ischemic stress, one of the most studied miRNA families is the **miR-15 family**, a group of 5 miRNAs (miR-15a, miR-15b, miR-16-1, miR-16-2, miR-195, and miR-497) that share the same seed region. The *miR-15* family has been shown to induce a strong inhibition of the cell cycle [30, 31]. Furthermore, therapeutic inhibition of the *miR-15* family with subcutaneous delivery of antimiR has been shown to reduce infarct size in murine MI [32, 33].

Lastly, **miR-29** has a key role in regulating fibrosis activation upon cardiac stress [34]. MiR-29 mimics have recently shown encouraging preclinical safety and efficacy data for idiopathic pulmonary fibrosis, and is currently investigated for a future potential clinical application towards wound healing and HF.

INJECTABLE HYDROGELS TO REPAIR THE HEART

A drawback of pre-clinical studies using miRNA therapeutics is that the far majority of the drugs often end up in the liver and kidney, revealing targeted delivery as one of the major challenges [32]. Delivery of agents to the heart remains a big hurdle in therapeutic strategies, making it an interesting subject for ongoing investigations. Delivery methods which have been tested include modified micelle, liposomes, nanoparticles, and others with varying levels of success [35]. Specific to miRNA therapeutics, its naked delivery is considered safe; however, the process is highly inefficient due to the electrostatic repulsions occurring at physiological pH between the anionic nucleic acid molecules and the negatively charged plasma membrane [35].

Biomaterial scaffolds may be exploited to deliver therapeutic gene molecules, providing a controlled release of these agents in desired locations as a means to avoid clearance mechanisms and reinforce their stability in the physiological milieu [36]. Hydrogels constitute a class of biomaterials formed by self-assembling or crosslinking of water-soluble polymers into a network. The porous and hydratable structure of hydrogels induces their gelation and swelling in the biological microenvironment, enabling their local administration by injection without the need for invasive surgery. In an effort to control the release kinetics and preserve the activity of therapeutic biomolecules, hydrogels have been widely investigated as gene delivery systems. These systems are either based on natural (e.g., extracellular matrix-derived or collagen/fibrin-based) materials that closely mimic the host tissue, or synthetic materials (e.g., poly (ethylene glycol) (PEG) or poly(N-isopropylacrylamide) - based) that are easily tunable, have controllable biochemical properties, and might be less vulnerable to batch-to-batch variation. Various injectable hydrogels are available, differing in composition, mechanical and gelation properties induced by changes in physiological conditions such as temperature, ionic strength, and pH [37].

After MI, hydrogels may serve as an injectable vehicle to create a local sustained-release drug delivery depot. For instance, ureido-pyrimidinone poly(ethylene glycol) (UPy-PEG) hydrogel was developed to be used as a catheter-injectable hydrogel to sustain drug release delivery in a porcine model of MI [38]. Hydrogels can be used for the delivery of antimiRs and miRNA mimics. However, the pharmacokinetics and dynamics of antimiRs and mimics formulated in a hydrogel need further optimization for a more local, safe, and efficient delivery.

THESIS OUTLINE

The studies described in this thesis were aimed to extend our insights on CM-specific gene regulation relevant for cardiac remodeling and to study a novel therapeutic approach for CM-specific delivery. We isolated and sequenced CMs from mouse models of pathological and physiological remodeling and used *in vitro* CM models to identify and investigate novel candidate gene targets. Additionally, we studied the safety and efficacy of a hydrogel-based delivery method to increase CM local delivery of miRNA therapeutics and to increase protection of the heart after MI.

In **chapter 2** we investigate CM-specific gene programs in pathological remodeling. Using a model of pressure overload, we identified a failure-induced gene program, which is conserved between mouse and human. Here, we identified phosphofructokinase-platelet isoform (*PFKP)* to play a role in CM remodeling during HF.

In **chapter 3** we investigate CM-specific gene programs driving physiological hypertrophy. Using a model of swimming, we identified the exercise-induced gene program in CMs. By focusing on transcription factors, we identified high expression of Sox17 in hypertrophic CMs. We investigated the potential cardioprotective role of Sox17 in a model of pressure overload by using adenoviral delivery which failed to preserve cardiac function during pathology.

In **chapter 4** we investigate the efficacy and safety of a new hydrogel-based delivery system in a model of ischemic injury. Hydrogel-based delivery of antimir-195 improved CM local delivery and enhanced target de-repression and CM proliferation.

Finally, in **chapter 5** we discuss all findings in a broader context together with future perspectives.

References

1. Group WCRCW. World Health Organization cardiovascular disease risk charts: revised models to estimate risk in 21 global regions. *Lancet Glob Health*. 2019;7:e1332-e1345.
2. Benjamin EJ, Muntner P, Alonso A, Bittencourt MS, Callaway CW, Carson AP, Chamberlain AM, Chang AR, Cheng S, Das SR, Delling FN, Djousse L, Elkind MSV, Ferguson JF, Fornage M, Jordan LC, Khan SS, Kissela BM, Knutson KL, Kwan TW, Lackland DT, Lewis TT, Lichtman JH, Longenecker CT, Loop MS, Lutsey PL, Martin SS, Matsushita K, Moran AE, Mussolino ME, O'Flaherty M, Pandey A, Perak AM, Rosamond WD, Roth GA, Sampson UKA, Satou GM, Schroeder EB, Shah SH, Spartano NL, Stokes A, Tirschwell DL, Tsao CW, Turakhia MP, VanWagner LB, Wilkins JT, Wong SS, Virani SS, American Heart Association Council on E, Prevention Statistics C and Stroke Statistics S. Heart Disease and Stroke Statistics-2019 Update: A Report From the American Heart Association. *Circulation*. 2019;139:e56-e528.
3. Wilkins E WL, Wickramasinghe K, Bhatnagar P, Leal J, Luengo-Fernandez R, Burns R, Rayner M, Townsend N. European Cardiovascular Disease Statistics 2017. *European Heart Network*. 2017.
4. Nakamura M and Sadoshima J. Mechanisms of physiological and pathological cardiac hypertrophy. *Nat Rev Cardiol*. 2018;15:387-407.
5. Ponikowski P, Voors AA, Anker SD, Bueno H, Cleland JG, Coats AJ, Falk V, Gonzalez-Juanatey JR, Harjola VP, Jankowska EA, Jessup M, Linde C, Nihoyannopoulos P, Parissis JT, Pieske B, Riley JP, Rosano GM, Ruilope LM, Ruschitzka F, Rutten FH, van der Meer P, Authors/Task Force M and Document R. 2016 ESC Guidelines for the diagnosis and treatment of acute and chronic heart failure: The Task Force for the diagnosis and treatment of acute and chronic heart failure of the European Society of Cardiology (ESC). Developed with the special contribution of the Heart Failure Association (HFA) of the ESC. *Eur J Heart Fail*. 2016;18:891-975.
6. Melo LG, Pachori AS, Kong D, Gnecchi M, Wang K, Pratt RE and Dzau VJ. Molecular and cell-based therapies for protection, rescue, and repair of ischemic myocardium: reasons for cautious optimism. *Circulation*. 2004;109:2386-93.
7. Chaanine AH and Hajjar RJ. AKT signalling in the failing heart. *Eur J Heart Fail*. 2011;13:825-9.
8. Burchfield JS, Xie M and Hill JA. Pathological ventricular remodeling: mechanisms: part 1 of 2. *Circulation*. 2013;128:388-400.
9. Fountoulaki K, Dagres N and Iliodromitis EK. Cellular Communications in the Heart. *Card Fail Rev*. 2015;1:64-68.
10. Saucerman JJ, Tan PM, Buchholz KS, McCulloch AD and Omens JH. Mechanical regulation of gene expression in cardiac myocytes and fibroblasts. *Nat Rev Cardiol*. 2019.

11. Saucerman JJ, Tan PM, Buchholz KS, McCulloch AD and Omens JH. Mechanical regulation of gene expression in cardiac myocytes and fibroblasts. *Nat Rev Cardiol*. 2019;16:361-378.

12. Man J, Barnett P and Christoffels VM. Structure and function of the Nppa-Nppb cluster locus during heart development and disease. *Cell Mol Life Sci*. 2018;75:1435-1444.

13. Goetze JP, Bruneau BG, Ramos HR, Ogawa T, de Bold MK and de Bold AJ. Cardiac natriuretic peptides. *Nat Rev Cardiol*. 2020;17:698-717.

14. Miyata S, Minobe W, Bristow MR and Leinwand LA. Myosin heavy chain isoform expression in the failing and nonfailing human heart. *Circ Res*. 2000;86:386-90.

15. Nascimben L, Ingwall JS, Lorell BH, Pinz I, Schultz V, Tornheim K and Tian R. Mechanisms for increased glycolysis in the hypertrophied rat heart. *Hypertension*. 2004;44:662-7.

16. Leong HS, Brownsey RW, Kulpa JE and Allard MF. Glycolysis and pyruvate oxidation in cardiac hypertrophy--why so unbalanced? *Comp Biochem Physiol A Mol Integr Physiol*. 2003;135:499-513.

17. Tran DH and Wang ZV. Glucose Metabolism in Cardiac Hypertrophy and Heart Failure. *J Am Heart Assoc*. 2019;8:e012673.

18. Cardoso AC, Lam NT, Savla JJ, Nakada Y, Pereira AHM, Elnwasany A, Menendez-Montes I, Ensley EL, Petric UB, Sharma G, Sherry AD, Malloy CR, Khemtong C, Kinter MT, Tan WLW, Anene-Nzelu CG, Foo RS, Nguyen NUN, Li S, Ahmed MS, Elhelaly WM, Abdisalaam S, Asaithamby A, Xing C, Kanchwala M, Vale G, Eckert KM, Mitsche MA, McDonald JG, Hill JA, Huang L, Shaul PW, Szweda LI and Sadek HA. Mitochondrial Substrate Utilization Regulates Cardiomyocyte Cell Cycle Progression. *Nat Metab*. 2020;2:167-178.

19. Zhao G, Jeoung NH, Burgess SC, Rosaaen-Stowe KA, Inagaki T, Latif S, Shelton JM, McAnally J, Bassel-Duby R, Harris RA, Richardson JA and Kliewer SA. Overexpression of pyruvate dehydrogenase kinase 4 in heart perturbs metabolism and exacerbates calcineurin-induced cardiomyopathy. *Am J Physiol Heart Circ Physiol*. 2008;294:H936-43.

20. Kuwahara K, Teg Pipes GC, McAnally J, Richardson JA, Hill JA, Bassel-Duby R and Olson EN. Modulation of adverse cardiac remodeling by STARS, a mediator of MEF2 signaling and SRF activity. *J Clin Invest*. 2007;117:1324-34.

21. Lazar E, Sadek HA and Bergmann O. Cardiomyocyte renewal in the human heart: insights from the fall-out. *Eur Heart J*. 2017;38:2333-2342.

22. Uygur A and Lee RT. Mechanisms of Cardiac Regeneration. *Dev Cell*. 2016;36:362-74.

23. Xin M, Kim Y, Sutherland LB, Murakami M, Qi X, McAnally J, Porrello ER, Mahmoud AI, Tan W, Shelton JM, Richardson JA, Sadek HA, Bassel-Duby R and Olson EN. Hippo pathway effector Yap promotes cardiac regeneration. *Proc Natl Acad Sci U S A*. 2013;110:13839-44.

24. Wu Y, Zhou L, Liu H, Duan R, Zhou H, Zhang F, He X, Lu D, Xiong K, Xiong M, Zhuang J, Liu Y, Li L, Liang D and Chen YH. LRP6 downregulation promotes cardiomyocyte proliferation and heart regeneration. *Cell Res*. 2020.

25. van Rooij E and Olson EN. MicroRNA therapeutics for cardiovascular disease: opportunities and obstacles. *Nat Rev Drug Discov*. 2012;11:860-72.

26. Eding JE, Demkes CJ, Lynch JM, Seto AG, Montgomery RL, Semus HM, Jackson AL, Isabelle M, Chimenti S and van Rooij E. The Efficacy of Cardiac Anti-miR-208a Therapy Is Stress Dependent. *Mol Ther*. 2017;25:694-704.

27. Wang Z. The guideline of the design and validation of MiRNA mimics. *Methods Mol Biol*. 2011;676:211-23.

28. Kamanu TK, Radovanovic A, Archer JA and Bajic VB. Exploration of miRNA families for hypotheses generation. *Sci Rep*. 2013;3:2940.

29. Jörg Täubel, Wilfried Hauke, Steffen Rump, Janika Viereck, Sandor Batkai, Jenny Poetzsch, Laura Rode, Henning Weigt, Celina Genschel, Ulrike Lorch, Carmen Theek, Arthur A Levin, Johann Bauersachs, Scott D Solomon, Thomas Thum. Novel antisense therapy targeting microRNA-132 in patients with heart failure: results of a first-in-human Phase 1b randomized, double-blind, placebo-controlled study. European Heart Journal. 2021; 42:178-88

30. Ofir M, Hacohen D and Ginsberg D. MiR-15 and miR-16 are direct transcriptional targets of E2F1 that limit E2F-induced proliferation by targeting cyclin E. *Mol Cancer Res*. 2011;9:440-7.

31. Porrello ER, Johnson BA, Aurora AB, Simpson E, Nam YJ, Matkovich SJ, Dorn GW, 2nd, van Rooij E and Olson EN. MiR-15 family regulates postnatal mitotic arrest of cardiomyocytes. *Circ Res*. 2011;109:670-9.

32. Hullinger TG, Montgomery RL, Seto AG, Dickinson BA, Semus HM, Lynch JM, Dalby CM, Robinson K, Stack C, Latimer PA, Hare JM, Olson EN and van Rooij E. Inhibition of miR-15 protects against cardiac ischemic injury. *Circ Res*. 2012;110:71-81.

33. Porrello ER, Mahmoud AI, Simpson E, Johnson BA, Grinsfelder D, Canseco D, Mammen PP, Rothermel BA, Olson EN and Sadek HA. Regulation of neonatal and adult mammalian heart regeneration by the miR-15 family. *Proc Natl Acad Sci U S A*. 2013;110:187-92.

34. van Rooij E, Sutherland LB, Thatcher JE, DiMaio JM, Naseem RH, Marshall WS, Hill JA and Olson EN. Dysregulation of microRNAs after myocardial infarction reveals a role of miR-29 in cardiac fibrosis. *Proc Natl Acad Sci U S A*. 2008;105:13027-32.

35. Bono N, Ponti F, Mantovani D and Candiani G. Non-Viral in Vitro Gene Delivery: It is Now Time to Set the Bar! *Pharmaceutics*. 2020;12.

36. Patel S, Athirasala A, Menezes PP, Ashwanikumar N, Zou T, Sahay G and Bertassoni LE. Messenger RNA Delivery for Tissue Engineering and Regenerative Medicine Applications. *Tissue Eng Part A*. 2019;25:91-112.

37. Carballo-Pedrares N, Fuentes-Boquete I, Diaz-Prado S and Rey-Rico A. Hydrogel-Based Localized Nonviral Gene Delivery in Regenerative Medicine Approaches-An Overview. *Pharmaceutics*. 2020;12.

38. Koudstaal S, Bastings MMC, Feyen DAM, Waring CD, van Slochteren FJ, Dankers PYW, Torella D, Sluijter JPG, Nadal-Ginard B, Doevendans PA, Ellison GM and Chamuleau SAJ. Sustained Delivery of Insulin-Like Growth Factor-1/Hepatocyte Growth Factor Stimulates Endogenous Cardiac Repair in the Chronic Infarcted Pig Heart. *Journal of Cardiovascular Translational Research*. 2014;7:232-241.

CHAPTER 2

GENE EXPRESSION PROFILING OF HYPERTROPHIC CARDIOMYOCYTES IDENTIFIES NEW PLAYERS IN PATHOLOGICAL REMODELING

Marta Vigil-Garcia[1]*, Charlotte J. Demkes[1,2]*, Joep E.C. Eding[1], Danielle Versteeg[1], Hesther de Ruiter[1], Ilaria Perini[1], Monika M. Gladka[1], Folkert W. Asselbergs[2,3,4], Aryan Vink[5], Magdalena Harakalova[2], Alexander Bossu[6], Toon A. B. van Veen[6], Cornelis J. Boogerd[1], and Eva van Rooij [1,2]

[1] Hubrecht Institute, Royal Netherlands Academy of Arts and Sciences and University Medical Center Utrecht, The Netherlands.

[2] Department of Cardiology, University Medical Centre Utrecht, The Netherlands.

[3] Institute of Cardiovascular Science, Faculty of Population Health Sciences, University College London, London, United Kingdom.

[4] Health Data Research UK and Institute of Health Informatics, University College London, London, United Kingdom.

[5] Department of Pathology, University Medical Centre Utrecht, The Netherlands. [6] Department of Medical Physiology, University Medical Centre Utrecht, The Netherlands.

* These authors contributed equally to this article

Adapted from:

Cardiovascular Research, doi:10.1093/cvr/cvaa233

Published online on 22 July 2020

Keywords: Hypertrophy, Pathological remodeling, RNA sequencing, Cardiomyocyte, Heart failure, PFKP

Abstract

Aims Pathological cardiac remodelling is characterized by cardiomyocyte (CM) hypertrophy and fibroblast activation, which can ultimately lead to maladaptive hypertrophy and heart failure (HF). Genome-wide expression analysis on heart tissue has been instrumental for the identification of molecular mechanisms at play. However, these data were based on signals derived from all cardiac cell types. Here, we aimed for a more detailed view on molecular changes driving maladaptive CM hypertrophy to aid in the development of therapies to reverse pathological remodelling.

Methods and Results Utilizing CM-specific reporter mice exposed to pressure overload by transverse aortic banding and CM isolation by flow cytometry, we obtained gene expression profiles of hypertrophic CMs in the more immediate phase after stress, and CMs showing pathological hypertrophy. We identified subsets of genes differentially regulated and specific for either stage. Among the genes specifically up-regulated in the CMs during the maladaptive phase we found known stress markers, such as *Nppb* and *Myh7*, but additionally identified a set of genes with unknown roles in pathological hypertrophy, including the platelet isoform of phosphofructokinase (PFKP). Norepinephrine-angiotensin II treatment of cultured human CMs induced the secretion of N-terminal-pro-B-type natriuretic peptide (NT-pro-BNP) and recapitulated the up-regulation of these genes, indicating conservation of the up-regulation in failing CMs. Moreover, several genes induced during pathological hypertrophy were also found to be increased in human HF, with their expression positively correlating to the known stress markers NPPB and MYH7. Mechanistically, suppression of Pfkp in primary CMs attenuated stress-induced gene expression and hypertrophy, indicating that Pfkp is an important novel player in pathological remodelling of CMs.

Conclusion Using CM-specific transcriptomic analysis, we identified novel genes induced during pathological hypertrophy that are relevant for human HF, and we show that PFKP is a conserved failure-induced gene that can modulate the CM stress response.

INTRODUCTION

Heart failure (HF) is a major cause of morbidity and mortality, that can originate from numerous diseases such as myocardial infarction and hypertension.[1] Independent of the aetiology, cardiac hypertrophy is an immediate response comprising compensatory alterations in size, shape, and function of the myocardium to restore cardiac output. However, if left untreated, it can progress into maladaptive alterations, including a decline in cardiomyocyte (CM) contractility, fibrosis, ventricular dilatation, chronic inflammation, and increased cellular apoptosis, which can ultimately lead to HF.[2] While the remodelling process involves all cardiac cell types, CMs function as key determinants of cardiac health and disease.[3] Within the CMs, stress induces changes in gene expression, including reactivation of the fetal gene programme, that can trigger cell growth resulting in the initial CM hypertrophy. Next, there is a cellular metabolic shift towards carbohydrates as energy substrate and a change in mitochondria-associated pathways to adapt to the increase in ATP demand.[2,4] As a result, CMs progress towards failure, presenting a significant reduction of mitochondria biogenesis.[5] At the same time, cardiac function progressively deteriorates, ultimately leading to HF.

Current HF therapies target neurohormonal activation to improve cardiac relaxation and energetics or are antiarrhythmic approaches. While important advances have been made in the treatment of HF, so far these have been mainly directed at symptom management and prevention of sudden cardiac death. To date, there is no cure available to stop disease progression. RNA sequencing on heart tissue has been instrumental for understanding the molecular mechanisms important during hypertrophy and failure.[6] These studies have shown us the relevance of genes encoding factors such as myocyte enhancer factor 2 (MEF2), periostin, angiotensin, and insulin-like growth factor during the transition into HF.[7,8] While insightful, most RNA sequencing efforts to date have been limited by the fact that the obtained signal was derived from tissue. The complex cell type composition dilutes out any cell type-specific signals and fails to provide information on cellular origin of the detected gene expression changes. An improved strategy for the discovery of new targets could be to decipher the changes occurring during the transition from hypertrophic towards failing CMs specifically. Identification of novel genes and pathways that play a role during CM failure combined with functional studies addressing the mechanisms by which these contribute to disease progression could further aid in the identification of novel druggable targets and form the basis for development of enhanced therapies.

Here, we set out to obtain genome-wide gene expression profiles from CMs during the early and maladaptive phase of cardiac remodelling. To do so we used a recently developed CM isolation method[9] combined with an animal model of pressure overload to comprehensively examine gene expression changes. In doing so, we identified specific molecular signatures for hypertrophic CM and CMs showing pathological hypertrophy and found multiple novel genes that are unknown for their

role in pathological remodelling. We further showed that these pathological genes are also up-regulated in human end-stage HF and in stressed human-induced pluripotent stem cell (hiPSC)-derived CMs. Amongst the failure-induced genes, we identified phosphofructokinase-platelet (*PFKP*) as a stress-induced glycolytic enzyme in CMs, and its *in vitro* inhibition blocked expression of the gene encoding natriuretic peptide B (*Nppb*) expression and hypertrophy. Together, these findings may set the basis for accelerating the field of molecular cardiology towards the identification of new therapeutic targets for HF.

RESULTS

Identifying the early and pathological hypertrophic states during cardiac remodelling

To define the gene expression profiles that mark hypertrophic and failing CMs, we used TAB in mice to model pressure overload-induced pathological hypertrophy. To establish the suitable timepoints for analysis, we collected molecular data for up to 8 weeks after surgery on wild-type mice (**Supplementary Figure S1A).** The aortic pressure gradient was significantly increased at 6 and 8 weeks post-banding (**Supplementary Figure S1B).** Histological and morphological analysis showed an increase in heart size [heart weight to tibia length (HW/TL)] and CM cross-sectional area (CSA) already 1 week after banding that was maintained for the duration of the study (**Supplementary Figure S1C–E, Table S1).** Additionally, collagen deposition was significantly increased after 4 weeks of banding (**Supplementary Figure S1F).** At a molecular level, cardiac stress markers natriuretic peptide A (*Nppa*)[15] and beta myosin heavy chain (*Myh7*) increased after TAB, while alpha myosin heavy chain (*Myh6*) decreased.[16]Collagen type III alpha 1 (*Col3a1*)[17] showed an initial increase after TAB, while there was a pronounced reduction in the expression of the metabolic regulators PPARG coactivator 1 alpha and beta (*Pgc1α* and *Pgc1β*)[5] after banding (**Supplementary Figure S1G).** Based on the increased heart size and signs of increased CM size at 1 week post-TAB, we concluded this timepoint to resemble early phase hypertrophy. The additional increase in fibrotic tissue and increased aortic pressure gradient at 8 weeks post-TAB indicated that disease state had advanced towards pathological remodelling and maladaptive hypertrophy at this timepoint.

Using flow cytometry to isolate CMs

To genetically label CMs, we crossed *Myh6-Cre* transgenic mice[18] with *Rosa26-td-Tomato* reporter mice (*R26-lsl-tdTomato*)[10] (**Figure 1A and B**). Mice were subjected to TAB or sham surgery and we collected heart tissue after either 1 or 8 weeks, after which we could confirm an increase in HW/TL ratio, CM size (CSA) and fibrosis (**Figure 1C–F**). We next used our optimized digestion protocol

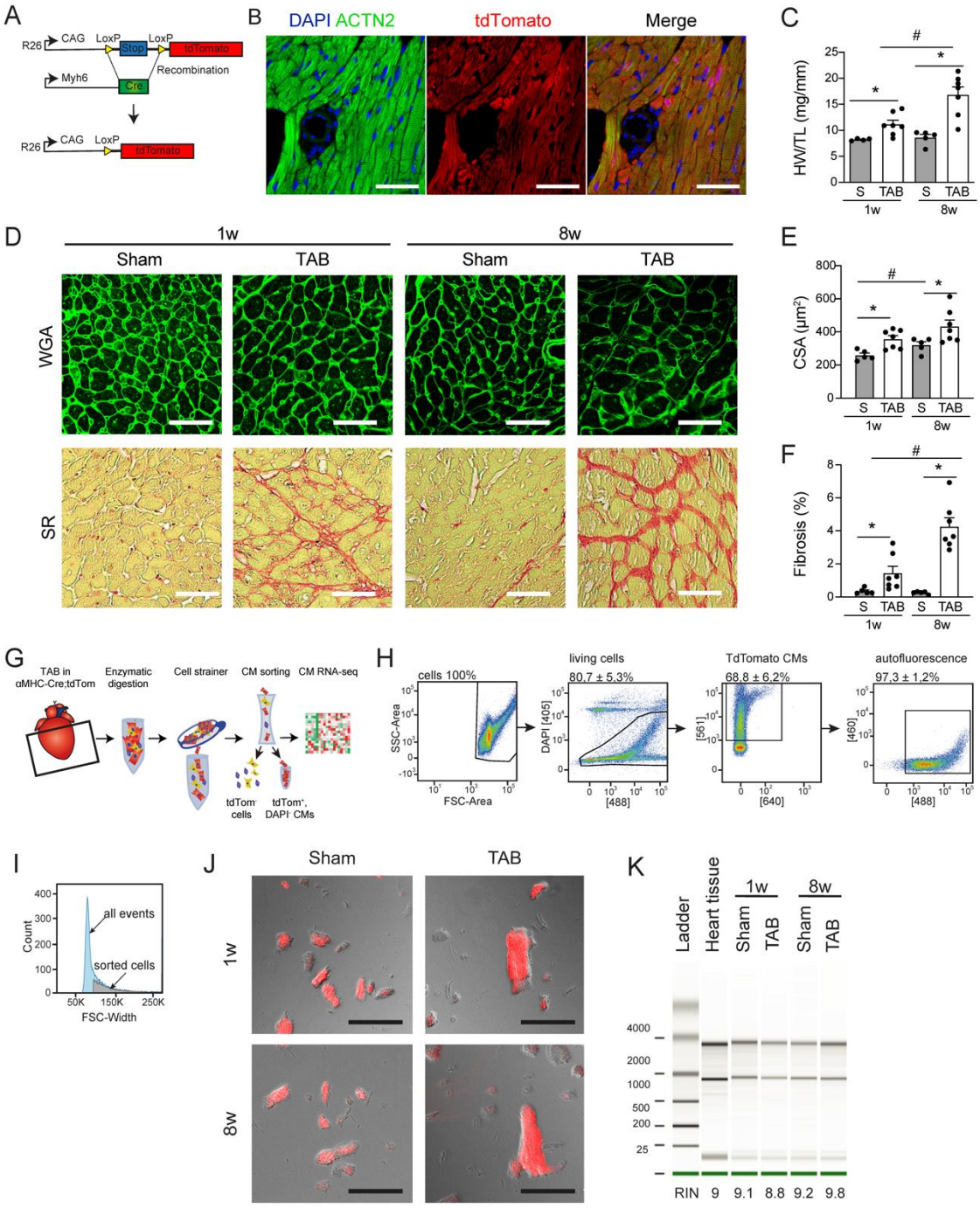

Figure 1. Sorting hypertrophic and failing cardiomyocytes (CMs). A, Strategy for the generation of a CM-specific reporter mouse (*Myh6*-Cre-*tdTomato*). **B,** Immunofluorescence indicating sarcomeric α actinin (ACTN2; CMs) and tdTomato. Scale bar is 200 µm. **C,** Wheat germ agglutinin (WGA, upper row) and picrosirius red (SR, bottom row) staining of hearts one week or eight weeks after transverse aortic banding (TAB) and corresponding sham controls. Scale bars are 200µm. **D,** Quantification of cross-sectional area (CSA) of CMs (≥50 cells per heart, n=5-7). **E,** Quantification of ventricular fibrosis (n=5-7). **F,** Representative FACS plots showing the gating strategy to obtain tdTomato positive CMs. Selections are based on DAPI negativity, tdTomato positivity and green auto-fluorescence. **G**, Forward scatter (FSC)-width plot showing the fraction of sorted cells compared to all events. **H,** Representative images of CMs after sort. **I**, Bioanalyzer plot showing the RNA quality isolated from the sorted CMs one week or eight weeks after TAB surgery and their respective sham controls. RIN**:** RNA Integrity Number. Data expressed as mean fold change ± SEM; * indicates $p<0.05$ compared to sham (S) in a One-way ANOVA test; # indicates $p<0.05$ comparing sham 1 week to sham 8 weeks with unpaired t-test (n=5-7).

followed by FACS[9] to collect CMs based on viability, tdTomato positivity, and sarcomere auto-fluorescence[19] (**Figure 1G and H).** To enrich for CMs, we selected cells with a higher forward scatter width (**Figure 1I, Supplementary Figure S2A and B).** Microscopy confirmed the sorted cells were tdTomato positive, rod-shaped and striated cells, indicative for CMs (**Figure 1J)**. RNA extracted from these cells appeared to be of good quality as indicated by RNA integrity number >8.0 (**Figure 1K and Supplementary Figure S2C and D).**

Hypertrophic and failing cardiomyocytes present a distinct gene expression profile

To comprehensively define the CM gene expression profiles in the compensatory hypertrophy state and in the pathological hypertrophy state, we performed RNA sequencing on sorted CM populations from hearts 1- and 8 weeks post-TAB and their respective sham controls. Principal component analysis (PCA) revealed high similarity between all sham transcriptomes, whereas CMs from TAB 1w animals, which will be termed 'hypertrophic CMs', and CMs from TAB 8w, which will be termed 'pathological CMs', had a clearly distinct gene expression pattern (**Figure 2A**). Moreover, component 2 of the PCA plot revealed higher similarity between control and hypertrophic CMs than with pathological CMs, indicating a progressive change in gene expression in response to stress. A total of 390 and 146 genes were up-regulated in hypertrophic and pathological CMs, respectively, with 52 overlapping genes between both conditions (**Figure 2B–D**). In contrast, 58 and 174 genes were down-regulated in hypertrophic and pathological CMs, respectively, with 22 genes down-regulated in both conditions (**Figure 2B–D and Supplementary Figure S3A–C).** Functional annotation of differentially expressed genes revealed a strong enrichment of cytoskeleton organization and angiogenesis-related genes in the early hypertrophic state whereas failing CMs were enriched for genes involved in muscle cell morphology and development (**Figure 2E).** Down-regulated genes were involved in metabolic pathways and immune response, respectively (**Figure 2F**). Additionally, almost all mitochondrial genes were down-regulated in the failing CMs (**Supplementary Figure S4),** indicating severe stress in this group of cells. Altogether, these results reinforce that hypertrophic and pathological CMs present a distinct transcriptomic profile, implicating different processes to be relevant during these different stages of disease.

Identification of novel genes regulated in hypertrophic and failing CMs

To explore genes that are key in driving maladaptive remodelling, we focused on the top 30 up-regulated genes in hypertrophic and/or pathological CMs (**Figure 3A**). Interestingly, genes specific to

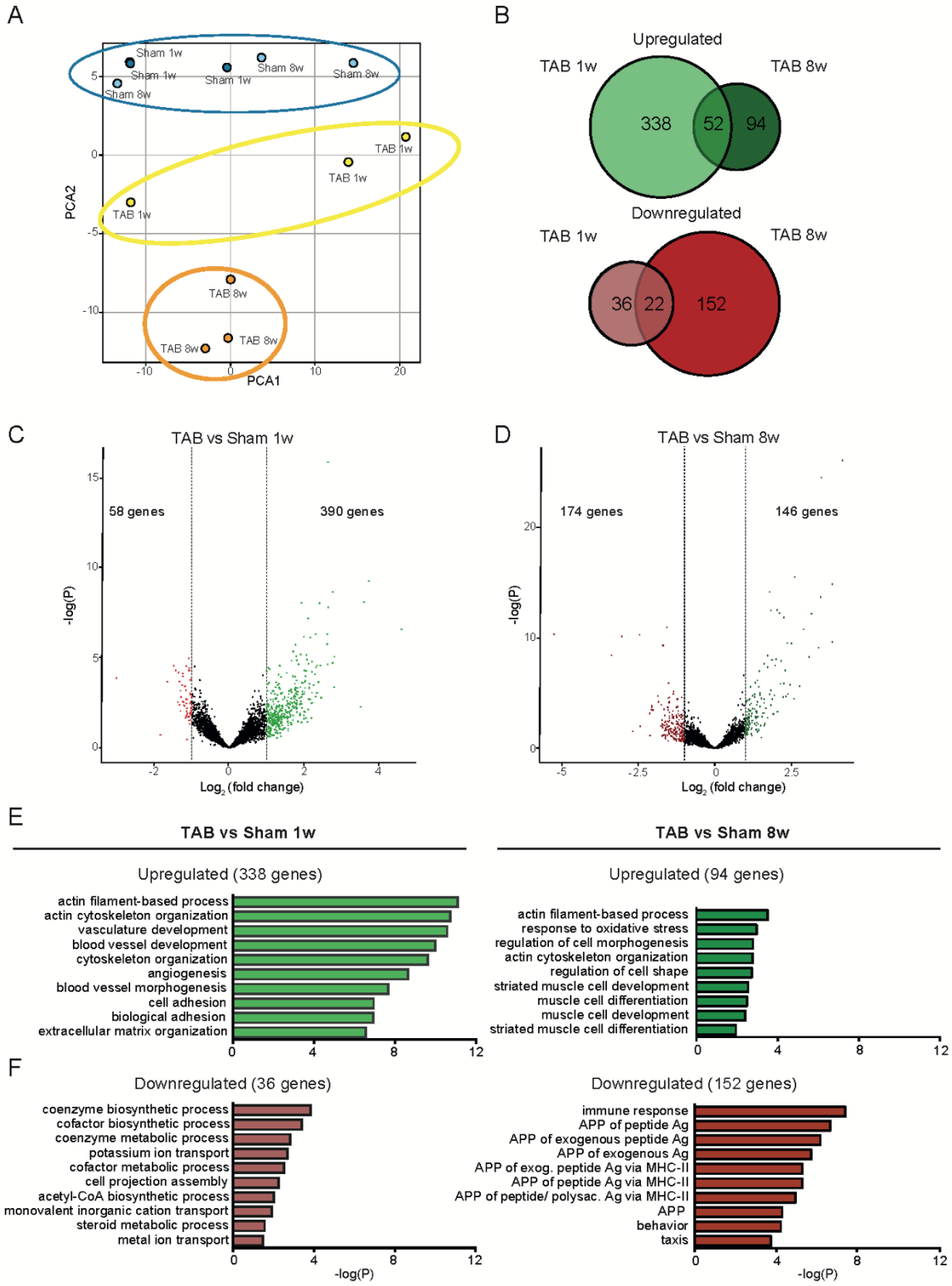

Figure 2. **RNA sequencing analysis reveals differential gene regulation in hypertrophic and failing CMs. A,** Principle component analysis (PCA) plot showing the distinct gene expression between groups (n=3). **B,** Venn diagrams showing the intersection between significantly upregulated genes (log2FC>1), upper panel in green, and significantly downregulated genes (log2FC<-1), lower panel in red, in CMs one week (TAB 1w) and eight weeks (TAB 8w) after TAB when compared to corresponding control (Sham 1w and Sham 8w), respectively (n=3). **C**, Volcano plot of all genes in TAB 1w samples compared to Sham 1w. Significant upregulated genes (22) based on Log2FC >1; and significant downregulated genes (red) based on Log2FC<-1. **D**, Volcano plot of all genes in TAB 8w samples compared to Sham 8w. Significant upregulated genes (22) based on Log2FC >1; and significant downregulated genes (red) based on Log2FC<-1. **E,** GO enrichment analysis for the upregulated genes in CMs

from TAB 1w and TAB 8w compared to corresponding control. **F**, GO enrichment analysis for the downregulated genes in CMs from TAB 1w and TAB 8w compared to corresponding control.

hypertrophic CMs (**Figure 3A, left panel)** presented a variable expression pattern during the pathological state. However, most of the genes specific to CM maladaptive remodelling (**Figure 3A, right panel**) were already showing some degree of up-regulation during hypertrophy, likely representing a gradual activation of this gene programme. Among the genes up-regulated in CM hypertrophy, we identified cyclin-dependent kinase 1 (*Cdk1),* a gene involved in cardiac hypertrophy.[20] Interestingly, *Col3a1*, previously shown to be up-regulated in CMs,[21,22] was also up-regulated in the hypertrophic cells. Since collagen genes are canonical fibroblast markers, we chose to confirm this finding in a single cell sequencing data set (**Supplementary Figure S5).** Also in this dataset expression of *Col3a1* increased five-fold after stress in CMs, indicating a possible relevant biological function during pathological remodelling (**Supplementary Figure S5C and D**). Additionally, maladaptive genes included natriuretic peptide B (*Nppb*), the clinically used biomarker for HF,[17] and *Myh7*, a known marker for diseased CMs.[16]

Real-time PCR on mRNA from sorted CMs confirmed the expression patterns indicated by RNA sequencing with up-regulation of *Cdk1* and *Col3a1* in hypertrophic CMs, and *Nppb* and *Myh7* in failing CMs (**Figure 3B).** In addition, *in situ* hybridization confirmed *Col3a1*, *Nppa*, and *Nppb* mRNA expression in hypertrophic and/or pathological CMs (**Figure 3C and D**).

Failure-induced genes are activated by stress in human CMs

In search for novel relevant players during maladaptive remodelling, we screened the top up-regulated genes during CM failure for genes that had not previously been functionally linked to hypertrophy and/or failure. In doing so we identified 16 candidate genes to further pursue (**Figure 3A, right panel genes in bold**).

To investigate whether up-regulation of these genes in pathological CMs is conserved between species, we utilized human iPSC-CMs. To mimic pathological remodelling in a physiological manner, we subjected a highly pure CM population (**Supplementary Figure S6)** to a 7-day-stress protocol with Norepinephrine (NE) and Angiotensin II (AngII).[23,24] After stimulation, the morphology of the stressed CMs remained grossly normal compared to control (**Figure 4A**). However, NE/AngII treatment significantly reduced the calcium cycle length and induced faster calcium influx (**Figure 4B–D**), characteristics of a beta-adrenergic stimulation.[17] Importantly, NE/AngII led to a strong induction of NT-pro-BNP protein secretion (**Figure 4E**), clinically used to detect and monitor HF in human patients.[25] *NPPB* mRNA levels were also highly induced, whereas *MYH7* was not (**Figure 4F),** which is

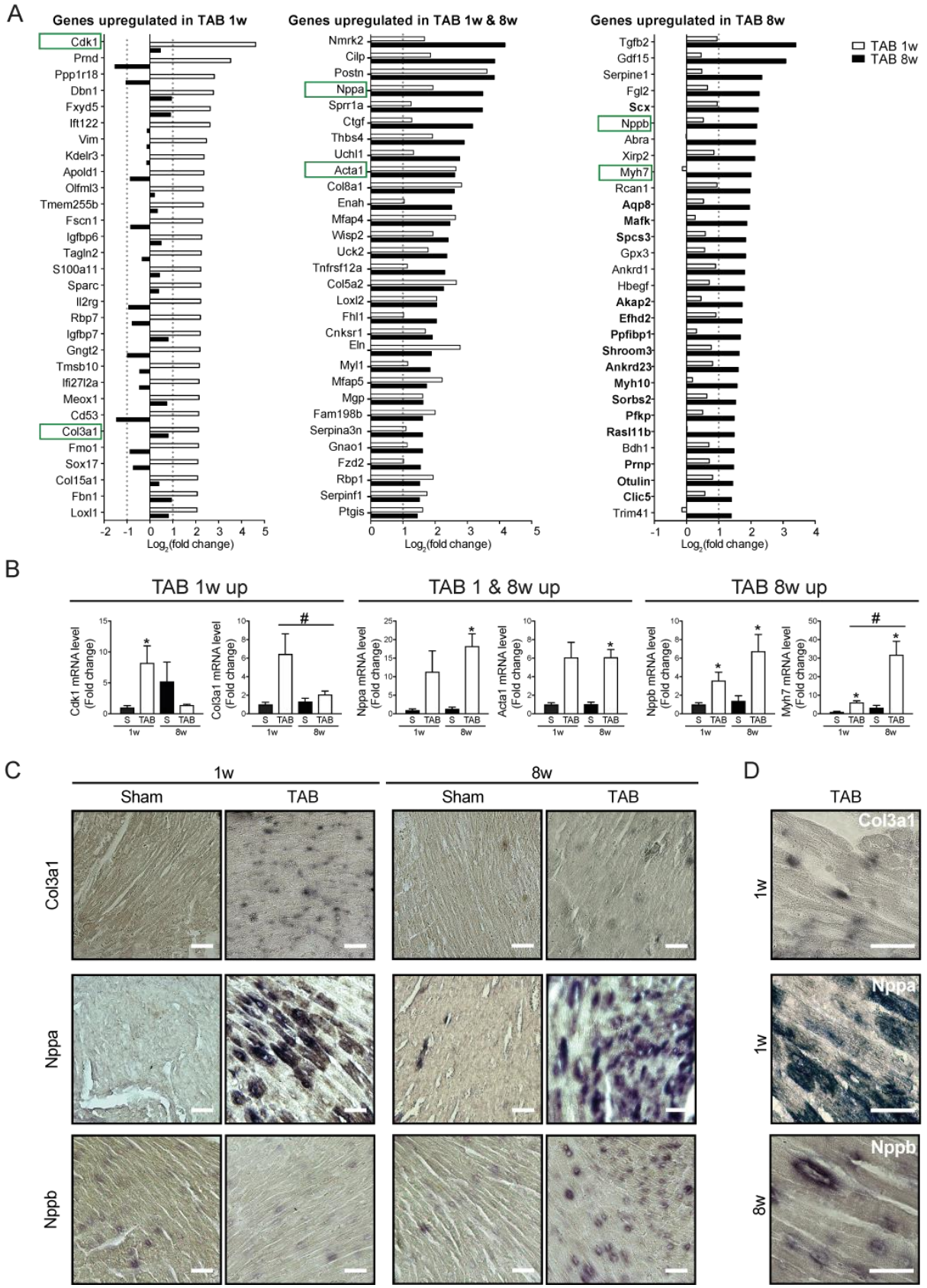

Figure 3. **Known cardiac stress markers are differentially regulated in hypertrophic and failing CMs. A,** Top 30 differentially upregulated genes in CMs from TAB 1w (left panel TAB 1w and TAB 8w (middle panel) and TAB 8w (right panel) compared to corresponding control. **B,** Real-time PCR on sorted CMs of differentially upregulated cardiac stress markers (n=3). **C**, In situ hybridization analysis for *Col3a1* (upper panels), *Nppa* (middle panels) or

Nppb (lower panels) mRNA. Scale bars represent 200µm. **D**, Larger inset of representative images in C showing CMs expressing *Col3a1* (upper panel), *Nppa* (middle panel) or *Nppb* (lower panel), respectively. Scale bars represent 50µm. Data expressed as mean fold change ± SEM; * indicates p<0.05 compared to control (S) and # indicates p<0.05 compared to TAB1w in a One-way ANOVA or unpaired t-test (n=3).

likely due to the relative immaturity of the hiPSC-CMs. Having established the stress response after stimulation, we next investigated the expression of the genes that were found to be up-regulated in failing mouse CMs and found eight of them to be significantly up-regulated in stressed hiPS-CMs and two were undetectable (**Figure 4F**). These data indicate that the failing gene expression programme is partly recapitulated in stressed hiPSC-CMs and suggest conservation of this response between mouse and human CMs.

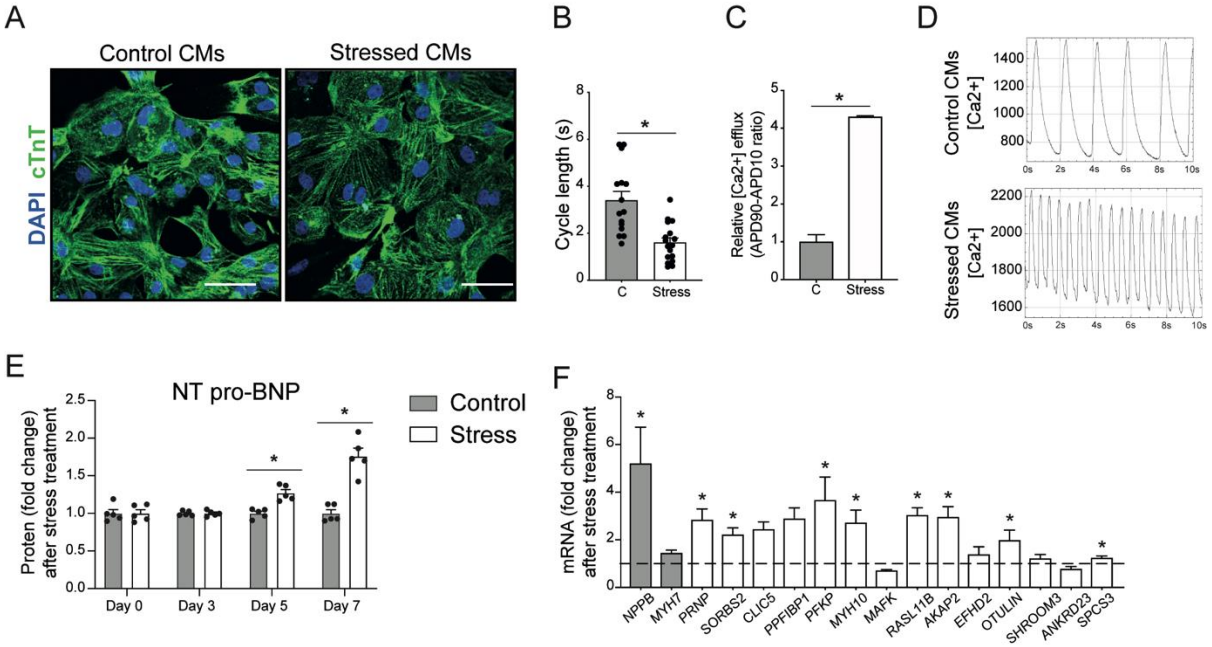

Figure 4. Failure-induced genes are increased in stressed human iPS-derived CMs. A, Representative images of hiPS-CMs in control conditions or after NE and AngII treatment. Immunofluorescence for cardiac troponin T (cTnnT) and nuclei DAPI**. B,** Calcium transient analysis of the frequency of spontaneous calcium transients and **C,** Calcium transient analysis of the calcium reuptake (left panel) and release (right panel) of control (C) or NE/Ang II treated (Stress) CMs (n=15-18 cells). **D,** Representative spontaneous calcium transients in control (left) and stressed (right) iPS- derived CMs. **E,** Real-time PCR analysis of stress markers and the newly identified genes on NE-AngII treated CMs (n=3-9). Data expressed as mean fold change ± SEM; * indicates p<0.05 compared to control (C) with unpaired t-test.

Increased expression of the failure-induced genes in human end-stage HF

remodelling were also differentially regulated in human failing hearts. To this end, we collected left ventricular biopsies from explanted hearts of patients presenting end-stage HF and non-failing donors. The selected patients presented a decline in cardiac function (**Figure 5A**), as well as an up-regulation of the failure markers *NPPB* and *MYH7* (**Figure 5B)** in accordance with our findings in sorted failing mouse CMs (**Figure 3A**). RNA sequencing analysis of these hearts revealed transcriptomic clustering for most of the HF samples and a good separation between healthy control and patient samples

(**Figure 5C).** The candidate genes induced during maladaptive remodelling presented heterogeneous expression levels between different patients, possibly due to different cell compositions of the tissue samples **(Figure 5D**). However, six candidate genes were significantly up-regulated in human HF (**Figure 5E**). These genes were the platelet isoform of phosphofructokinase (*PFKP*), prion protein (*PRNP*), sorbin and SH3 domain-containing protein 2 (*SORBS2*), myosin heavy chain 10 (*MYH10*), MAF BZIP transcription factor K (*MAFK*) and RAS like family 11 member B (*RASL11b*). Notably, except for *MAFK*, all these genes were also up-regulated in stressed hiPSC-CM (**Figure 4F**). To further examine the association of these genes with HF, we performed correlation analysis to *NPPB* and *MYH7*expression. *NPPB* expression was positively correlated to *PFKP*, *RASL11B*, *MAFK*, and *MYH10* (**Figure 5F**), while *MYH7* was positively correlated to *SORBS2*, *PRNP*, and *MYH10* (**Figure 5G**). Altogether, these results demonstrate that the induction of *PFKP*, *PRNP*, *SORBS2*, *MYH10*, MAFK, and *RASL11B* in CMs showing pathological hypertrophy is conserved between human and mouse and correlates to the expression of known markers of cardiac failure.

PFKP protein is upregulated in human failing hearts and involved in cardiomyocyte remodeling

As *PFKP* is a rate-limiting enzyme of glycolysis,[26] and there being a shift in metabolism during HF, we wanted to investigate the relevance of PFKP during CM failure in greater detail. To validate PFKP expression at protein level, we performed immunohistochemistry in human failing hearts. PFKP expression was induced in a subset of CMs in explanted hearts from patients with dilated cardiomyopathy, hypertrophic cardiomyopathy, and ischaemic heart disease (**Figure 6A).** Next, to further validate the RNA sequencing results of *Pfkp*expression on mouse isolated CMs, we performed real-time PCR analysis. We could confirm a higher *Pfkp* mRNA level in CMs showing pathological remodelling compared to sham, whereas this was not observed in hypertrophic CMs compared to sham (**Figure 6B**). Interestingly, no differential expression was found in the real-time results on full mouse heart tissue (**Figure 6C**), probably due to the high expression of this isoform in other cell types of the heart.

In addition to the platelet isoform, there are two other known *PFK* isoforms in mammals: the muscle isoform *PFKM*, and the liver isoform *PFKL.*[26] To determine if the differential regulation in failing CMs is specific for the platelet isoform, we analysed the expression of the liver and muscle isoforms in mouse and human samples. RNA-Seq analysis indicated that *Pfkm* and *Pfkl* were not differentially regulated in failing mouse CMs when compared to sham (**Figure 6D).** Moreover, *PFKP* was significantly up-regulated in human failing hearts compared to control, whereas the other isoforms *PFKM* and *PFKL* were not significantly changed (**Figure 6E**). Similarly, *PFKP* was also the only

isoform up-regulated in hiPS-CMs after NE/AngII treatment (**Figure 6F).** Taken together, these results provide strong support for a conserved mechanism that leads to the up-regulation of the platelet isoform of PFK in response to pathological remodelling in CM.

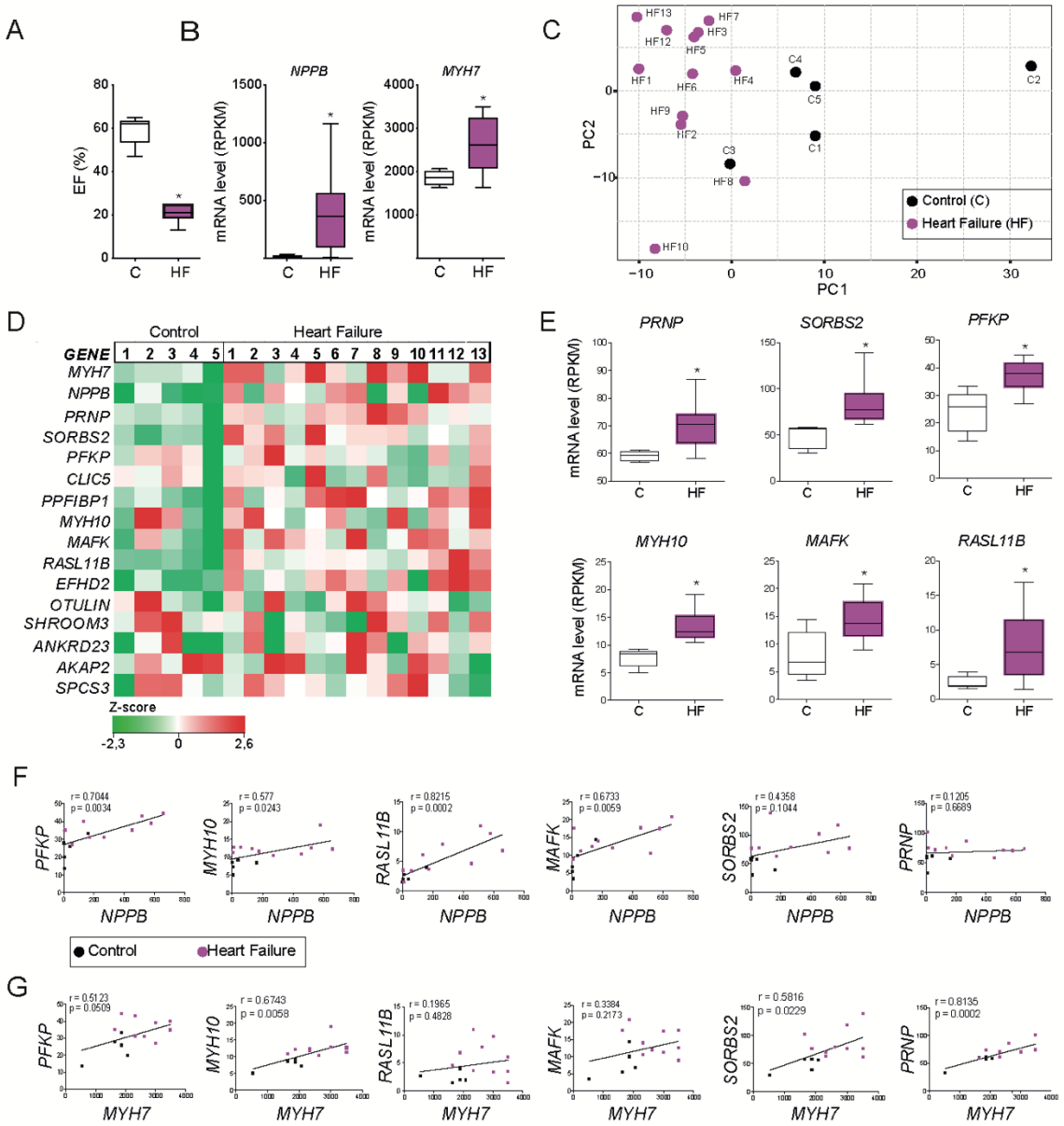

Figure 5. Failure-induced gene expression in human heart failure. A, Average percentage ejection fraction (EF %) in non-failing controls (C) and heart failure patients (HF). **B,** Expression analysis of cardiac failure markers *NPPB* and *MYH7* from control and diseased hearts. RPKM: reads per kilobase million. **C,** Unsupervised principal component analysis (PCA) plot. Each dot represents an expression profile of an individual sample plotted by PCA score showing diseased hearts cluster together and are distinct from controls. **D,** Gene expression map representing the expression of *MYH7* and *NPPB* and 14 novel genes identified in the failing CMs, in control and disease hearts. **E,** RPKM levels of six novel genes showing a significant upregulation in disease hearts (HF) when compared to control (C). **F,** Correlation between the cardiac failure marker *NPPB* and the 6 significantly upregulated genes identified in E. **G,** Correlation between the cardiac failure marker *MYH7* and the 6 significantly upregulated genes identified in E. Spearman r values and p-values are shown in the graphs. Data expressed as mean ± SEM or mean fold change ± SEM; * indicates $p<0.05$ compared to control in an unpaired t-test (n=5-13).

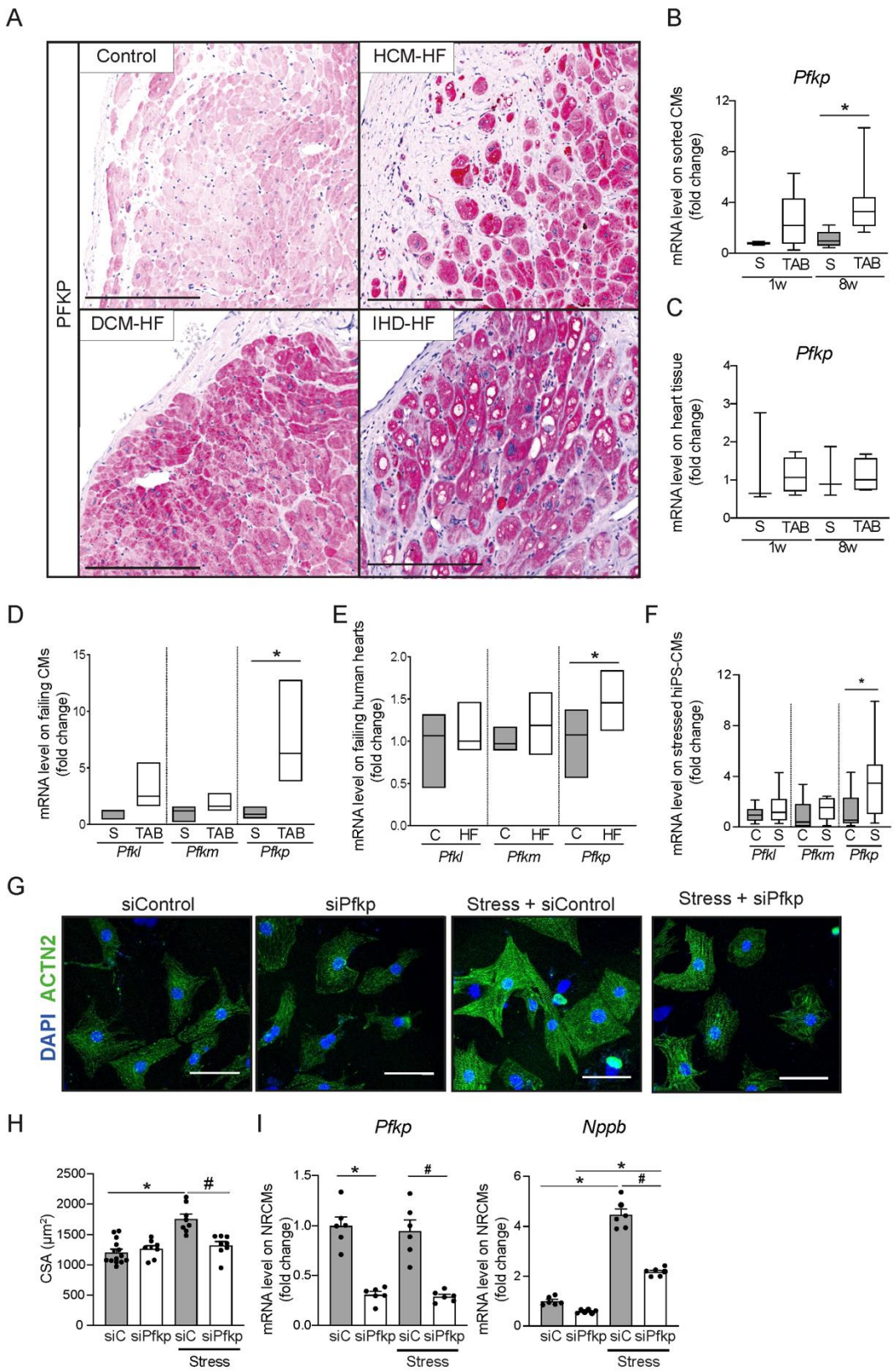

Figure 6. PFKP is expressed in human failing CMs. A, Immunohistochemistry of PFKP in healthy and HF dilated cardiomyopathy (DCM-HF), hypertrophic cardiomyopathy (HCM-HF) and ischemic heart disease (IHD-HF). **B**, Real-time PCR of *PFKP* on mouse sorted CMs (n=3) on sham (S) or TAB conditions. **C**, Real-time PCR of *PFKP* on mouse heart tissue (n=4-7) on sham (S) or TAB conditions. **D**, Expression analysis of *PFK* isoforms *PFKM* (Phosphofructokinase- muscle) and *PFKL* (Phosphofructokinase-liver) from RNA sequencing of mouse sorted CMs (n=3). **E**, Expression analysis of *PFK* isoforms *PFKM* (Phosphofructokinase- muscle) and *PFKL*

CMs (n=3). **E**, Expression analysis of *PFK* isoforms *PFKM* (Phosphofructokinase- muscle) and *PFKL* (Phosphofructokinase-liver) from RNA sequencing of human failing hearts (n=5-13). **F**, Real-time PCR of *PFK*-isoforms on NE/AngII treated hiPS- derived CMs (n=6-9). **G,** Representative images of PE-treated NRCMs transfected with scramble siRNA control or *Pfkp* siRNA. Immunofluorescence for sarcomeric α actinin (ACTN2) and nuclei DAPI. **H,** Cardiomyocyte cross sectional area (CSA) quantification (n=>50), and **I,** Real-time PCR analysis of the cardiac stress markers *Nppb* and *Pfkp* of PE-treated NRCMs transfected with *Pfkp* siRNA (siPFKP) or scrambled siRNA control (si-C) (n=5-6). Data expressed as mean fold change ± SEM; * indicates p<0.05 compared to control (C) or sham (S) and # indicates p<0.05 compared to siRNA control-stressed (siC-Stress) in a One-way ANOVA or unpaired t-test.

To investigate whether *PFKP* is functionally involved in CM failure, we used NRCMs as they are a well-established model to induce hypertrophy upon pharmacological stimulation and also present efficient gene silencing results.[27,28] To induce stress in NRCMs, we exposed the cells with 10 µm Phenylephrine (PE). This led to an increase in CM cell size (**Figure 6G and H**) and induction of the failure marker *Nppb* (**Figure 6I**), indicating a strong stress response. Next, *Pfkp* gene silencing using small interfering RNAs (siRNA) efficiently reduced *Pfkp* mRNA expression with more than 70% in control and stress conditions (**Figure 6I).** *Pfkp* inhibition blocked the hypertrophic response and *Nppb* expression (**Figure 6H and I**), indicating a functional link between *Pfkp* up-regulation and CM stress. Collectively, we identified *PFKP* as the stress-induced PFK isoform that may reinforce the metabolic switch towards glycolysis during pathological remodelling of CM and its suppression may be beneficial for blocking the progression towards cardiomyocyte failure.

Discussion

In this study, we identified gene programmes specific to hypertrophic CMs and CMs showing signs of pathological remodelling. Our data demonstrate that using flow sorting and deep sequencing of healthy and diseased CM populations allows for the identification of known and novel marker genes for disease, which would not be necessarily revealed by RNA sequencing on tissue. The relevance of the novel genes for pathological CMs is supported by the observations that (i) the majority of genes identified in pathological mouse CMs was also up-regulated in failing human CMs, (ii) multiple candidate genes are found to be up-regulated in human HF samples, and (iii) expression of these genes positively correlated to known markers of cardiac failure, like *NPPB* and *MYH7*, in human failing hearts. Using this approach, we were able to identify and confirm *PFKP* as the failure-induced isoform of PFK. Furthermore, inhibition of *Pfkp* blocked CM remodelling and *Nppb* expression, suggesting that PFKP is involved in the CM stress response.

We show that hypertrophic CMs and CMs showing signs of pathological remodelling differ widely in gene expression with more up-regulated genes in the hypertrophic cells and more down-regulated

genes in the more diseased CMs. These results imply an active response of many pathways during the primary, compensatory response to overcome the initial stress and support cell growth. This is consistent with a previous study of single CM sequencing showing an increase of regulated genes during hypertrophy.[29] Additionally, the genes that are significantly induced during the maladaptive phase, already show an early, less pronounced activation during the hypertrophic stage. This suggests that the pathological gene programme is already slightly activated during the compensatory phase, and becomes more pronounced during failure, but is initially still overridden by the early hypertrophic gene programme. Based on our results, we propose that these failure-induced genes are potential therapeutic targets, as inhibition strategies at earlier phases could block or reduce disease progression. In the failing CMs we also found almost all mitochondrial genes down-regulated, corroborating transcriptional regulation of the decline in mitochondrial biogenesis during pathological remodelling.[5]

Another observation that our CM-specific sequencing data allowed us to make, is that stress markers that have been linked to other cell types, like *Col3a1,* are also expressed in CMs, but at a significant lower level when compared with fibroblasts. The function of *Col3a1* expression in CMs has not been studied, however, its up-regulation is in accordance with studies showing that multiple ECM genes expressed in fibroblasts are also expressed in CMs and regulated during stress.[21,22] Furthermore, it was recently shown that fibrosis-like conditions can induce collagen gene expression in human iPS-CMs.[30] Taken together, these observations further reinforce the relevance of cell-specific sequencing to identify meaningful factors in disease development.

Our study identified five new genes that could be linked to pathological remodelling in both mouse and human CMs. While they might have a known cardiac role, they have so far not been functionally linked to pathological hypertrophy. For instance, structural protein MYH10 is the only non-muscle myosin expressed in the heart.[31] MYH10 is required for normal heart development, as loss of MYH10 in CMs during embryogenesis led to HF.[31]However, the role of MYH10 in adult CMs has not been reported, and the relevance of its up-regulation in HF requires further functional studies. Another structural protein is SORBS2. It is considered an adapter protein involved in cytoskeleton organization, myofibril assembly and z-band signalling and it is highly expressed in CMs.[32] Its up-regulation in pathological hypertrophy might be involved with the structural changes occurring in failing CMs, but this for now remains speculative. Moreover, RASL11B is a small GTPase protein with pro-apoptotic functions in cancer cells.[33] No role has been reported in CMs but we could hypothesize a similar function considering it is overexpressed in myocytes that might be at risk of apoptosis. PRNP is a membrane glycoprotein associated to pathogenesis on muscle and nervous system when overexpressed.[34] PRNP overexpression in mice led to muscle degradation with aging due to autophagy

activation.[34] These results suggest a detrimental effect of PRNP induction in failing CMs. Finally, PFKP is the platelet isoform of PFK, a glycolytic enzyme catalyzing one of the key regulatory and rate-limiting steps of glycolysis.

PFKP was selected for further study due to its function as a limiting enzyme in glycolysis. The failing heart is characterized by an increase in glucose uptake and glycolytic rates but not by an increase in glucose oxidation.[4] *PFK* activity is increased, enhancing the glucose flux into glycolysis and forming pyruvate and lactate which at elevated levels lead to contractile dysfunction.[4] In a meta-analysis of human, mouse, rat, and dog microarray datasets, *PFKP* was found associated with HF.[35] Those findings are in line with our finding that *PFKP*induction in failing CMs is conserved between mouse and humans. Recent studies in cancer have linked the up-regulation of *PFKP* with increased glycolysis and tumourigenesis of the cancer cells by the activation of AKT.[36] This suggests that the up-regulation of *PFKP* in cancer cells, as in CMs, is stressed-induced and may have an important role in disease development. Accordingly, our data indicate that *PFKP* inhibition reduces stress responses in pathological CMs. For future targeted therapies, it is relevant to identify the molecular mechanisms behind *PFKP* overexpression in failing CMs along with the impact of *PFKP* inhibition on HF development.

While follow up analysis indicates the validity of our findings, using flow cytometry to isolate CMs may come with some limitations. There is a variation between sorts and the possibility that the sorted fraction is influenced by disease changing cell morphology and composition. For these reasons, it is key that findings are confirmed by additional studies, like the cell-based assays and immunohistochemistry used in our studies. In addition, to reduce age-related changes, we included proper sham controls at each timepoint.

To model aspects of CM failure *in vitro* we used NE/AngII to stress hiPS-CMs, which impaired calcium transients and induced expression of *NPPB*. However, the relatively immature phenotype of hiPSC-CMs makes it difficult to assess how well this resembles a truly failing CM. The same issue is partially true for neonatal CMs, although to a lesser extent. Advances in tissue engineering, maturation and disease modelling will help for improving these cell-based assays to better mimic the adult diseased conditions.

In summary, our study provides a resource for CM-specific genes related to hypertrophy pathological remodelling that might be relevant for the different stages of disease. Our data also show that PFKP is functionally involved in CM failure and remodelling. Using these data for follow-up functional studies might further reveal biological implications of the newly defined genes in the process of CM hypertrophy or maladaptive remodelling and may aid in the development novel therapeutic strategies aimed to reverse cardiac remodelling and reduce HF.

Materials and Methods

Animals

Animal studies were performed according to the guidelines from Directive 2010/63/EU of the European Parliament on the protection of animals used for scientific purposes. Animal experiments were approved by the institutional guidelines and regulations of the Animal Welfare Committee of the Royal Netherlands Academy of Arts and Sciences (HI 13.2304, AVD8011002015250 16.2305/IVD366) and following the guide for the care and use of laboratory animals.

To generate cardiomyocyte specific tdTomato expressing mouse, *Rosa26-tdTomato* reporter mice (*R26R*^{TdT}, TdTomato expression driven by Rosa26 promoter; bred on a C57/BL6N background) (10) were crossed with *Myh6-Cre* transgenic mice (*Myh6*^{cre}; a generous gift from Jeffery Molkentin, Cincinnati Children's Hospital Medical Center).

Digestion of the mouse heart and cardiomyocyte sorting

Perfused hearts were used for digestion. After perfusing the heart, the ventricles were collected and the tissue was minced into fine pieces using a scalpel and transferred into a glass vial with 1,5ml of cold digestion buffer. The tissues were digested using a gently shaking (100rpm) 37°C water-bath for 15 min. The obtained cell suspension was gently pipetted up and down (10x) and transferred onto a 100μm cell strainer placed on top of a 50ml falcon tube. The cell pellet was suspended in 2-3ml of DMEM with DAPI 1:1000 for cell sorting using a FACS Aria SORP (BD bioscience (9). Living single cells were sorted based on multiple scatter strategies. Forward scatter and side scatter area (FSC-Area and SSC-Area) were selected for cells that were DAPI negative, tdTomato fluorescent in 640 and 561 nm and auto-fluorescent in 488 and 460, considering that living heart cells are brighter in those channels. Next, based on FSC-Height and FSC-Area we selected for single cells and excluded cell debris. Finally, by using FSC-Width we were able to pick more elongated cells. Cells were sorted into Eppendorf tubes containing TRIzol and frozen down at -80°C.

RNA sequencing of sorted CMs

For sorted cells bulk sequencing, CELseq1 (11) preparation was done using the MessageAMP II aRNA amplification kit (ThermoFisher Scientific) until IVT step. Final library preparation was continued according to the CELseq2 manual.

RNA isolation and quality control

To isolate RNA, we used TRIzol® reagent (Life Technologies) following the manufacturer's instructions. To assess the RNA quality, an aliquot of RNA was diluted to 200-5000pg/μl and put on a bioanalyzer using Agilent RNA 6000 Pico Kit according to the manufacturer's instructions.

Quantitative real-time PCR

Total RNA (1µg) was applied to mRNA based reverse transcription using an iScript cDNA Synthesis Kit (Bio-Rad). Real-time PCR was performed according to based SYBRgreen methodology (Bio-Rad). Transcript quantities were normalized for endogenous loading.

Histology and microscopy

Adult hearts were excised from euthanized mice, washed in cold PBS and fixed with 4% formalin at room temperature for 48h, embedded in paraffin and sectioned at 4µm. Cultured CMs on cover-slips were washed with PBS and fixed with 4% formaldehyde at room temperature for 20 minutes. Hematoxylin and eosin (H&E) and picrosirius red (SR) staining were used following standard procedures. Fluorescein isothiocyanate (FITC) labeled Wheat Germ Agglutinin (WGA) lectin (100 µg/ml final concentration, Sigma-Aldrich, L4895). For immunohistochemistry, sections were put to heat-induced antigen retrieval and blocking with 1% BSA. The sections were incubated with specific primary antibodies ON at 4°C. After washing with PBS, the sections were incubated with secondary antibodies for 1 hour at RT, washed and sealed with a mounting medium containing DAPI (Vector Laboratories). Cultured CMs on cover-slips were incubated with Blocking buffer with 1% Fish gelatin and incubated with specific primary antibody 25 minutes at RT. After washing with blocking buffer, the cover-slips were incubated with secondary antibodies for 25 minutes at RT, washed with MQ water and sealed with a mounting medium containing DAPI. For in situ hybridization, the probes were generated as described before (12). Primers used for partial coding sequence amplification can be found in online supplementary Table S4. Amplified sequences were ligated into pSPT18 vectors (Roche). Mouse heart paraffin embedded sections of 8 um mounted on Starfrost slides were used for ISH.

Human Heart Samples

Approval for human tissue samples was obtained from the Medical Ethics Committee of the University Medical Center Utrecht, The Netherlands (12#387). The study met the criteria of the code of conduct for responsible use of human tissue in the Netherlands and conforming the principles outlined in the Declaration of Helinki. Collection of the human heart tissue was approved by the scientific advisory board of the biobank of University Medical Center Utrecht, Utrecht, the Netherlands (protocol no. 12/387). Written informed consent was obtained or in certain cases waived by the ethics committee when not possible due to death of the patient. We included tissue from the left ventricular free wall or septum from explanted hearts of patients with heart failure and left ventricular free wall of nonfailing donor hearts that were not used for transplantation.

Human RNA sequencing

RNA was isolated using ISOLATE II RNA Mini Kit (Bioline) according to the manufacturers' instructions with minor adjustments

Human induced pluripotent stem cell (hiPSC)-derived cardiomyocytes

The *LUMC0099iCTRL04* hiPSCs were used to generate CMs using defined medium with timed addition of growth factors and small molecules as described previously (13). hiPSCs were plated at a density of 50,000 cell/cm^2 three days prior to differentiation to allow for attachment to the Geltrex (Gibco) coated cell-culture plates. To enrich for CMs, purification was done for 4 days using selection medium. Differentiation efficiency was determined by flow cytometry for cardiac troponin T (cTnT) expression, using an antibody directed to cTnT (1:1000 ab45932, Abcam). CMs were dissociated after selection and reseeded in a density of 400,000 cells/cm^2 on Geltrex coated cell-culture plates.

hiPSC-CMs NE/ Angiotensin II stimulation

CMs were dissociated and seeded at a cell density of 1 million cells per well in a Geltrex coated 6-well plate for RNA analysis or with a cell density of 50.000 cells per well on a Geltrex coated cover-slip in a 24-well plate for immunofluorescence or calcium transient analysis. CMs were exposed to culture medium with or without addition of 10μM final concentration L-Norepinephrine (NE, Sigma-Aldrich) and 1μM final concentration of Angiotensin II (AngII, Sigma-Aldrich) to induce control and stress conditions for 7 days. The medium was refreshed every 48h.

Intracellular calcium transients

hiPSC-CMs plated on glass coverslips were loaded for 15 min with Fluo-4 AM 0.2 mM (Invitrogen). Fluorescent signals were acquired using a custom build upright microscope. Line-scan images were acquired at the sampling rate of 1 ms per line and 10 seconds were imaged using a high-speed camera (Andor Zyla 4.2 plus sCMOS). Cells were recorded at 37°C in Tyrode's solution). The recordings were all baseline measurements using software Micro-Manager, version 1.4.23, along with ImageJ. Following background subtractions, data were analyzed with a custom-written program within MATLAB (Peaks, T.P. de Boer).

Primary cardiomyocyte culture

Neonatal rat ventricular CMs (NRCMs) were isolated by enzymatic dissociation of 1-2-day old neonatal rat hearts. To increase the purity of the cardiomyocyte culture, the cells were carefully separated from the non-cardiomyocyte fraction by differential plating. Pure CMs were plated on 6-well plates (1 million cells per well) or 24-well plate (125.000 cells per well).

NRCMs β-adrenergic stimulation

CMs were exposed to culture medium with or without addition of 10μM final concentration of Phenylephrine (PE, Sigma-Aldrich) for 24h to induce control or stress conditions.

Transfection of CMs with siRNA Oligo duplexes

The 27-nucleotide siRNA duplexes were synthesized and purified by OriGene. The transfection was performed with 10μmol of siRNA and Lipofectamine 2000 (Invitrogen) according to manufacturer's instructions. The siRNA control used was the Universal-scrambled negative control from OriGene.

Statistical analysis

Values are presented as mean ± SEM. Outliers were identified and excluded using a ROUT test (GraphPad, using Q=1%). Statistical significance was evaluated using an unpaired *t*-test for comparisons between two groups or one-way ANOVA for comparison of several groups. Analyses were performed using the GraphPad Prism Version 8.0 software. * indicates $p < 0.05$ and was considered statistically significant compared to control.

AUTHOR CONTRIBUTION

Conception and design of the research: M.V.G., C.D., M.G., T.V., C.B., E.V.R.; acquisition of data: M.V.G., C.D., D.V., H.R., I.P., L.K., F.A., A.V., .M.H., A.B.; analysis and interpretation of the data: M.V.G., C.D., J.E., A.V., M.H., A.B., T.V., C.B., E.V.R.; statistical analysis: M.V.G., C.D., J.E., M.H.; supervising the experiments: M.G., T.V., C.B., E.V.R.; drafting the manuscript: M.V.G., C.D., C.B., E.V.R.; critical revision of the manuscript for important intellectual content: J.E., F.A., A.V., M.H., T.V.

ACKNOWLEDGEMENTS

We would like to thank Anko de Graaff and the Hubrecht Imaging Center for supporting the imaging. We gratefully acknowledge Jeroen Korving for help with histology. We thank Stefan van der Elst and the Hubrecht FACS facility for help with sorting cells and Judith Vivié for help with library preparation. We thank Petra van der Kraak, Joyce van Kuik and Erica Sierra-de Koning for technical support with the immunostainings of the human tissue. We thank Michal Mokry (Epigenomic facility UMC Utrecht) and the Utrecht Sequencing Facility for support in processing human RNA-seq data.

REFERENCES

1. Braunwald E. The war against heart failure: the Lancet lecture. Lancet 2015;385:812–824.
2. Burchfield JS, Xie M, Hill JA. Pathological ventricular remodeling: mechanisms: part 1 of 2. Circulation 2013;128:388–400.
3. Fountoulaki K, Dagres N, Iliodromitis EK. Cellular Communications in the Heart. . Card Fail Rev 2015;1:64–68. .
4. Bertero E, Maack C. Metabolic remodelling in heart failure. Nat Rev Cardiol 2018;15: . 457–470. .
5. Rosca MG, Hoppel CL. Mitochondria in heart failure. Cardiovasc Res 2010;88:40–50. .
6. Liu Y, Morley M, Brandimarto J, Hannenhalli S, Hu Y, Ashley EA, Tang WH, Moravec . CS, Margulies KB, Cappola TP, Li M; MAGNet consortium. RNA-Seq identifies novel . myocardial gene expression signatures of heart failure. Genomics 2015;105:83–89. .
7. el Azzouzi H, van Oort RJ, van der Nagel R, Sluiter W, Bergmann MW, De Windt LJ. . MEF2 transcriptional activity maintains mitochondrial adaptation in cardiac pressure . overload. Eur J Heart Fail 2010;12:4–12. .

8. Koentges C, Pepin ME, Musse C, Pfeil K, Alvarez SVV, Hoppe N, Hoffmann MM, . Odening KE, Sossalla S, Zirlik A, Hein L, Bode C, Wende AR, Bugger H. Gene ex- . pression analysis to identify mechanisms underlying heart failure susceptibility in mice . and humans. Basic Res Cardiol 2018;113:8. .
9. Gladka MM, Molenaar B, de Ruiter H, van der Elst S, Tsui H, Versteeg D, Lacraz . GPA, Huibers MMH, van Oudenaarden A, van Rooij E. Single-cell sequencing of the . healthy and diseased heart reveals cytoskeleton-associated protein 4 as a new modulator of fibroblasts activation. Circulation 2018;138:166–180
10. Madisen L, Zwingman TA, Sunkin SM, Oh SW, Zariwala HA, Gu H, Ng LL, Palmiter RD, Hawrylycz MJ, Jones AR, Lein ES, Zeng HA. robust and high-throughput Cre reporting and characterization system for the whole mouse brain. Nat Neurosci 2010; 13:133–140.
11. Hashimshony T, Senderovich N, Avital G, Klochendler A, de Leeuw Y, Anavy L, Gennert D, Li S, Livak KJ, Rozenblatt-Rosen O, Dor Y, Regev A, Yanai I. CEL-Seq2: sensitive highly-multiplexed single-cell RNA-Seq. Genome Biol 2016;17:77.
12. Lacraz GPA, Junker JP, Gladka MM, Molenaar B, Scholman KT, Vigil-Garcia M, Versteeg D, de Ruiter H, Vermunt MW, Creyghton MP, Huibers MMH, de Jonge N, van Oudenaarden A, van Rooij E. Tomo-Seq identifies SOX9 as a key regulator of cardiac fibrosis during ischemic injury. Circulation 2017;136:1396–1409.
13. Burridge PW, Matsa E, Shukla P, Lin ZC, Churko JM, Ebert AD, Lan F, Diecke S, Huber B, Mordwinkin NM, Plews JR, Abilez OJ, Cui B, Gold JD, Wu JC. Chemically defined generation of human cardiomyocytes. Nat Methods 2014;11:855–860.
14. van Rooij E, Fielitz J, Sutherland LB, Thijssen VL, Crijns HJ, Dimaio MJ, Shelton J, De Windt LJ, Hill JA, Olson EN. Myocyte enhancer factor 2 and class II histone deacety- lases control a gender-specific pathway of cardioprotection mediated by the estro- gen receptor. Circ Res 2010;106:155–165.
15. Gohar A, Rutten FH, Ruijter H, Kelder JC, Haehling S, Anker SD, Mo¨ckel M, Hoes AW. Mid-regional pro-atrial natriuretic peptide for the early detection of non-acute heart failure. Eur J Heart Fail 2019;21:1219–1227.
16. Morkin E. Regulation of myosin heavy chain genes in the heart. Circulation 1993;87: 1451–1460.
17. Harvey PA, Leinwand LA. The cell biology of disease: cellular mechanisms of cardio- myopathy. J Cell Biol 2011;194:355–365.
18. Agah R, Frenkel PA, French BA, Michael LH, Overbeek PA, Schneider MD. Gene re- combination in postmitotic cells. Targeted expression of Cre recombinase provokes cardiac-restricted, site-specific rearrangement in adult ventricular muscle in vivo. J Clin Invest 1997;100:169–179.

19. Chorvat D Jr, Kirchnerova J, Cagalinec M, Smolka J, Mateasik A, Chorvatova A. Spectral unmixing of flavin autofluorescence components in cardiac myocytes. Biophys J 2005;89:L55–L57.
20. Tamamori M, Ito H, Hiroe M, Terada Y, Marumo F, Ikeda MA. Essential roles for G1 cyclin-dependent kinase activity in development of cardiomyocyte hypertrophy. Am J Physiol 1998;275:H2036–H2040.
21. DeLaughter DM, Bick AG, Wakimoto H, McKean D, Gorham JM, Kathiriya IS, Hinson JT, Homsy J, Gray J, Pu W, Bruneau BG, Seidman JG, Seidman CE. Single-cell resolution of temporal gene expression during heart development. Dev Cell 2016;39: 480–490.
22. CuiY,ZhengY,LiuX,YanL,FanX,YongJ,HuY,DongJ,LiQ,WuX,GaoS,LiJ, Wen L, Qiao J, Tang F. Single-cell transcriptome analysis maps the developmental track of the human heart. Cell Rep 2019;26:1934–1950.
23. Eisenhofer G, Friberg P, Rundqvist B, Quyyumi AA, Lambert G, Kaye DM, Kopin IJ, Goldstein DS, Esler MD. Cardiac sympathetic nerve function in congestive heart fail- ure. Circulation 1996;93:1667–1676.
24. Chinnaiyan KM, Alexander D, McCullough PA. Role of angiotensin II in the evolution of diastolic heart failure. J Clin Hypertens (Greenwich) 2005;7:740–747.
25. Verdu JM, Comin-Colet J, Domingo M, Lupon J, Gomez M, Molina L, Casacuberta JM, Munoz MA, Mena A, Bruguera-Cortada J. Rapid point-of-care NT-proBNP optimal cut-off point for heart failure diagnosis in primary care. Rev Esp Cardiol (Engl Ed) 2012;65:613–619.
26. WangJ,ZhangP,ZhongJ,TanM,GeJ,TaoL,LiY,ZhuY,WuL,QiuJ,TongX.The platelet isoform of phosphofructokinase contributes to metabolic reprogramming and maintains cell proliferation in clear cell renal cell carcinoma. Oncotarget 2016;7: 27142–27157.
27. Bass GT, Ryall KA, Katikapalli A, Taylor BE, Dang ST, Acton ST, Saucerman JJ. Automated image analysis identifies signaling pathways regulating distinct signatures of cardiac myocyte hypertrophy. J Mol Cell Cardiol 2012;52:923–930.
28. LaMorte VJ, Thorburn J, Absher D, Spiegel A, Brown JH, Chien KR, Feramisco JR, Knowlton KU. Gq- and ras-dependent pathways mediate hypertrophy of neonatal rat ventricular myocytes following alpha 1-adrenergic stimulation. J Biol Chem 1994; 269:13490–13496.
29. Nomura S, Satoh M, Fujita T, Higo T, Sumida T, Ko T, Yamaguchi T, Tobita T, Naito AT, Ito M, Fujita K, Harada M, Toko H, Kobayashi Y, Ito K, Takimoto E, Akazawa H, Morita H, Aburatani H, Komuro I. Cardiomyocyte gene programs encoding morpho- logical and functional signatures in cardiac hypertrophy and failure. Nat Commun 2018;9:4435.
30. Heras-Bautista CO, Mikhael N, Lam J, Shinde V, Katsen-Globa A, Dieluweit S, Molcanyi M, Uvarov V, Jutten P, Sahito RGA, Mederos-Henry F, Piechot A, Brockmeier K, Hescheler J, Sachinidis A,

Pfannkuche K. Cardiomyocytes facing fibrotic conditions re-express extracellular matrix transcripts. Acta Biomater 2019;89: 180–192.

31. Ma X, Takeda K, Singh A, Yu ZX, Zerfas P, Blount A, Liu C, Towbin JA, Schneider MD, Adelstein RS, Wei Q. Conditional ablation of nonmuscle myosin II-B delineates heart defects in adult mice. Circ Res 2009;105:1102–1109.
32. Bang C, Batkai S, Dangwal S, Gupta SK, Foinquinos A, Holzmann A, Just A, Remke J, Zimmer K, Zeug A, Ponimaskin E, Schmiedl A, Yin X, Mayr M, Halder R, Fischer A, Engelhardt S, Wei Y, Schober A, Fiedler J, Thum T. Cardiac fibroblast-derived microRNA passenger strand-enriched exosomes mediate cardiomyocyte hypertrophy. J Clin Invest 2014;124:2136–2146.
33. He H, Dai J, Zhuo R, Zhao J, Wang H, Sun F, Zhu Y, Xu D. Study on the mechanism behind lncRNA MEG3 affecting clear cell renal cell carcinoma by regulating miR-7/ RASL11B signaling. J Cell Physiol 2018;233:9503–9515.
34. Joshi-Barr S, Bett C, Chiang WC, Trejo M, Goebel HH, Sikorska B, Liberski P, Raeber A, Lin JH, Masliah E, Sigurdson CJ. De novo prion aggregates trigger autoph- agy in skeletal muscle. J Virol 2014;88:2071–2082.
35. Barth AS, Kumordzie A, Frangakis C, Margulies KB, Cappola TP, Tomaselli GF. Reciprocal transcriptional regulation of metabolic and signaling pathways correlates with disease severity in heart failure. Circ Cardiovasc Genet 2011;4:475–483.
36. LeeJH,LiuR,LiJ,ZhangC,WangY,CaiQ,QianX,XiaY,ZhengY,PiaoY,Chen Q, de Groot JF, Jiang T, Lu Z. Stabilization of phosphofructokinase 1 platelet isoform by AKT promotes tumorigenesis. Nat Commun 2017;8:949.

SUPPLEMENTARY MATERIAL

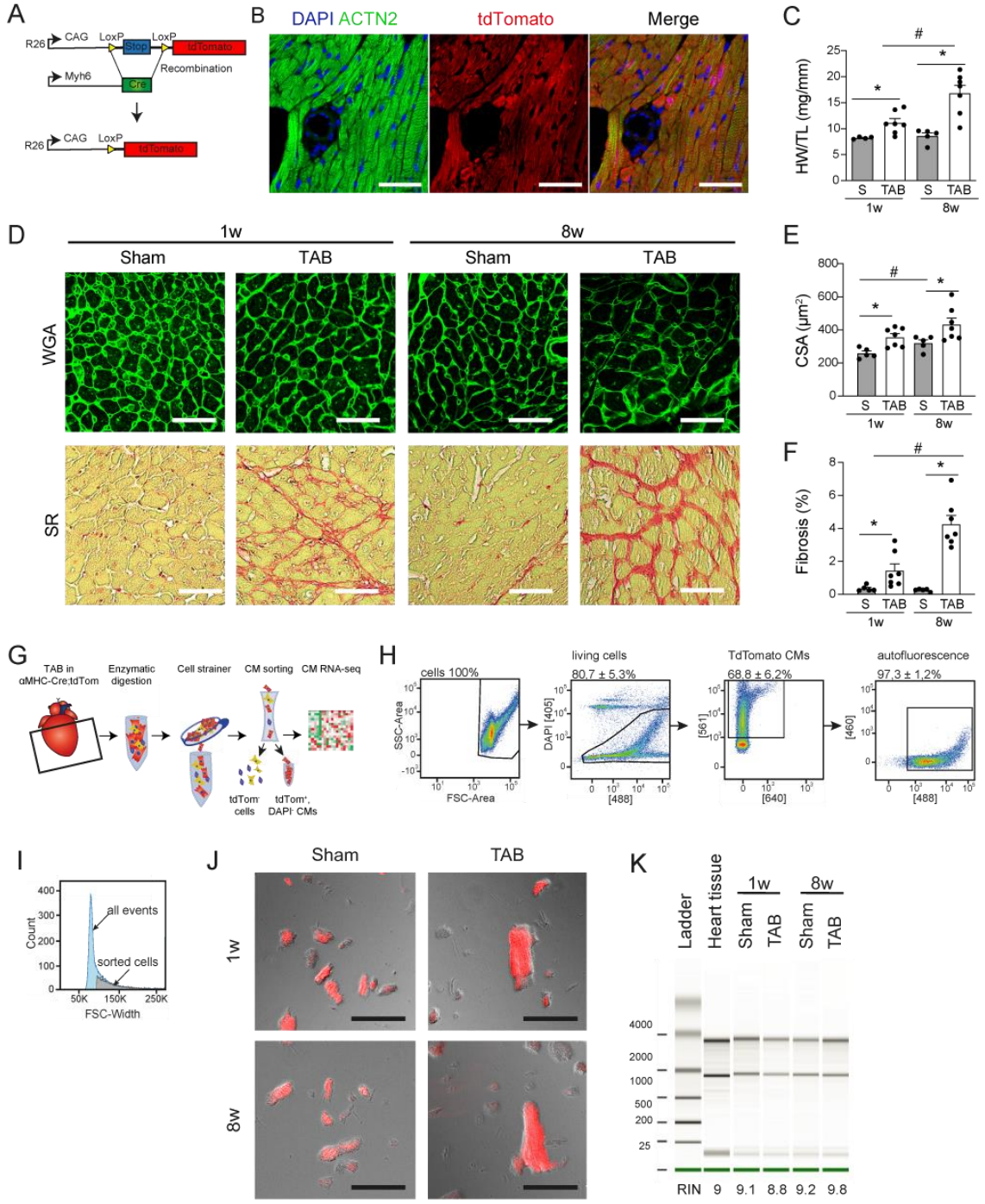

Supplementary Figure 1. Time-course analysis after pressure overload to identify adaptive and pathological hypertrophic stages. A, Schematic of transverse aortic banding (TAB) time-course study. **B**, Aortic pressure gradient determined by echocardiography (n=7-8). **C**, Representative images of H&E, wheat germ agglutinin (WGA, middle row) and Picrosirius red (SR, bottom row) stained cardiac sections. Scale bars represent 200µm or 50µm. **D**, Heart weight to tibia length (HW/TL) ratios (n=7-8). **E**, Quantification of cross-sectional area (CSA) of CMs (~80 cells per animal, n= 3-4 per group). **F**, Quantification of ventricular fibrosis (n=2-4 per group). **G**, Real-time PCR analysis of *Nppa, Myh7, Myh6*, *Col3a1, Pgc1*a and *Pgc1*! on cardiac tissue collected at the indicated timepoints after TAB (n=3-4). Data expressed as mean fold change ±SEM; *indicates p<0.05 compared to sham (S) in a One-way ANOVA or unpaired t-test.

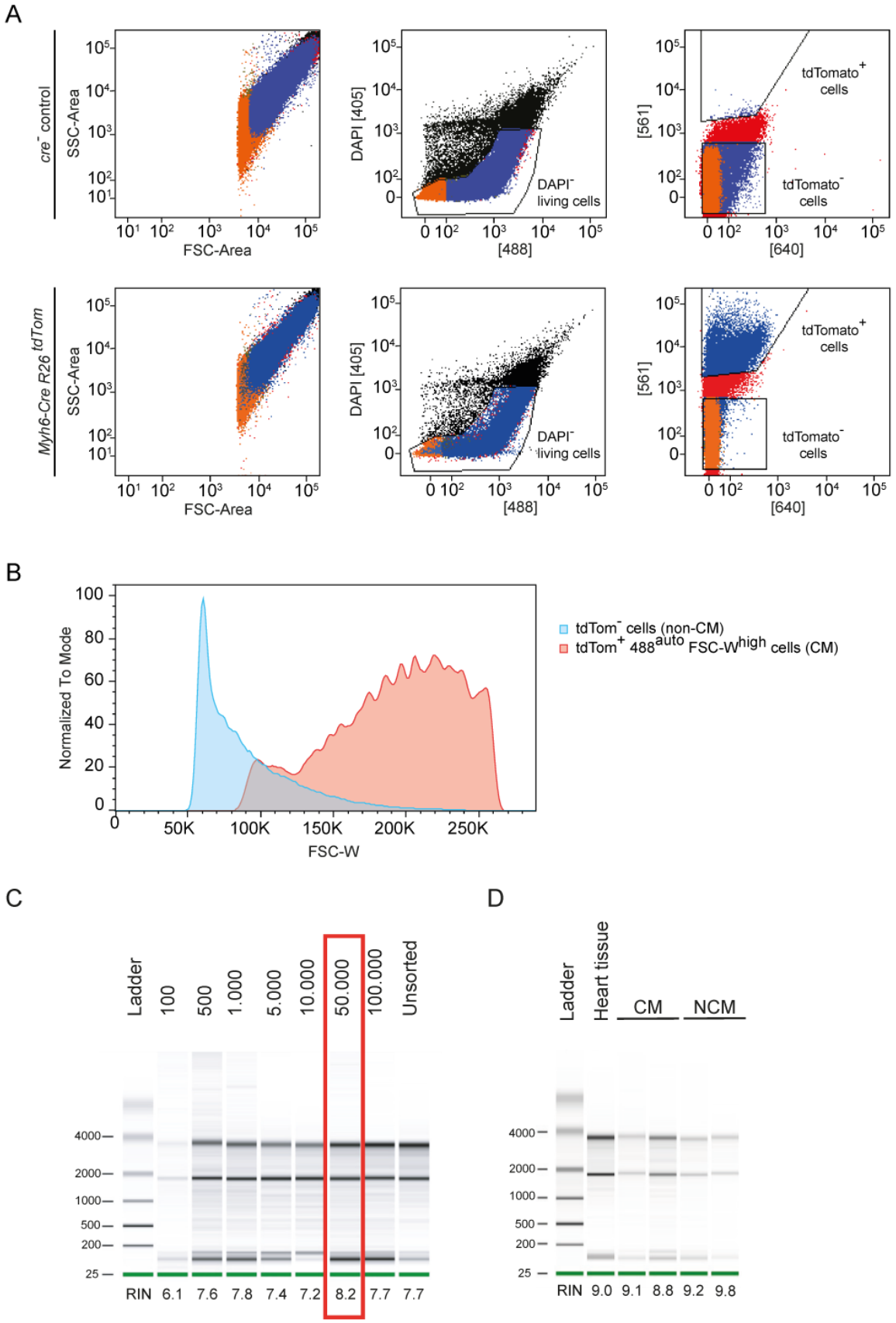

Supplementary Figure 2. Fluorescence-activated cell sorting (FACS) strategy for enriching for CMs and RNA quality from sorted CMs. A, FACS plots showing the gating strategy to distinguish tdTomato positive CMs from

tdTomato negative nonCMs in Cre negative (upper row) and Myh6-Cre;tdTomato positive (lower row) hearts. B, Histogram showing size distribution of sorted CM (DAPI- tdTomato+ 488auto FCSWhigh) and nonCM (DAPI- tdTom-) based on forward scatter width (FSC-W) C, Bioanalyzer plot of RNA isolated from increasing amounts of sorted CMs in Sham conditions, and their respective RNA integrity number stated below. D, Bioanalyzer plot of RNA isolated from 50,000 sorted CMs (CMs) and 50,000 sorted cells that are not selected with the cardiomyocyte gating strategy, mostly non-CMs (NCMs).

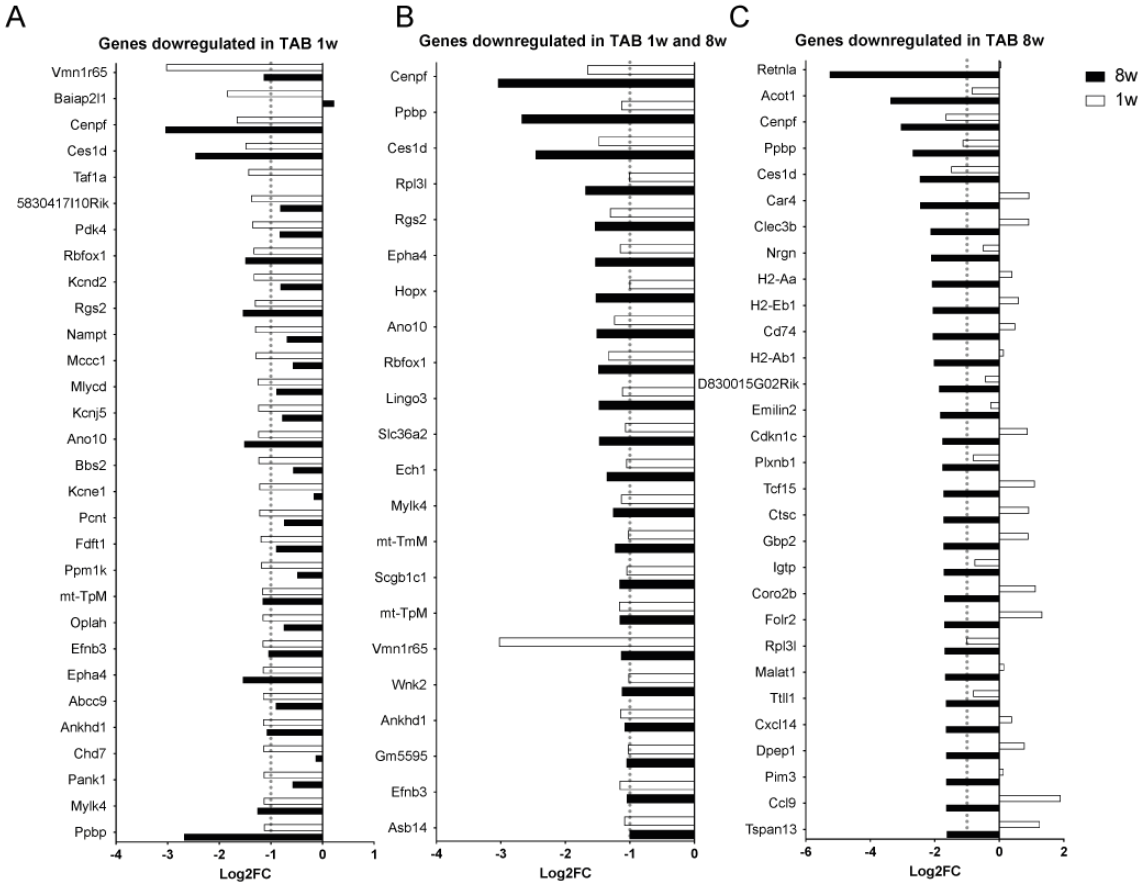

Supplementary Figure 3. Downregulated genes in hypertrophic or pathological CMs. List of genes downregulated in hypertrophic and/or failing CMs. **A,** List of the top 30 downregulated genes in one-week TAB CMs (log2FC > 1). **B,** List of all the genes (22 genes) that are downregulated in one and eight-week TAB CMs (log2FC < -1). **C,** List of the top 30 downregulated genes in eight-week TAB CMs (log2FC > 1).

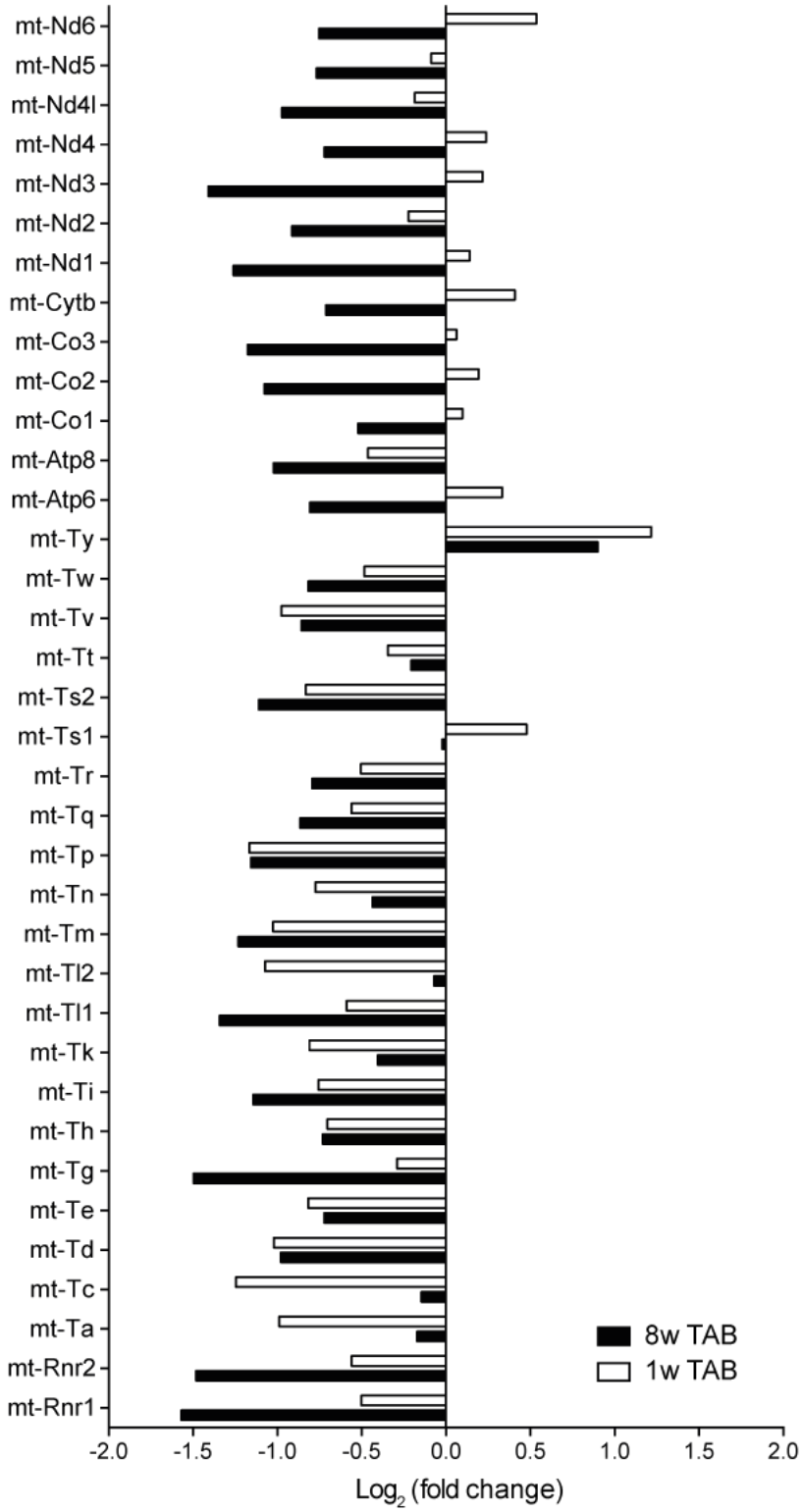

Supplementary Figure 4. List of mitochondrial genes in hypertrophic and pathological CMs. Regulation of all mitochondrial genes detected in one and eight-week TAB CMs.

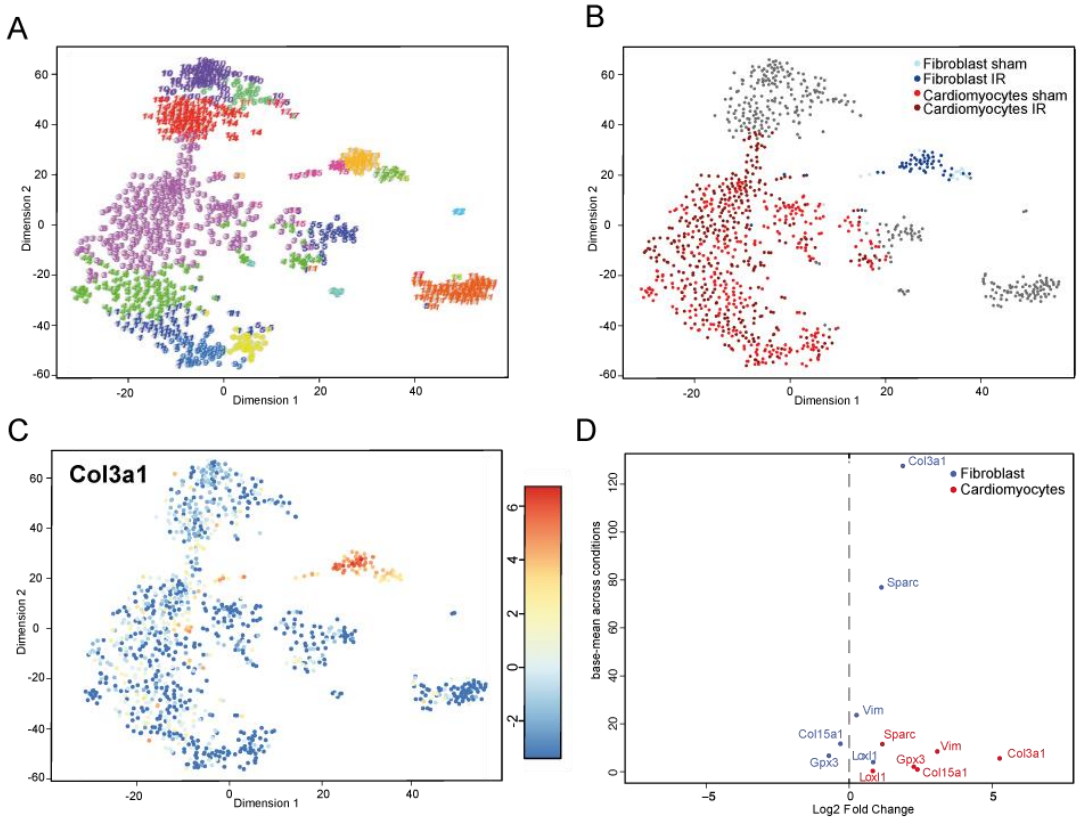

Supplementary Figure 5. Single-cell sequencing analysis on sham and post-IR hearts to identify fibroblast marker changes (n=3). A, t-SNE map indicating transcriptome similarities among all individual cells. Different numbers and colors highlight the different clusters. **B,** t-SNE map indicating the origin of fibroblast and cardiomyocyte population: fibroblasts from sham (light blue) and post-IR (dark blue) hearts, and CMs from sham (light red) and post-IR (dark red) hearts. **C,** t-SNE map indicating the expression of *Col3a1* in cell populations indicated as fibroblasts and CMs. **D,** Scatter plot showing the expression changes of well stablished fibroblast markers in the fibroblast population (blue) and in the cardiomyocyte population (red). Data obtained from single-cell RNA sequencing data set, and differences are based on base-mean reads across all conditions and Log2 fold change.

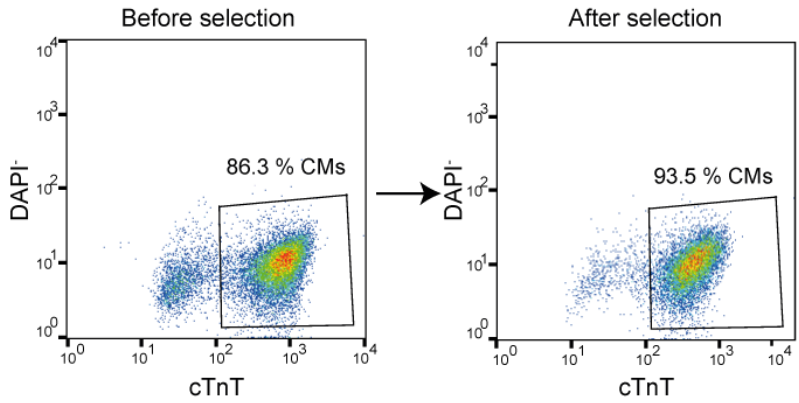

Supplementary Figure 6. hiPSC-derived CM purity after differentiation. FACS plots representing the % of CMs before and after lactate selection based on cardiac troponin T (cTnT) expression.

Supplementary Table S1. Echocardiography results from control (Sham) and transverse aortic banding (TAB)-operated mice after 1, 2, 4, 6, or 8 weeks (w) of TAB.

Left ventricular anterior wall (LVAW); Left ventricular internal diameter (LVID); Left ventricular posterior wall (LVPW) are measured in both diastole (;d) and systole (;s). Ejection fraction (EF) and fractional shortening (FS) were calculated from short axes M-mode measurements by Vevo® LAB 1.7.1 software. Average ± SD is shown. * indicates p<0.05 compared to Sham with One-way ANOVA test.

	FS (%)	EF (%)	LVPW;s (mm)	LVID;s (mm)	LVAW;s (mm)	LVPW;d (mm)	LVID;d (mm)	LVAW;d (mm)	Velocity (mm/s)
Sham (n=7)	22,25 ±4,27	44,78 ±6,80	1,04 ±0,14	3,26 ±0,28	1,27 ±0,16	0,81 ±0,09	4,12 ±0,27	0,98 ±0,16	-649,64 ±69,51
1w TAB (n=8)	28,07 ±4,99 *	52,66 ±10,40	1,42 ±0,20 *	2,92 ±0,34	1,45 ±0,21	1,08 ±0,24 *	3,96 ±0,19	1,03 ±0,10	-905,86 ±116,72 *
2w TAB (n=7)	24,08 ±2,45	48,72 ±4,24	1,43 ±0,21 *	3,04 ±0,33	1,43 ±0,13	1,11 ±0,19 *	3,98 ±0,34	1,06 ±0,10	-1006,25 ±65,37 *
4w TAB (n=8)	21,83 ±2,79	44,20 ±4,85	1,39 ±0,21 *	3,48 ±0,23	1,81 ±0,39 *	1,14 ±0,22 *	4,44 ±0,17 *	1,45 ±0,27 *	-1099,76 ±91,84 *
6w TAB (n=7)	18,32 ±2,29	37,95 ±4,40	1,65 ±0,23 *	3,77 ±0,59	1,64 ±0,21 *	1,36 ±0,22 *	4,60 ±0,63	1,26 ±0,15 *	-1188,07 ±85,81 *
8w TAB (n=7)	16,12 ±3,52 *	33,63 ±6,63 *	1,36 ±0,11 *	3,75 ±0,37 *	1,62 ±0,18 *	1,20 ±0,09 *	4,51 ±0,29 *	1,31 ±0,13 *	-1751,43 ±390,98 *

Supplementary Table S2. Morphological measurements from control (Sham) and transverse aortic banding (TAB)-operated mice after 1, 2, 4, 6, or 8 weeks (w) of TAB.

Heart weight (HW), bodyweight (BW), tibia length (TL) are shown, as HW, Lung weight (Lu) and liver weight (Li) normalized to BW or TL. Average ± SD is shown. * indicates p<0.05 compared to Sham with One-way ANOVA test.

	Li/TL (mg/mm)	Lu/TL (mg/mm)	HW/TL (mg/mm)	Li/BW (mg/g)	Lu/BW (mg/g)	HW/BW (mg/g)	TL (mm)	BW (g)	HW (mg)
Sham (n=7)	89,45 ±4,50	10,58 ±0,59	8,56 ±0,92	53,68 ±1,46	6,36 ±0,42	5,13 ±0,46	16,66 ±0,10	27,76 ±0,99	142,54 ±14,91
1w TAB (n=8)	94,69 ±4,00 *	11,13 ± 0,70	13,22 ±2,11 *	58,63 ±1,87 *	6,96 ±0,41 *	8,23 ±1,48 *	16,44 ±0,18 *	26,51 ±0,80 *	217,61 ±35,99 *
2w TAB (n=7)	78,10 ±6,31 *	11,42 ±2,10	11,23 ±1,49 *	50,07 ± 2,76 *	7,33 ±1,33	7,23 ±1,09 *	16,40 ±0,18 *	25,56 ±1,10 *	184,23 ±24,83 *
4w TAB (n=8)	89,06 ±8,93	17,14 ±6,40 *	12,76 ±2,73 *	52,87 ±2,84	9,04 ±1,40 *	8,11 ±1,26 *	16,73 ±0,13	27,80 ±1,42	228,14 ±37,00 *
6w TAB (n=7)	94,56 ±5,94	11,75 ±1,39	17,22 ±2,01 *	52,12 ±1,85	6,50 ±0,88	9,47 ±0,70 *	17,10 ±0,26 *	31,03 ±1,67 *	294,41 ±33,28 *
8w TAB (n=7)	90,86 ±7,85	11,53 ±1,55	14,17 ±2,44 *	50,20 ±2,82 *	6,39 ±0,91	7,83 ±1,26 *	16,91 ±0,22 *	30,57 ±1,43 *	239,91 ±43,60 *

Supplementary Table S3. Primer pairs used in real-time PCRs to quantify mRNA.

Gene	Species	Forward primer	Reverse primer
Actn2	Mouse (Mmu)	AGATGACCCTGGGTATGATCTG	TGTATGGAGCTGTCTTCCTCTG
Cdk1	Mouse (Mmu)	AAGTGTGGCCAGAAGTCGAG	TGAGAGCAAATCCAAGCCGT
Col3a1	Mouse (Mmu)	GATGGCAAAGATGGATCACCTGG	GACCCTTTTCTCCTGGGATGC
Gapdh	Mouse (Mmu)	TGTCGTGGAGTCTACTGGTG	ACACCCATCACAAACATGG
Myh6	Mouse (Mmu)	GTTAAGGCCAAGGTCGTGTC	GCCATGTCCTCGATCTTGTC
Myh7	Mouse (Mmu)	TGACGCAGGAGAGCATCAT	GAGTGCATTTAACTCAAAGTCCTTC
Nppa	Mouse (Mmu)	AGGCCATATTGGAGCAAATC	CCTCATCTTCTACCGGCATC
Nppb	Mouse (Mmu)	GAGTCCTTCGGTCTCAAGGC	CAACTTCAGTGCGTTACAGC
Pgc1α	Mouse (Mmu)	TCAAGAACGAAAGTCGGAGG	GGACATCTAAGGGCATCAC
Pgc1β	Mouse (Mmu)	GGCCTTGTGTCAAGGTGGAT	GCACCGAAGTGAGGTGCTTA
AKAP2	Human (Hsa)	GGAGGCTACCACTCCCTGC	GAGGGATGGTCCATGGGATG
ANKRD23	Human (Hsa)	GGACCATGGACTTCATCAGCATTCAGCA	TCAGCACCGGGTGCGGGGATGCGCCACGT
CLIC5	Human (Hsa)	CCCAAACTGGCTGCAAAACA	TAGGCCTCTTTCAAGAGCAGC
EFDH2	Human (Hsa)	GACGGCTTCATCGACCTGAT	GACGTCGATCTCAGAGAGGC
KCNJ2	Human (Hsa)	ACCGCTACAGCATCGTCTCT	TCCACACACGTGGTGAAGAT
MAFK	Human (Hsa)	CATTAAAGGTCAAGAAGGAGGCG	GACATGGACACCAGCTCATCA
MYH10	Human (Hsa)	CTGAGGCGCTGGATCTGTG	AAAAGCAATTGCCTCTTCAGCC
NPPA	Human (Hsa)	CCGTGAGCTTCCTCCTTTTA	CCAAATGGTCCAGCAAATTC
NPPB	Human (Hsa)	CTCCAGAGACATGGATCCCC	GTTGCGCTGCTCCTGTAAC
OTULIN	Human (Hsa)	ACATGTACCGTGCTGCAGAT	AATCTCGGTTCTGATGCCCC
PFKL	Human (Hsa)	TTTACAAGCTCCTCGCCCAC	TTCTTGCACCTGACCCTTGG
PFKM	Human (Hsa)	TTCGAGACCTGCAGGCAAAT	TCCAGTTCATAGCCTTGGCG
PFKP	Human (Hsa)	AGGAACGGCCAGATCGATAA	CACCTCCAGAACGAAGGTCC
PPFIBP1	Human (Hsa)	GGTACTGGCCCAAGGCAAA	ACTGGAGTGGGTGATGGACT
PRNP	Human (Hsa)	GACCGAGGCAGAGCAGTC	AGTGTTCCATCCTCCAGGCTTC
RASL11B	Human (Hsa)	CCGGTTCCTCACCAAACGAT	GGCTGTTCTCATGGACCTGAA

RPL32	Human (Hsa)	CAACGTCAAGGAGCTGGAAG	TGGGGTTGGTGACTCTGATG
SHROOM3	Human (Hsa)	CTGGAGCACGGAGAACCATTA	CACATCTCTGCGCACTACCA
SORBS2	Human (Hsa)	GCCTCACTCAACTCCAGCAT	TCTGAGGATCGGTACAGGGG
SPSC3	Human (Hsa)	CGATGGAAATGGTCTCAAGGGA	CCAGCATTTGGTACGACGTT
Pfkp	Rat (rno)	CATGAATGCTGCTGTCCGTG	CATGCCTTGGTAACCCTCGT
Nppb	Rat (rno)	CCTGCTTTTCCTTAATCTGTCG	GCCATTTCCTCTGACTTTTCTC

Supplementary Table S4. In Situ Hibridization primers for probes.

Target	**Forward (Fw) & reverse (Rv) primer**	**Cloning strategy**
Col3a1	Fw: GCTCTAGAGGGGAATGGAGCAAGACAGT	XbaI
	Rv: GCGAGCTCGTTCACCAGCAACAGCAGAA	SacI
Nppa	Fw: GCTCTAGAAGCAAACATCAGATCGTGCC	XbaI
	Rv: GCGAGCTCATATGCAGAGTGGGAGAGGC	SacI
Nppb	Fw: GCTCTAGAAGGAAATGGCCCAGAGACAG	XbaI
	Rv: GCGAGCTCCAAAAGCAGGAAATACGCTATGT	SacI

CHAPTER 3

GENE EXPRESSION PROFILE OF CARDIOMYOCYTES AFTER EXERCISE

Marta Vigil-García [1], Charlotte J. Demkes [1], Joep E.C. Eding [1], Maya Wright Clark [1], Celine Peterse [1], Hesther de Ruiter [1], Lieneke Kooijman [1], Danielle Versteeg [1], Mauro Giacca [3], Cornelis J. Boogerd [1], Eva van Rooij [1,2].

[1] Hubrecht Institute, Royal Netherlands Academy of Arts and Sciences and University Medical Center Utrecht, The Netherlands.

[2] Department of Cardiology, University Medical Centre Utrecht, The Netherlands.

[3] International Centre for Genetic Engineering and Biotechnology, Trieste, Italy.

Manuscript in preparation

Key words: Exercise, cardiac hypertrophy, Sox17, AAV9

ABSTRACT

Aims Physical exercise provides benefits and protection during cardiovascular disease. Here we aimed for a better understanding of the molecular changes occurring in cardiomyocyte (CM) hypertrophy in response to exercise and investigated the role of the exercise-induced transcription factor *Sox17*.

Methods and results Utilizing CM-specific reporter mice exposed to a swimming model of exercise and CM isolation by flow cytometry, we obtained the gene expression profile of physiologically hypertrophied CMs. To identify potential protective factors, we compared this transcriptome to the transcriptome of hypertrophic and failing CMs obtained from a model of pathological remodeling induced by pressure-overload. In doing so, we identified a subset of genes that appeared induced in CMs after exercise and reduced during pathological remodeling. These upregulated genes presented enrichment of pathways related to angiogenesis and positive regulation of transcription, with transcription factor *Sox17* being among them. To investigate the *in vivo* function of Sox17, we generated an AAV9-Sox17 to specifically increase Sox17 in CMs. AAV9-Sox17 injections led to *Sox17* mRNA and protein overexpression after 2 weeks, with an induced expression of exercise-related genes under homeostatic conditions. To study the potential cardioprotective function of Sox17, we injected AAV9-mediated *Sox17* and the respective AAV9-control in mice subjected to transverse aortic banding (TAB), just after surgery. Pressure-overload induced by the banding led to cardiac dysfunction after 8 weeks in both AAV9-control and AAV9-Sox17 groups.

Conclusion Swimming stimulates adaptive hypertrophy, improves cardiac function, and induces gene expression changes characteristic of physiological remodeling. During adaptive hypertrophy, we identified the upregulation of exercise related genes in CMs, including the transcription factor *Sox17*. However, AAV9-mediated *Sox17* overexpression does not exert protection against pathological remodeling in a mouse model of pressure overload.

INTRODUCTION

Cardiac muscle cells can adapt to an increase in volume or pressure load by inducing hypertrophy [1]. This occurs upon physiological stimuli, such as exercise, or pathological stresses, like hypertension or myocardial infarction. During the earlier stages, both stimuli induce similar adaptive changes, yet pathological remodeling can lead to heart failure, while physiological remodeling does not. Thus, understanding the molecular differences occurring between both processes may have important clinical implications. Previous studies have shown the role of many transcription factors in pathological remodeling, and several pharmacological treatments in research are targeted towards their inhibition to slow down adverse remodeling. However, currently no cure to slow down the remodeling is available. Exercise-related protective pathways and associated transcription factors are less well known, yet they might have the potential to provide novel therapeutic candidates [1].

Exercise protects the heart from disease [2]. It improves cardiac function, increases cardiac mass by increasing cardiomyocyte (CM) size and proliferation, induces angiogenesis, alters cell metabolism and reduces cell apoptosis [3, 4]. Expression analysis of exercised hearts has identified an increase in the expression of transcription factors associated with cell cycle progression [5], angiogenesis and hypertrophy [3]. For instance, the activation of the transcription factor hypoxia-inducible factor α (HIF1α) by Akt1 signaling exerts pro-angiogenic effects [6], and the repression of the transcription factor CCAAT/enhancer binding proteins beta (C/EBPβ) induces regulation of CM hypertrophy, proliferation and differentiation [5]. In fact, C/EBPβ heterozygosity recapitulates the exercise phenotype and regulates the "exercise gene set" that includes Tbx5, Gata4 and Nkx2.5 among others [5].

The Sox (SRY related-HMG box) family of transcription factors has 20 members that have been evolutionarily conserved and that participate in the differentiation of tissues and organs [7]. Sox genes have also been associated to key biological processes during heart disease, such as Sox9 which regulates cardiac fibrosis after ischemic injury [8]. The SoxF subgroup (Sox7, 17, 18) has a key role in the differentiation of various cell types. Furthermore, this group is necessary for the modulation and development of the cardiovascular system. Particularly, compound heterozygosity of Sox17 and Sox18 causes problems in early heart and vascular development in the mouse embryo [9]. In addition, endothelial cell-specific inactivation of Sox17 in the mouse embryo is accompanied by a lack of arterial differentiation and vascular remodeling, which induces early lethality [9]. In humans, Sox17 mutations are linked to pulmonary arterial hypertension with congenital heart disease [10].

Collective work in the field suggests that the activation of adaptive or protective factors, could be a useful strategy in patients with heart failure [11, 12]. Here, we aim to identify adaptive factors by using CM (CM)-specific transcriptomic data from hypertrophic CMs after swimming-induced exercise. To do so we used a CM isolation method [13] combined with an animal model of exercise and investigated

gene expression changes occurring in CMs in response to exercise. We identified exercise-related signatures and found novel transcription factors regulated in hypertrophic CMs that were not previously studied for their function in CM remodeling. Sox17, a transcription factor functioning upstream of the Notch signaling and downstream of the canonical Wnt signaling [7], was upregulated during adaptive hypertrophy. AAV9-mediated overexpression of Sox17 increased the expression of protective genes under homeostatic conditions. However, in response to pressure overload induced hypertrophy, Sox17 was unable to induce a cardioprotective response.

RESULTS

Exercise training induces physiological hypertrophy in the heart

To define the gene expression profile that marks exercise-induced hypertrophy, we used a mouse model of swimming-induced cardiac hypertrophy. We subjected mice to a training protocol of 9 days ramp up phase followed by 2 weeks of swimming for 90 minutes 2 times per day, with a minimum of 4 hours of rest in between rounds (**Figure 1A)**. The control sedentary (Sed) mice swam two times a 5-minutes session a day. Echocardiography revealed a significant decrease in interventricular relaxation time (IVRT) (14,13±1,97*) after swimming (Ex) when compared to Sed mice (17,69 ±1,47) (**Figure 1B-C, Table S1**), indicating increase in diastolic function [14, 15]. Exercise induced physiological hypertrophy as shown by an increase in heart size (heart weight (HW)/ tibia length (TL)) and CM size (cell surface area (CSA)) (**Figure 1D-F**). In addition, connective tissue staining by Picrosirius Red (SR) shows that cardiac collagen deposition did not change after exercise (**Figure 1D, G**). Gene expression analysis by real-time PCR revealed a decrease in beta myosin heavy chain (Myh7) and an increase in alpha myosin heavy chain (Myh6), indicating a better cardiac performance [16] (**Figure 1H**). Additionally, the genetic reprograming induced by pathological hypertrophy was not activated. This is shown by no change in natriuretic peptide a (*Nppa*) and natriuretic peptide b (*Nppb*) expression levels, and a decrease in expression of Actin alpha 1, skeletal muscle (*Acta1*). Moreover, collagen 3a1 (*Col3a1*) showed a trend towards decrease in expression levels (**Figure 1H**). Based on the functional improvement and the increase in CM size, the swimming model introduced hallmarks of physiological remodeling.

Using flow cytometry to isolate hypertrophic CMs

We used CM specific Myh6-Cre [17]/ R26-td-Tomato [18] reporter mice to genetically label CMs **(Figure 2A)** and we confirmed robust and specific labeling of alpha-actinin2 (ACTN2) positive CMs (**Figure 2B**). Myh6-Cre / R26-td-Tomato reporter mice were subjected to sedentary or exercise protocols, which induced hypertrophy shown by HW/TL and CSA (**Figure 2C-E**). To isolate CMs, we followed the same strategy as previously published [19] in which cells were sorted based on viability, tdTomato positivity, sarcomere auto-fluorescence and enrichment for cells with a higher forward scatter width (**Figure 2F,**

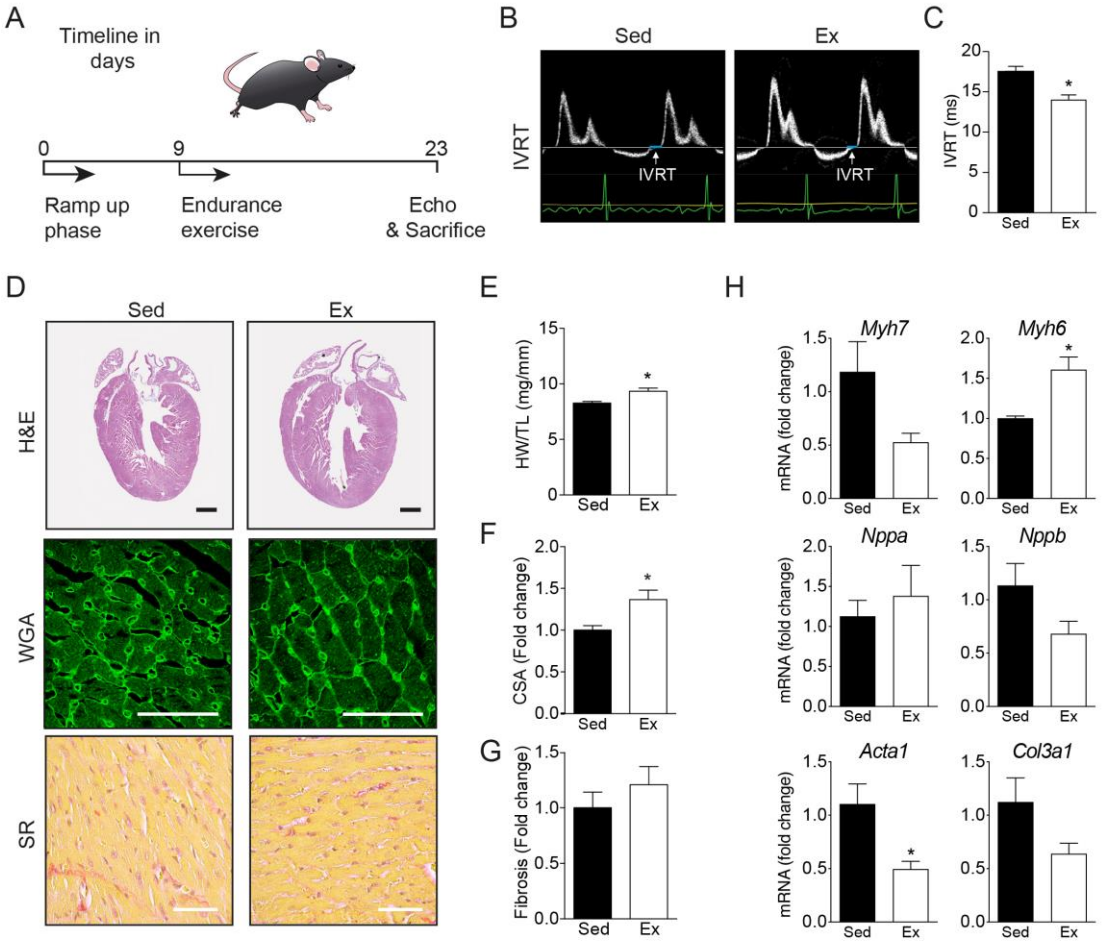

Figure 1. Swimming training induces physiological hypertrophy. A, Schematic of time-course for swimming study. B, Representative echocardiography images for the interventricular relaxation time (IVRT). C, IVRT (ms). D, Representative images of H&E, wheat germ agglutinin (WGA, middle row) and Picrosirius red (SR, bottom row) stained cardiac sections. E, Heart weight to tibia length (HW/TL) ratios (n=6-12). F, Quantification of cell surface area (CSA) of CMs (~80 cells per n= 3-4 per group). G, Quantification of ventricular fibrosis (n=2-4 per group). H, Real-time PCR analysis of Myh7, Myh6, Nppa, Nppb, Acta1 and Col3a1 on cardiac tissue collected from control (Sed) and after exercise (Ex) (n= 6-12). Data expressed as mean fold change ±SEM; *indicates $p<0.05$ compared to sedentary (Sed) with unpaired t-test.

Figure S1). After sorting, the cells expressed tdTomato and exhibited a rod-shape like structure (**Figure 2G).** In addition, we were able to extract good quality RNA from these cells with an RNA integrity number above 7.0 (**Figure 2H**). Together, these results illustrate the successful isolation of hypertrophic CMs.

RNA-sequencing of hypertrophic CMs after swimming reveals gene expression changes characteristic of exercise-induced hypertrophy

To comprehensively define the exercise-induced gene program, we performed RNA-sequencing on sorted CMs from Sed and Ex hearts. Principal Component Analysis (PCA) revealed a clearly distinct gene expression signature between Sed and Ex CM transcriptomes (**Figure 3A**). A total of 396 genes

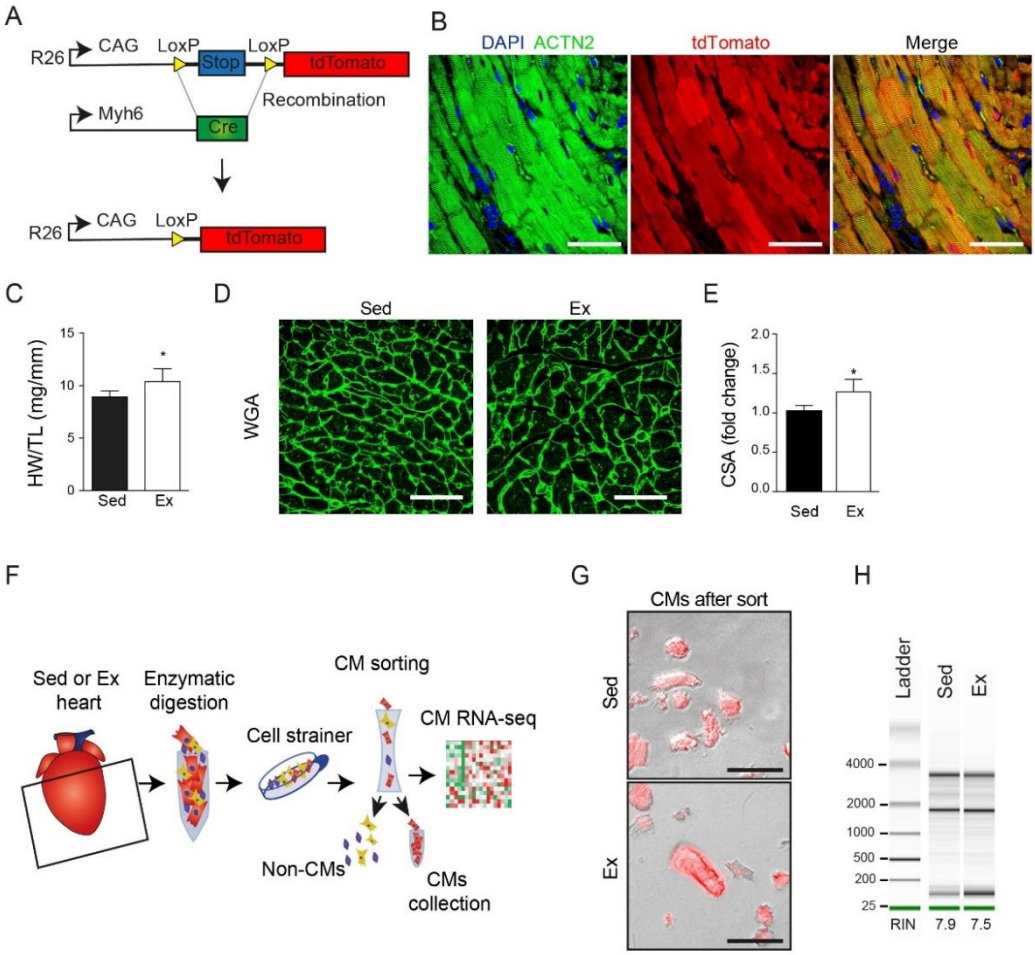

Figure 2. Isolating CMs after exercise. A, Strategy for the generation of a CM-specific reporter mouse (Myh6-Cre/ tdTomato). B, Immunofluorescence indicating sarcomere α actinin (ACTN2; CMs) and tdTomato. Scale bar is 200 µm. C, Heart weight to tibia length (HW/TL) ratio of Sed and Ex groups (n=5-6). D, Wheat germ agglutinin (WGA) staining of hearts of Ex and Sed groups. Scale bars are 200µm. E, Quantification of CSA of CMs (>50 cells per heart, n=5-6). F, Schematic drawing of the CM isolation and sorting strategy. G, Representative images of CMs after sort. H, Bioanalyzer plot showing the RNA quality isolated from the sorted CMs after Sed or Ex protocols. RIN: RNA Integrity Number. Data expressed as mean fold change ± SEM; * indicates $p<0.05$ compared to Sed with unpaired t-test.

were upregulated in hypertrophic CMs ($p> 0.05$; fold change (FC)> 1.5) and 175 genes were downregulated ($p>0.05$; FC<0.6) (**Figure 3B**). When we looked at the top 30 differentially upregulated genes, we could find genes associated to cardioprotection and exercise (**Figure 3C**). Interestingly, the top hit was the nuclear transcription factor Nuclear Receptor Subfamily 4 Group A Member 1 (*Nr4a1*), which has previously been found to be increased after exercise [20] and to protect against cardiac remodeling [21]. Additionally, we observed an induction of the apoptotic regulator BCL2-like 1 (*Bcl2l1*) which encodes for the protein BCL-XL, with pro-survival functions and a protective role against ischemia [12]; and the cell cycle regulator Cyclin Dependent Kinase Inhibitor 1A (*Cdkn1a*), which is known to be downregulated during pathological remodeling and to prevent heart failure in a model of cardiac hypertrophy induced by Angiotensin II [22]. Real-time PCR confirmed the induction of these markers on full heart tissue and in sorted CMs (**Figure 3D-E**). Gene ontology analysis of the upregulated genes

revealed pathways involved in angiogenesis (*Sox17*, *Apold1*), cell cycle regulation (*Cdkn1a*) and apoptotic processes (*Nr4a1, Bcl2l1*) [3] (**Figure 3F**). The downregulated genes were enriched for pathways related to metabolism (**Figure 3G**).

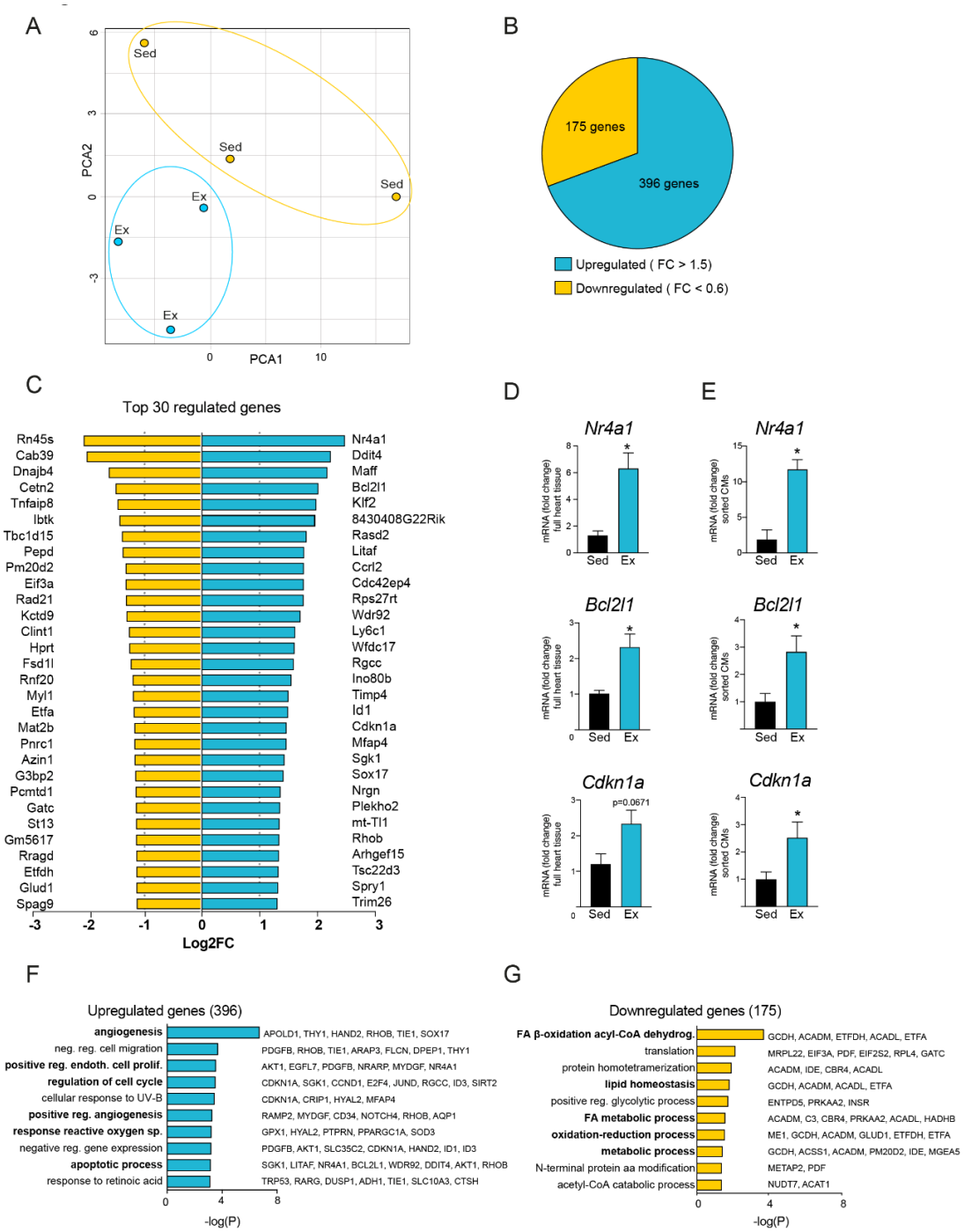

Figure 3. Gene expression analysis in CMs after exercise. A, Principal Component Analysis (PCA) plot indicating the gene expression differences between CMs from Sed and Ex mice. B, Pie chart showing the number of significantly regulated genes (p> 0.05; fold change (FC)> 1.5 or FC<0.6) after Ex compared to Sed. C, Top 30 upregulated (blue) and downregulated (yellow) genes in Ex versus Sed CMs. D, Real-time PCR analysis of upregulated genes (*Nrfa1*, *Bcl2l1* and *Cdkn1a*) related to exercise in heart tissue (n=5-6). E, Real-time PCR analysis of upregulated genes (*Nrfa1*, *Bcl2l1* and *Cdkn1a*) related to exercise in sorted CMs (right column) (n=-5-6). F, Gene ontology enriched pathways of the upregulated genes in Ex compared to Sed. G, Gene ontology enriched pathways of the downregulated genes in Ex compared to Sed. Data expressed as mean fold change ± SEM; * indicates p<0.05 compared to Sed with unpaired t-test.

Comparative analysis of RNA-sequencing of CMs after pathological and physiological remodeling identifies Sox17 as a potential cardioprotective factor

To identify the factors with a potential cardioprotective role, we combined CM RNA-sequencing results from the exercised CMs to a previous CM RNA-sequencing data set from hypertrophic and failing CMs obtained from a model of pressure overload induced by transverse aortic binding (TAB) [19]. In the initial stages, TAB induces an adaptive hypertrophic response during the first week after surgery (TAB 1w), while the latter stage of remodeling is characterized by pathological hypertrophy and a decline in cardiac function (TAB 8w) [19]. To identify genes that are up during both adaptive types of cardiac remodeling and down during CM failure, we compared the significantly upregulated genes in hypertrophic CMs from exercise and TAB 1w, and the significantly downregulated genes in failing CMs (TAB 8w). In doing so we identified 69 genes that were upregulated during adaptive remodeling and that were going down during failure (**Figure 4A-B**). To explore this group of genes, we performed gene ontology analysis which showed enrichment for pathways related to negative regulation of apoptosis, positive regulation of gene expression and angiogenesis (**Figure 4C**). Interestingly, transcription factor *Sox17* was present in the top upregulated genes and in the pathways related to angiogenesis and positive regulation of gene expression. *Sox17* is a transcription factor known to have a pro-angiogenic role [23], and we hypothesized that it could have a potential cardioprotective function in the heart. Real-time PCR confirmed the induction of *Sox17* on heart tissue and sorted CMs after exercise (**Figure 4D).** In the TAB model, *Sox17* did not present a significant change in heart tissue probably due to the presence of different cell types which can dilute out the signal (**Figure 4E**). In the TAB sorted CMs, *Sox17* expression did not show a significant change in TAB 1w. However, it was significantly downregulated in TAB 8w (**Figure 4E**), validating the RNA-seq data. These results identify *Sox17* as a transcription factor upregulated in CMs during adaptive hypertrophy and repressed during CM failure.

AAV9-mediated Sox17 overexpression in the mouse heart increases cardioprotective genes

To study a potential role of Sox17 in CM protection, we generated a AAV9 virus encoding a mouse *Sox17*, as AAV9 serotype preferentially infects CMs [24]. We performed tail vein injections in wildtype mice with a single bolus injection ($3x10^{12}$ vg) of either empty AAV9 (AAV9-control) or AAV9-Sox17 and collected the hearts 2 weeks later (**Figure 5A**). The virus resulted in a clear increase of exogenous *Sox17* and ~7-fold upregulation of the total *Sox17* mRNA in the heart (**Figure 5B, C**). SOX17 protein

was successfully translated and overexpressed (**Figure 5E, F**). Morphological analysis indicated no change in HW to body weight (BW) ratio (**Figure 5D**) and no significant changes in off target organs (**Figure S2**). We then set out to examine the stress induced by Sox17 overexpression in the heart at a molecular level. We looked at the regulation of the known cardiac stress markers *Myh6, Myh7, Nppa* and *Nppb* which showed no significant induction, except for *Myh7* (**Figure 5G**). We also observed no significant induction of angiogenic markers (data not shown). When we examined the regulation of the exercise-induced genes with cardioprotective functions in CMs (**Figure 3D**), AAV9-Sox17 infected

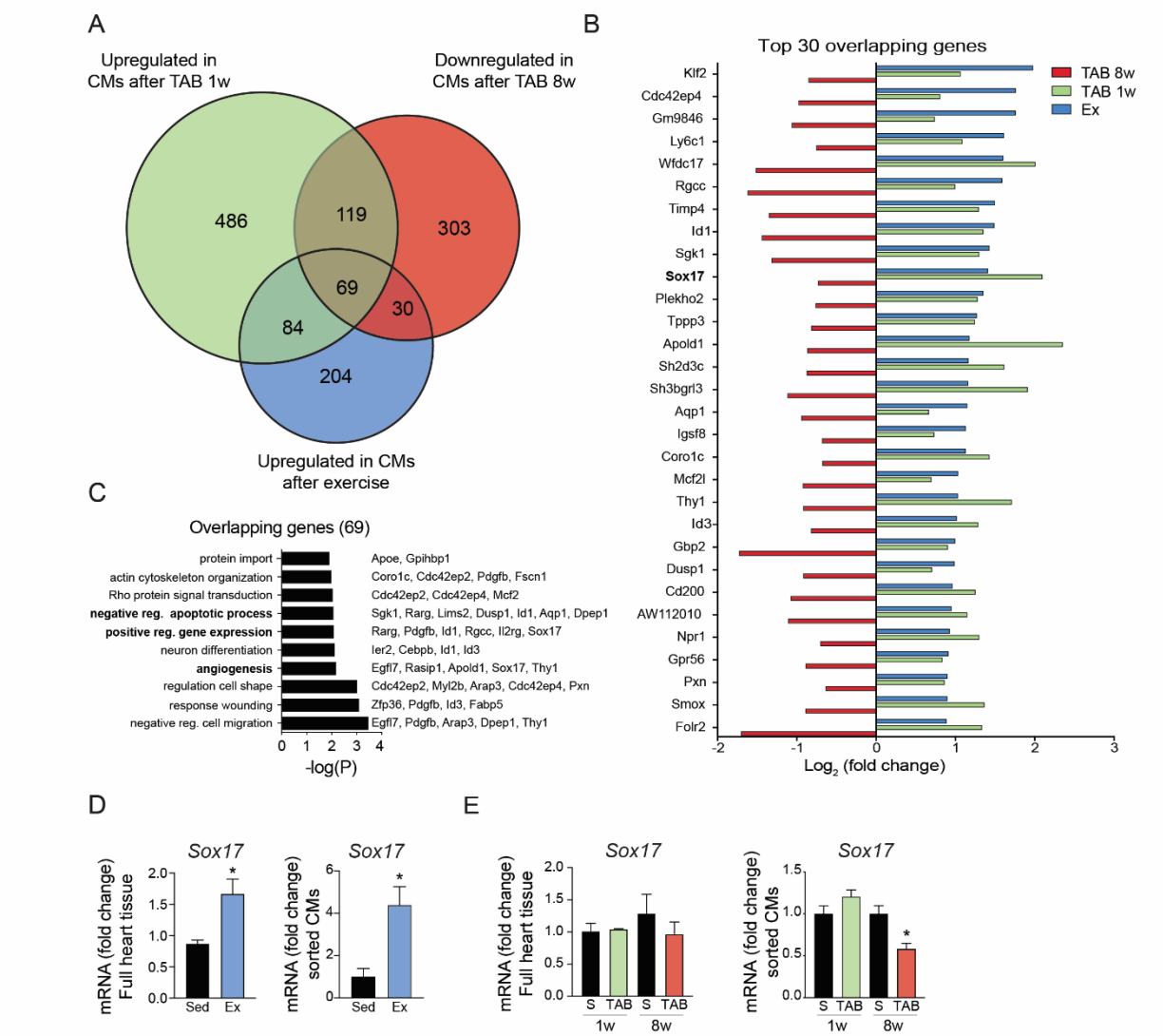

Figure 4. CMs undergoing adaptive hypertrophy express *Sox17*. A**,** Venn diagram showing the intersection between significantly upregulated genes (log2FC>1) in CMs one week after TAB (green), CMs after exercise (blue), and significantly downregulated genes (log2FC<-1) in CMs eight weeks after TAB (red), when compared to corresponding control (Sham 1w, sedentary and Sham 8w), respectively (n=3 per group). B, Top 30 differentially upregulated genes in CMs one week after TAB (green) and exercise (blue) and differentially downregulated genes in eight weeks after TAB (red). C, Gene ontology enriched pathways of the 69 differentially upregulated genes in CMs one week after TAB and exercise and differentially downregulated genes in eight weeks after TAB. D, Real-time PCR analysis of *Sox17* in heart tissue (left) and sorted CMs (right) in Ex or Sed groups. E, Real-time PCR of *Sox17* in heart tissue (left) and sorted CMs (right) in TAB or sham (S) groups (n=3). Data expressed as mean fold change ± SEM; * indicates p<0.05 compared to Sed or sham (S) with unpaired t-test.

hearts showed a significant upregulation of *Nr4a1*, while *Bcl2l1* and *Cdkn1a* showed a trend towards upregulation (**Figure 5H**). These results indicate that systemic delivery of AAV9-Sox17 successfully promotes SOX17 overexpression in the heart, which can in turn lead to the upregulation of cardioprotective genes.

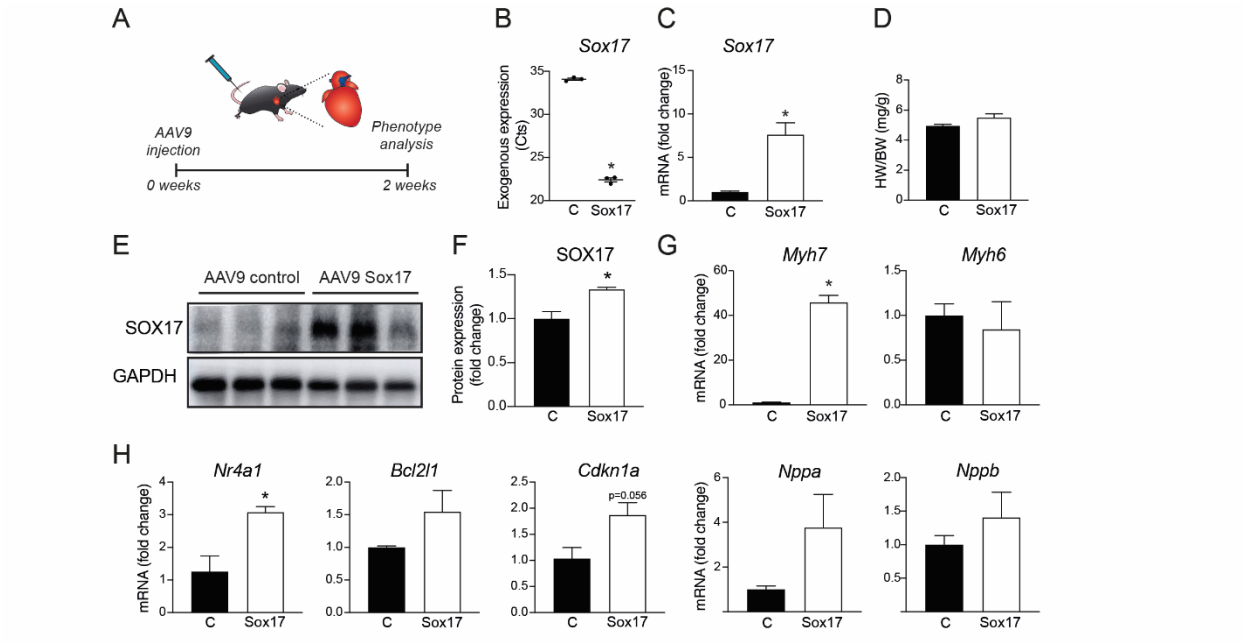

Figure 5. AAV9-mediated Sox17 overexpression in the heart induces as many stress genes and exercise-induced gene expression. A**,** Schematic of AAV9 injection strategy. B, Real-time PCR analysis of exogenous *Sox17* expression in heart tissue after AAV9 injection in AAV9-control (C) and AAV9-Sox17 (Sox17) groups (n=3). C, Real-time PCR analysis of exogenous and endogenous *Sox17* expression in heart tissue after AAV9 injection in C and Sox17 groups (n=3). D, Heart weight to body weight ratio (HW/BW) (n=3). E, Western blot analysis of SOX17 protein levels and loading control GAPDH after AAV9 injection of C and Sox17 (n=3). F, Protein level quantification. G, Real-time PCR analysis of cardiac markers *Myh7, Myh6, Nppa* and *Nppb* in heart tissue after AAV9 injection of C and Sox17 groups (n=3). H, Real-time PCR analysis of exercise-induced markers *Nr4a1, Bcl2l1* and *Cdkn1a* in heart tissue after AAV9 injection of C and Sox17 groups (n=3). Data expressed as mean fold change ± SEM; * indicates $p<0.05$ compared to C with unpaired t-test.

AAV9-mediated Sox17 overexpression during pressure overload does not improve cardiac function

To investigate if Sox17-mediated induction of cardioprotective factors protects during pathological remodeling, we exposed wildtype mice to pressure overload followed by empty AAV9 (control) or AAV9-Sox17 tail injections (**Figure 6A**). We performed the phenotypic analysis at 8 weeks post-surgery, when TAB surgery has induced a significant decline in cardiac function, activation of fibrosis and pathological hypertrophy. Exogenous and total *Sox17* mRNA levels were significantly higher in AAV9-Sox17 injected sham and TAB groups (**Figure 6B, C**). Interestingly, mRNA expression levels of *Sox17* after TAB in AAV9-control group showed a significant downregulation. SOX17 protein levels were highly variable between samples. In sham conditions, AAV9-Sox17 injections led to a non-significant upregulation of SOX17 protein (**Figure 6D**). In TAB conditions, AAV9-control and AAV9-Sox17 groups presented a comparable increase in SOX17 protein levels. The underlying reason for the

levels of SOX17 in TAB AAV9-control is not clear, yet we can hypothesize that the stress induced by TAB during the period of 8 weeks might allow for an additional regulatory response to become activated leading to high SOX17 protein levels. Cardiac function analysis by echocardiography revealed a decline in cardiac function 8 weeks after TAB in both AAV9-control and AAV9-Sox17 groups as shown by ejection fraction (EF)% (42.25%±7.01 and 45.17%±17.95, respectively) when compared to sham (55.47%±11.54 and 59.03%±12.35, respectively), indicating no functional improvement after Sox17 overexpression (**Figure 6E, Table S1).** TAB groups also showed similar interventricular septum size during systole and diastole (IVD;s and IVD;d) (**Figure 6F, Table S1)**. Noteworthy, the left ventricular posterior wall (LVPW) was increased only in TAB AAV9-Sox17 mice during systole, indicating that Sox17 overexpression might lead to a more severe hypertrophic response (**Figure 6F, G**). Morphologically, TAB surgery induced a similar increase in HW/TL ratio (**Figure 6I**). However, only AAV9-Sox17 group showed an increase in CSA after TAB (**Figure 6J),** further indicating Sox17-related induction of CM hypertrophy**.** No significant change in the weights of off target organ was observed (**Figure S3**). The fibrotic response was activated after TAB surgery in both AAV9-control and Sox17 groups, although Sox17 overexpression led to a more significant induction (**Figure 6K**). At a molecular level, gene expression analysis of cardiac markers *Myh6, Nppa, Nppb* and exercise-induced genes *Nr4a1, Bcl2l1* and *Cdkn1a* showed no significant difference between AAV9-C and AAV9-Sox17 groups (**Figure S4A, B**). Interestingly, *Myh7* was again highly induced after Sox17 overexpression when compared to empty AAV9. These results indicate that Sox17 overexpression does not improve cardiac function in a model of pressure overload but induces a stronger pathological response.

Transcriptome analysis of AAV9-mediated Sox17 overexpression during heart failure

To better comprehend the effects of Sox17 overexpression during pressure overload, we performed RNA-sequencing on TAB hearts after AAV9-control and AAV9-Sox17 injection. PCA showed clustering of the AAV9-Sox17 TAB samples, indicating different gene expression profiles in the Sox17 treated mice compared to control (**Figure 7A**). As shown in the volcano plot, more genes were induced after AAV9-Sox17 overexpression (**Figure 7B**) with 196 genes significantly upregulated (fold change>1.5 and p.val<0.05) and 86 genes downregulated (fold change<0.7 and p.val<0.05) (**Figure 7C**). When looking at the top regulated genes, we could identify the downregulation of cardiac stress marker *Acta1* [25] (**Figure S5**). Interestingly, the most upregulated gene was Dickkopf-related protein 2 (*Dkk2*) (**Figure S5)**, a Wnt signaling ligand previously linked to Sox17 [7].

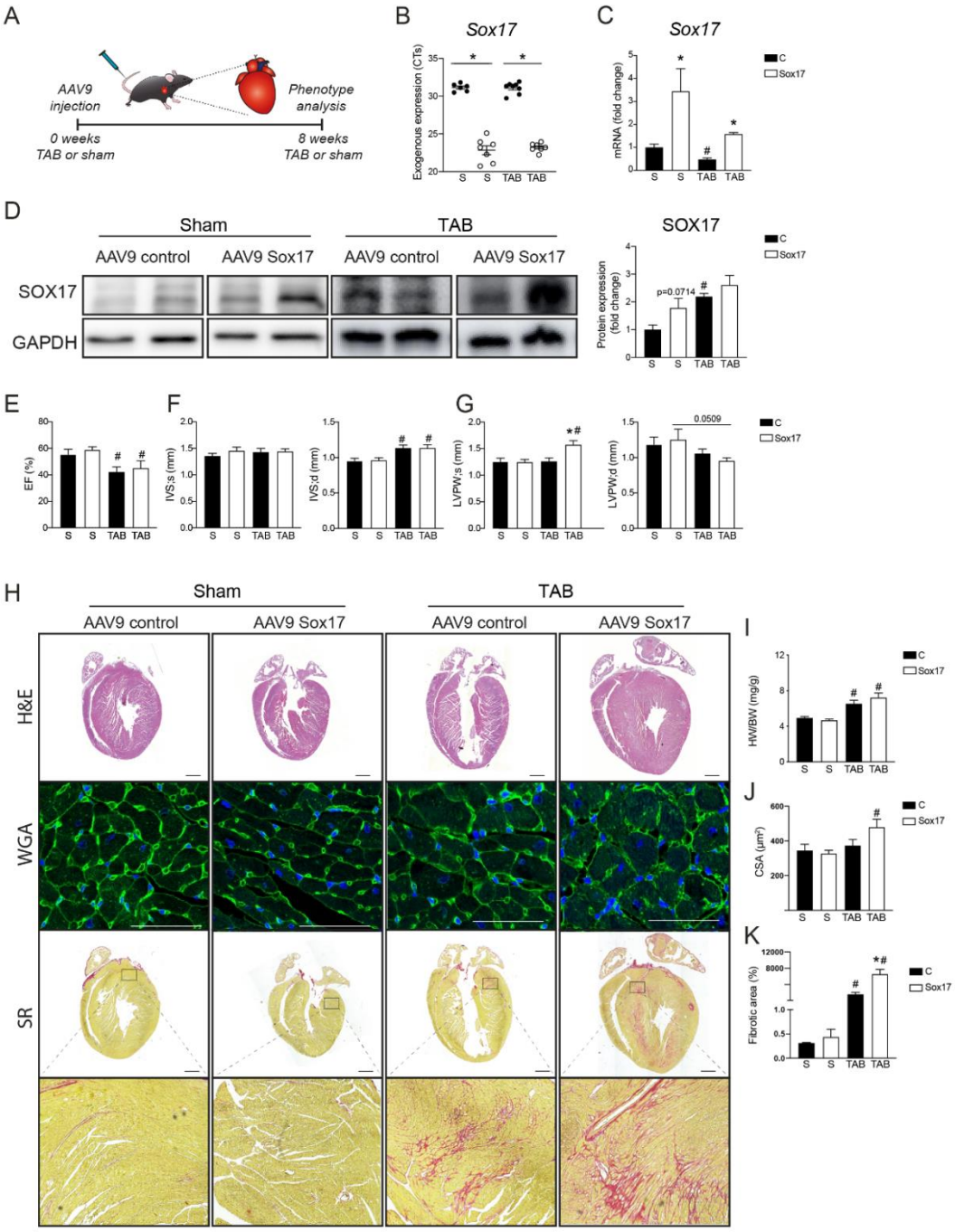

Figure 6. AAV9-mediated Sox17 overexpression during pressure overload does not improve cardiac function. A, Schematic of AAV9 injection strategy. B, Real-time PCR analysis of exogenous Sox17 expression in heart tissue after empty AAV9 (C) or AAV9-Sox17 injection (Sox17) in sham (S) or TAB groups (n=6-8). C, Real-time PCR analysis of endogenous Sox17 expression in heart tissue after empty AAV9 (C) or AAV9-Sox17 (Sox17) injection, in S or TAB groups (n=6-8). D, Representative western blot images of SOX17 protein levels and loading control GAPDH in heart tissue after AAV9 control or AAV9-Sox17 injections in S or TAB groups (n=6-8) and the respective quantification (left panel). E, Ejection fraction (EF%). F-G, interventricular septum thickness in systole and diastole (IVS;s and IVS;d). G, left ventricular posterior wall thickness in systole and diastyle (LVPS;s and LVPS;d) as determined by echocardiography (n=6-8). H, Representative images of H&E, wheat germ agglutinin (WGA, middle row) and Picrosirius red (SR, bottom row) stained cardiac sections. I, Heart weight to body weight (HW/BW) ratios (n=6-8). J, Quantification of cross-sectional area (CSA) of CMs (~80 cells per n= 3). K, Quantification of ventricular fibrosis (n=3). Data expressed as mean fold change ± SEM; * indicates p<0.05 compared to C with unpaired t-test. # indicates p<0.05 compared to S with unpaired t-test.

Next, to reinforce the link between Sox17 overexpression with the upregulation genes, we performed in silico HOMER analysis (**Figure 7D**). Sox17 motif was the most significantly enriched motif, targeting 21.47% of the promotors and further confirming the correlation of the upregulated genes with Sox17 overexpression. These group of genes also presented highly enriched promotors for Sox15, the T-box transcription factor T (Brachyury) and C/EBPβ motifs. Next, to elucidate which genes contained a Sox17 motif, we performed in silico oPOSSUM analysis[5] with the promoter region encompassing 100 bp upstream and 100 bp downstream of the transcription starting site (**Table S2)**. Cytoplasmic tyrosine-protein kinase BMX (*Bmx*) presented the highest % score, followed by slow skeletal muscle troponin 1 (Tnnt1), endothelin1 (*Edn1*), *Dkk2* and *Myh7,* between others. Gene expression analysis by real-time PCR confirmed the upregulation of these genes in AAV9-Sox17 TAB hearts (**Figure 7E, Figure S4**).

Next, to examine the pathways enriched after Sox17 overexpression, we performed GO-term enrichment analysis. We found enrichment of pathways related to mitosis, cell cycle and cell division (**Figure 7F, Table S3**) in the group of upregulated genes, while the downregulated genes showed enrichment for skeletal muscle fiber development and positive regulation of apoptosis and vasodilation (**Figure 7G, Table S3**). Altogether, we show that AAV9-Sox17 infection induces transcriptional changes at 8 weeks post-TAB surgery and enriches for cell cycle related pathways.

Discussion

In this study we present a gene program specific to CMs during physiological hypertrophy and show that exercise induces the expression of protective genes in these cells. We investigated the transcriptional changes occurring in hypertrophic CMs after exercise and compared them to the ones occurring after pressure overload during the adaptive and pathological hypertrophic stages. With this comparison we identified a group of regulated genes that potentially drive adaptive hypertrophy, with Sox17 transcription factor among those as Sox17 is highly upregulated during the adaptive phase of remodeling. While investigating the role of Sox17 overexpression during progression towards failure, we showed that Sox17 does not induce cardioprotection under conditions of pressure overload.

Sox17 overexpression under healthy conditions after 2 and 8 weeks did not induce hypertrophy of CMs. Under TAB conditions, Sox17 overexpression led to larger CM size and to a stronger fibrotic response. These results could suggest that high levels of exogenous protein for a lengthy period of time during stress might have non-specific and cardiotoxic effects. This has been previously suggested as a limitation of overexpression studies using viral gene transfer [26]. To elucidate whether long-term SOX17 overexpression is detrimental, additional experiments where overexpression is initiated at a later stage and induced for a shorter period could provide more insights.

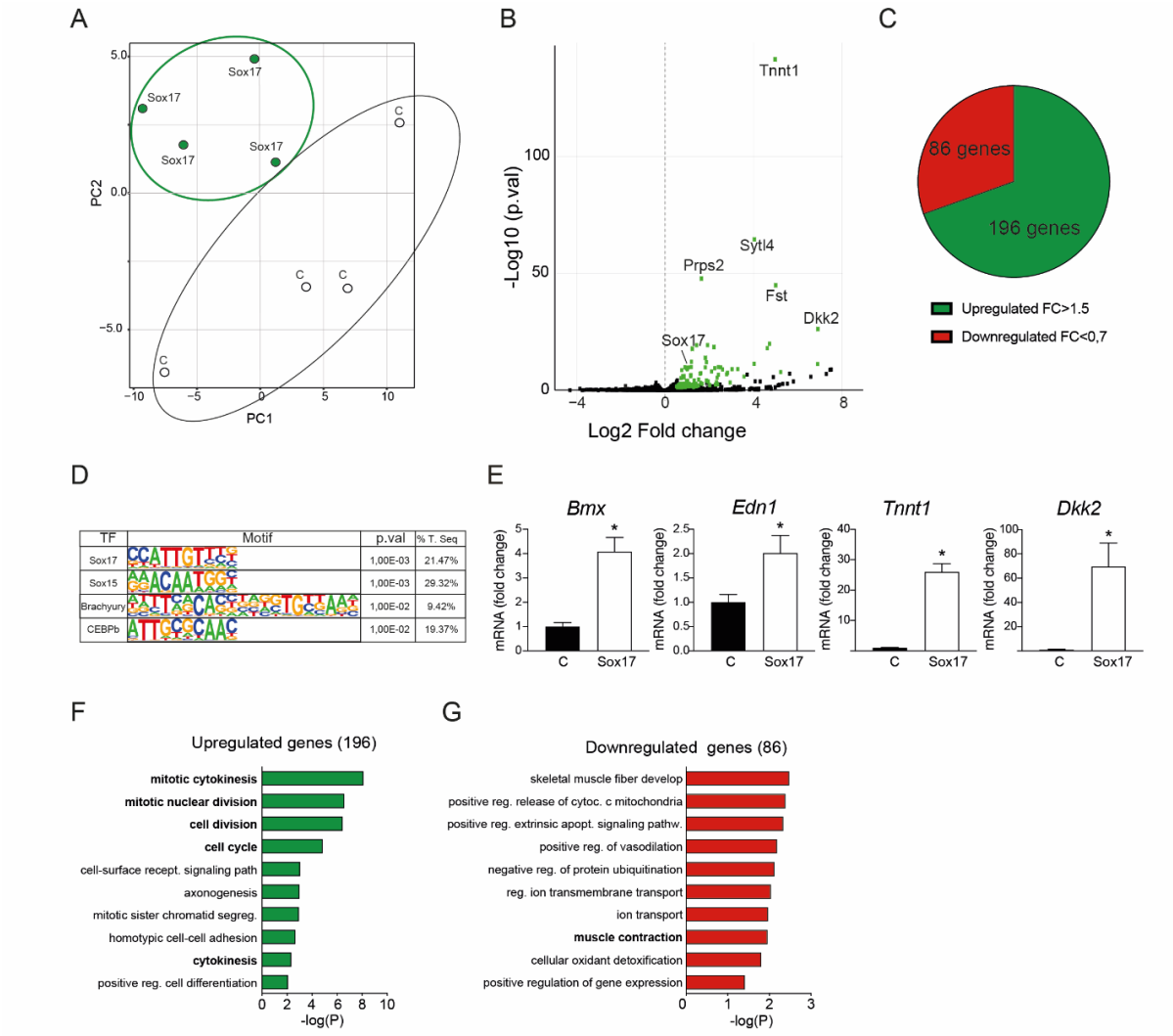

Figure 7. Cardiac gene expression changes after Sox17 overexpression during pressure overload. A, Principal Component Analysis (PCA) plot indicating the gene expression differences in heart tissue after empty AAV9 (C) or AAV9-Sox17 (Sox17) injection TAB groups (n=4). B, Volcano plot showing all genes expressed in TAB hearts after AAV9-Sox17 injection (Sox17) when compared to control (C). Significantly upregulated genes (with a Log2FC >1) are represented in green. C, Pie chart showing the number of significantly regulated genes (p> 0.05; fold change FC> 1.5 or FC<0.7) after AAV9-Sox17 compared to control. D, Motif analysis showing the most enriched motifs in the significantly upregulated genes after TAB AAV9-Sox17 compared to control. E, Real-time PCR of enriched genes with known or potential Sox17 binding sites on RNA collected from hearts after TAB (n=8). F, Enriched pathways based on gene ontology for the upregulated genes in Sox17 group compared to control. G, Enriched pathways based on gene ontology for the downregulated genes in Sox17 group compared to control. Data expressed as mean fold change ± SEM; * indicates p<0.05 compared to Control with unpaired t-test.

In our studies we identified a discrepancy between mRNA and protein levels. Sox17 mRNA induction was significant during adaptive hypertrophy and repressed during the failing state. However, at protein level, SOX17 was significantly present in the failing hearts. With the current data, the underlying reason for the mismatch is not clear, yet we can hypothesize that the stress induced by TAB during the period of 8 weeks might allow for an additional regulatory system to become activated and the regulatory processes that control steady-state protein abundance might be post-

transcriptional. For instance, SOX17 protein might have a long life-span to compensate for mRNA degradation during stress conditions.

Our study showed that Sox17 mRNA overexpression led to the upregulation of genes with enriched C/EBPβ binding sites. As previously mentioned, C/EBPβ has a strong link to exercise-induced genes [5], suggesting a link between Sox17 and the exercise-induced program. Moreover, the brachyury motif was also enriched. Brachyury belongs to the group of T-box transcription factors, which have been linked to Sox proteins and function as cardiac enhancers in the developing heart [27]. To confirm the interaction of Sox17 to these genes, data should be complemented with *in vitro* and *in vivo* models and chromatin immunoprecipitation sequencing (ChIP-seq) experiments.

Sox17 overexpression induced a set of genes that have been shown to be regulated in response to stress (Bmx, Edn1, Tnnt1, Dkk2 and Myh7). For instance, Bmx is a non-receptor tyrosine kinase expressed in endothelial cells, and deletion of Bmx has been shown to inhibit cardiac hypertrophy in mice[28]. Edn1, is an endothelium-derived vasoconstrictor peptide and its cognate receptors are therapeutic targets in the treatment of pulmonary arterial hypertension. Increased or decreased expression of Edn1 has been linked to detrimental cardiac function and cardiac hypertrophy, becoming critical for maintaining normal cardiac contractile function, for controlling superoxide levels, and for ensuring that the myocardium has sufficient collagen to prevent overstretching [29]. Sox17-induced Edn1 and Bmx upregulation could potentially be triggering the stronger hypertrophic and fibrotic response during cardiac stress that we observe 8 weeks after banding.

On the other hand, Sox17 overexpression also led to the upregulation of Dkk2, which has a potential protective role. Dkk2 is a glycoprotein previously shown to be regulated by Sox17 [7] and with a role in angiogenesis regulation. A study showed that DKK2 protein injections enhanced neovascularization of the infarcted area in a mouse model of myocardial infarction leading to an improved cardiac function [30].

Interestingly, *Myh7* was highly upregulated in response to Sox17 overexpression, and it was found to contain a binding site for Sox17. There is no previous research indicating a link between *Sox17* and *Myh7,* hence experiments validating their interaction could provide new insights as it could potentially link *Sox17* to CM stress.

Furthermore, RNA sequencing on TAB hearts after AAV9-control and AAV9-Sox17 injection suggested a link between Sox17 potential target genes to cell division and cell cycle pathways. Studies have shown that exercise has a regulatory role in CM proliferation through transcription factors [5]. Additional studies with short term Sox17 overexpression in stress models of ischemic injury could lead to data suggesting a link between Sox17 and CM proliferation.

Our study comes with some limitations. While AAV vectors have been used extensively for gene delivery in the last decade and hold promise as a vehicle for human gene therapy, overexpression studies need to be interpreted with care. In this regard, as previously stated, high levels of exogenously expressed proteins can lead to non-specific and cardiotoxic effects [26]. Additionally, the overexpression of SOX17 specifically in CMs needs to be confirmed to optimally validate its function. The findings link Sox17 overexpression with proteins mainly expressed in endothelial cells which could be due to cell-to-cell crosstalk.

In summary, we provide a resource for CM-specific exercise related genes that might be relevant for adaptive hypertrophy. Our data also show that Sox17 might be involved in the regulation of cell cycle factors, although we failed to show cardiac improvement in a model of pressure overload. Using these data for follow up functional studies might further reveal biological implications in the process of CM proliferation and may aid in the development novel therapeutic strategies aimed to protect the heart from cardiac remodeling.

Materials and Methods

Animals

Animal studies were performed according to the guidelines from Directive 2010/63/EU on the protection of animals used for scientific purposes. Animal experiments were approved by the institutional guidelines and regulations of the Animal Welfare Committee of the Royal Netherlands Academy of Arts and Sciences and following the guide for the care and use of laboratory animals.

To characterize the effects of exercise and pressure overload, wildtype C57Bl/6J mice were used. To generate CM-specific tdTomato expressing mouse, *Rosa26-tdTomato* reporter mice ($R26R^{TdT}$, TdTomato expression driven by Rosa26 promoter; bred on a C57Bl/6J background) [18] were crossed with *Myh6-Cre* transgenic mice ($Myh6^{cre}$; a generous gift from Jeffery Molkentin, Cincinnati Children's Hospital Medical Center). Mice were maintained on a C57Bl/6J background (stock number 000663, Charles River).

Swim exercise training

Physiological hypertrophy was induced in C57Bl/6J $R26R^{TdT}/Myh6^{cre}$ male mice by swimming exercise. The mice were subjected first to 8 days training period that was increased 10 minutes each day until two 90-minute sessions were achieved on the 9th day. The first day of swimming practice consisted of 1-minute session followed by a 2-minute session separated by at least 4 hours and a last 5-minutes-session after 4 hours. The next day the exercise group swam two 10-minutes sessions separated by at least 4 hours. Thereafter, for long-term swimming exercise, mice were made to swim in water tanks twice daily for 90 minutes 7 days a week for 4 weeks. The control group swam two 5-minutes session a day. Swimming mice were continuously monitored to ensure equal exertion [31]. After swimming, each

mouse was dried under an infrared heat lamp for 15 minutes and returned to their normal housing conditions.

Transverse aortic banding (TAB) surgery

Pathological remodeling was induced in wildtype C57Bl/6J male mice by constriction of the aorta. In brief, mice were anaesthetized with a mixture of ketamine and xylazine by IP injection and hairs were shaved from thorax. A tracheal tube was placed, connecting the mouse to a ventilator. After disinfection with Iodine and 70% ethanol, skin was incised left of the midline to allow access to the first intercostal space (between the first and second rib). Pectoral muscles were retracted, and the intercostal muscles cut caudal to the first rib. Retractors were placed to separate the thymus from the heart. The aorta was identified within the fatty tissue around the heart and a 6.0 silk suture was placed around the aorta between the first and the second branch. Suture was closed with a 26G needle in between to have a standard size aorta opening. Needle was removed immediately after closing suture. Thymus was replaced and the rib cage will be with 5.0 silk sutures. Pectoral muscles were replaced, and the skin was closed with a wound clip. After surgery, the tracheal tubing was removed, and the mice were placed on a nose cone with 100% oxygen until waking up. Buprenorphine (0.05-0.1 mg/kg) was administered postoperatively. During the whole procedure and recovery period the mice were placed on a 38°C heating pad.

Mouse injections

Sox17 overexpression was induced in wildtype C57Bl/6J male mice by tail vein injections with $3x10^{12}$ viral genomes and sacrificed 2 weeks or 8 weeks after injection, after which heart and other organs were harvested. Injections were performed just after TAB surgery, sham surgery, or without surgery.

Echocardiography

Cardiac function and heart dimensions were evaluated by 2-dimensional echocardiography using a Vevo® 2100 Ultrasound system (Visual Sonics). Mice were sedated with 5% isoflurane and anesthesia was maintained with 1-2% isoflurane. M-mode tracings from short axis view were used to measure internal diameter, anterior and posterior wall thicknesses at end diastole and end systole. The mean value of at least 9 cardiac cycles were used to determine the measurements for each animal. LV trace measurements from short axis view in M-mode were used to calculate fractional shortening (FS) and ejection fraction [32] and calculated by the Vevo® LAB 1.7.1 software as: FS(%) = 100* [(LVID;d – LVID;s)/ LVID;d], EF (%) = 100* [(LV Volume;d – LV Volume;s)/ LV Volume;d]. Blood flow was assessed using pulsed wave (PW)-mode, assisted by Color Doppler mode in aortic arch view.

Tissue collection

For cardiac tissue collection, mice were euthanized by cervical dislocation. The chest was opened to expose the heart. The heart was removed, washed in ice cold PBS, and weighed. For protein/RNA

analysis, the heart was snap frozen in liquid nitrogen. For CM sorting, the atria were removed, and the heart was immediately perfused by injection of 10ml of cold perfusion buffer into the left ventricle. After perfusion, the heart was removed and washed in cold perfusion buffer. Perfusion buffer contained 135mM NaCl, 4mM KCl, 1mM MgCl2, 10mM HEPES, 0,33 mM NaH2PO4, 10mM glucose, 10mM 2,3-butanedione monoxime (Sigma, St Louis, MO), 5mM taurine (Sigma), adjust pH to 7,2 at 37°C. Make a 10x stock without BDM and taurine, filter, and store at 4°C. Add BDM and taurine fresh. Perfused hearts were used for digestion. Left leg was collected, enzymatically digested with ProtK (Promega, 0.6µg/µl final concentration) in lysis buffer, and tibia length was measured with a digital caliper.

Digestion of the heart and CM isolation

After perfusing the heart, the ventricles were collected, and the tissue was minced into fine pieces using a scalpel and transferred into a glass vial with 1.5ml of cold digestion buffer. Digestion buffer was prepared as described below. The tissues were digested using a gently shaking (100rpm) 37°C water-bath for 15 min. The obtained cell suspension was gently pipetted up and down (10x) and transferred onto a 100µm cell strainer placed on top of a 50ml falcon tube. The tissue was gently rubbed through the strainer using the plunger of a 1ml syringe, after which the strainer was washed with 8.5ml of DMEM to obtain a total volume of 10ml, which was centrifuged for 6 min at 4°C at 300g. The cell pellet was suspended in 2-3ml of DMEM with DAPI 1:1000 for cell sorting [13].

1x digestion solutions (Suitable for 1/2 or 1/4 heart):

Liberase (Roche, 5401020001)
150µl Liberase TL (end conc. 0.5mg/ml)
30µl DNase I (end conc. 20ug/ml)
15µl Hepes 1M
1305µl DMEM
Comments: Dilute 1 vial in 1ml RNAse free water to final concentration of 50 mg/ml. Rotate 1/2h on roller bank at 4°C.

Imaging of the cells

After digestion of the heart 5000 cells were sorted into 96 wells plate and imaged using EVOS Cell Imaging Systems to visualize the morphology of the digested or sorted cells.

Fluorescence-activated cell sorting (FACS)

Freshly collected cardiac cell lysates were resuspended in 2-3mL DMEM with DAPI 1:1000 and stored on ice until sorting using a FACS Aria SORP (BD bioscience). Living single cells were sorted based on

multiple scatter strategies. Forward scatter and side scatter area (FSC-Area and SSC-Area) we selected for cells that were DAPI negative, tdTomato fluorescent in 640 and 561 nm and auto-fluorescent in 488 and 460 nm, considering that living heart cells are brighter in those channels. Next, based on FSC-Height and FSC-Area we selected for single cells and excluded cell debris. Finally, by using FSC-Width we were able to pick more elongated cells. Cells were sorted into Eppendorf tubes containing TRIzol and frozen down at -80°C.

RNA isolation and quality control

To isolate RNA, we used TRIzol® reagent (Life Technologies) following the manufacturer's instructions. The RNA concentration was assessed by a NanoDrop Spectrophotometer. To assess the RNA quality, an aliquot of RNA was diluted to 200-5000pg/µl and put on a bioanalyzer using Agilent RNA 6000 Pico Kit according to the manufacturer's instructions.

Quantitative real-time PCR

Total RNA (1µg) was applied to mRNA-based reverse transcription using an iScript cDNA Synthesis Kit (Bio-Rad). Real-time PCR was performed according to based SYBRgreen methodology (Bio-Rad). Transcript quantities were normalized for endogenous loading. Fold changes in gene expression were calculated according to the $2^{-\Delta\Delta Ct}$-method and expressed as mean fold change ± SEM.

Protein isolation and Western blotting

Protein was isolated from left ventricular tissue by grinding the tissue in RIPA buffer supplemented with protease inhibitor cocktail (Roche #11836170001) followed by protein quantification using the Bradford protein assay (Bio-Rad). Proteins were separated by SDS-PAGE and transferred to PVDF membranes (Bio-Rad). Membranes were blocked for 1 hour at room temperature (RT), and overnight incubated with primary antibodies at 4 °C. The next day, membranes were washed with TBS-T (3x 5 min) and incubated with an HRP-conjugated secondary antibody for 45 min at RT. Western blots were developed using ECL kit (Bio-Rad) and visualized using an ImageQuant LAS4000 (GE Healthcare Europe). For SOX17 detection we used mouse anti-Sox17 (Santa Cruz, #sc-130295).

Histology and microscopy

Adult hearts were excised from euthanized mice, washed in cold PBS, and fixed with 4% formalin at RT for 48h, embedded in paraffin and sectioned at 4µm. Cultured CMs on coverslips were washed with PBS and fixed with 4% formaldehyde at RT for 20 min. Sections were used for different staining.

Hematoxylin and eosin (H&E) and picrosirius red (SR) staining

We used standard procedures. 4-chamber views or short axis cross-section view and high magnification images were made using a Leica DM 4000 microscope and Leica LAS software. The fibrotic area in the ventricles was quantified using ImageJ 1.49v software. Quantifications were based on 2-4 hearts per experimental group.

WGA-staining

Tissue sections went through a process of deparaffinization, cell borders were stained with fluorescein isothiocyanate (FITC) labeled Wheat Germ Agglutinin (WGA) lectin (100 µg/ml final concentration, Sigma-Aldrich, L4895). Images were generated using a Leica TCS SPE and Leica LAS software. Cell surface area (CSA) was measured using ImageJ 1.49v software. Quantifications were based on >50 cells per heart and 5-6 hearts per experimental group.

Immunohistochemistry

Tissue sections went through a process of deparaffinization, rehydration, heat induced antigen retrieval and blocking with 1% BSA. The sections were incubated with specific primary antibodies overnight at 4°C. After washing with PBS, the sections were incubated with secondary antibodies for 1 hour at RT, washed and sealed with a mounting medium containing DAPI (Vector Laboratories). Cultured CMs on cover-slips were incubated with Blocking buffer with 1% Fish gelatin, and incubated with a specific primary antibody 25 min at RT. After washing with blocking buffer, the cover-slips were incubated with secondary antibodies for 25 minutes at RT, washed with milliQ water and sealed with a mounting medium containing DAPI. The images were taken using the Leica TCS SPE confocal microscope. Antibodies used:

Antibody	**Source**
Mouse anti- a actinin (ACTN2)	Sigma-Aldrich #A7732
Goat anti-tdTomato	Sicgen AB8181-200
Anti-mouse Alexa-488	Life technologies
Anti-goat Alexa-568	Life technologies

RNA-sequencing of sorted CMs

For sorted cells bulk sequencing, CELseq1 [33] preparation was applied using the MessageAMP II aRNA amplification kit (ThermoFisher Sceintific) until in vitro transcription (IVT) step. Final library preparation was continued according to the CELseq2 manual[5]. Primers consisted of a 24 bp polyT stretch, a 4bp random molecular barcode, a cell-specific 6bp barcode, the 5' Illumina TruSeq small RNA kit adaptor and a T7 promoter. After addition of this CELseq primers, mRNA was then reverse transcribed, converted into double-stranded cDNA, pooled and IVT for linear amplification following the CEL-Seq 2 protocol. The aRNA that resulted from the IVT was then again reverse transcribed using a Random Hexamer primer as described in the CELseq2 protocol. From this cDNA, Illumina sequencing libraries were then prepared with the TruSeq small RNA primers (Illumina) and sequenced paired-end at 75 bp read length.

Data analysis of CM RNA-sequencing

Paired-end reads from Illumina sequencing were mapped with BWA-ALN to the reference genome *Mus musculus* GRCm38 (version 0.7.10). Transcript count for every gene was recorded. Differential gene expression between groups was calculated using R and the DESeq2 package [34]. Up- and downregulated genes were identified as genes that changed log2 fold change of 1 or -1 (up or down, respectively) in TAB animals compared to sham animals at the same timepoint. Lists of up- or downregulated genes were submitted to the online database for annotation, visualization and integrated discovery (DAVID) [35],[36] to identify enriched GO-terms in these differentially expressed genes.

RNA-sequencing of heart tissue

RNA from ventricular tissue of sham and TAB animals was used for whole-transcriptome (RNA-seq) analysis. RNA-seq libraries were created from rRNA-depleted RNA using Truseq stranded total RNA library prep kit with ribo-zero (Illumina). Next, strand-specific single-end 75bp reads were generated on an Illumina Nextseq 500.

Data analysis of heart tissue RNA-sequencing

Reads were aligned and quantified against the *Mus musculus* reference genome (GRCm38) using STAR workflow. Lists of significantly upregulated ($p<0.05$; fold change >1.5) and downregulated ($p<0.05$; fold change <0.7) were submitted in the database for annotation to DAVID to identify enriched GO-terms in these differentially expressed genes. Indicated pathways have a significant gene enrichment score ($p<0.10$).

AAV9 generation

The murine Sox17 cDNA was amplified using the forward (5'gcgctagtcgacATGAGCAGCCCGGATGCG3') and reverse (5'gcgctaaagcttTCAAATGTCGGGGTAGTTGC3') primers and cloned via SalI and HindIII restriction sites into the AAV vector (under control of CMV promoter) and was subsequently used for AAV generation. AAV9 were generated in collaboration with M. Giacca, by the AAV Vector Unit at ICGEB Trieste (http://www.icgeb.org/avu-core-facility.html) following a protocol previously described [37]. AAV9s encoding empty pAAV vector were used as control.

HOMER

Transcription factor motif enrichment analysis in proximal promoters was performed using the findMotifs.pl function from the Homer suite (v4.10, Heinz et al., 2010), using all expressed genes ($p<0.05$; fold change >1.5 or <0.7) as background and promoter length set to -100 to +100bp [38].

oPOSSUM

Identification of genes containing predicted transcription binding sites was performed using the web-based system for the detection of over-represented transcription factor binding sites oPOSSUM (http://opossum.cisreg.ca/oPOSSUM3/) in the upregulated gene set. The list of SOX17 target gene

hits was used, and genes with the motif present at the promoter region encompassed between 100 bp upstream and 100 bp downstream of the transcription starting site were selected. Genes were ordered by the absolute score of the predicted binding site sequence given by the weight matrix profile.

Statistical analysis.

Values are presented as mean ± SEM in bar graphs or ±SD in tables. Outliers were identified and excluded using a Grubbs test (GraphPad, using α=0.05). Statistical significance was evaluated using an unpaired *t*-test for comparisons between two groups or one-way ANOVA for comparison of several groups. Analyses were performed using the GraphPad Prism Version 8.0e software. * indicates $p < 0.05$ and was considered statistically significant compared to control.

Autor contribution

Conception and design of the research: M.V.G., C.D., E.V.R.; acquisition of data: M.V.G., C.D., D.V., H.R., L.K., J.E., M.W., C.P.; analysis and interpretation of the data: M.V.G., C.D., K.B., E.V.R.; statistical analysis: M.V.G., C.D.; supervising the experiments: C.B., E.V.R.; drafting the manuscript: M.V.G., C.D., E.V.R.; critical revision of the manuscript for important intellectual content: E.V.R.

Acknowledgements

We thank Utrecht Sequencing Facility for providing sequencing service and data. Utrecht Sequencing Facility is subsidized by the University Medical Center Utrecht, Hubrecht Institute, Utrecht University and The Netherlands X-omics Initiative (NWO). We thank Jeroen Korving for his help with the histology and we thank Anko de Graaff and the Hubrecht Imaging Center for supporting the imaging. We thank ICMS animation studio for providing help with animation.

References

1. Nakamura M and Sadoshima J. Mechanisms of physiological and pathological cardiac hypertrophy. *Nat Rev Cardiol*. 2018;15:387-407.

2. Shephard RJ and Balady GJ. Exercise as cardiovascular therapy. *Circulation*. 1999;99:963-72.

3. Chaanine AH and Hajjar RJ. AKT signalling in the failing heart. *Eur J Heart Fail*. 2011;13:825-9.

4. Bei Y, Fu S, Chen X, Chen M, Zhou Q, Yu P, Yao J, Wang H, Che L, Xu J and Xiao J. Cardiac cell proliferation is not necessary for exercise-induced cardiac growth but required for its protection against ischaemia/reperfusion injury. *J Cell Mol Med*. 2017;21:1648-1655.

5. Bostrom P, Mann N, Wu J, Quintero PA, Plovie ER, Panakova D, Gupta RK, Xiao C, MacRae CA, Rosenzweig A and Spiegelman BM. C/EBPbeta controls exercise-induced cardiac growth and protects against pathological cardiac remodeling. *Cell*. 2010;143:1072-83.

6. Zhang Z, Yao L, Yang J, Wang Z and Du G. PI3K/Akt and HIF1 signaling pathway in hypoxiaischemia (Review). *Mol Med Rep*. 2018;18:3547-3554.

7. Mukherjee S, Chaturvedi P, Rankin SA, Fish MB, Wlizla M, Paraiso KD, MacDonald M, Chen X, Weirauch MT, Blitz IL, Cho KW and Zorn AM. Sox17 and beta-catenin co-occupy Wnt-responsive enhancers to govern the endoderm gene regulatory network. *Elife*. 2020;9.

8. Lacraz GPA, Junker JP, Gladka MM, Molenaar B, Scholman KT, Vigil-Garcia M, Versteeg D, de Ruiter H, Vermunt MW, Creyghton MP, Huibers MMH, de Jonge N, van Oudenaarden A and van Rooij E. Tomo-Seq Identifies SOX9 as a Key Regulator of Cardiac Fibrosis During Ischemic Injury. *Circulation*. 2017;136:1396-1409.

9. Zhou Y, Williams J, Smallwood PM and Nathans J. Sox7, Sox17, and Sox18 Cooperatively Regulate Vascular Development in the Mouse Retina. *PLoS One*. 2015;10:e0143650.

10. Zhu N, Welch CL, Wang J, Allen PM, Gonzaga-Jauregui C, Ma L, King AK, Krishnan U, Rosenzweig EB, Ivy DD, Austin ED, Hamid R, Pauciulo MW, Lutz KA, Nichols WC, Reid JG, Overton JD, Baras A, Dewey FE, Shen Y and Chung WK. Rare variants in SOX17 are associated with pulmonary arterial hypertension with congenital heart disease. *Genome Med*. 2018;10:56.

11. Wan WG, Jiang XJ, Li XY, Zhang C, Yi X, Ren S and Zhang XZ. Enhanced cardioprotective effects mediated by plasmid containing the short-hairpin RNA of angiotensin converting enzyme with a biodegradable hydrogel after myocardial infarction. *J Biomed Mater Res A*. 2014;102:3452-8.

12. Huang J, Ito Y, Morikawa M, Uchida H, Kobune M, Sasaki K, Abe T and Hamada H. Bcl-xL gene transfer protects the heart against ischemia/reperfusion injury. *Biochem Biophys Res Commun*. 2003;311:64-70.

13. Gladka MM, Molenaar B, de Ruiter H, van der Elst S, Tsui H, Versteeg D, Lacraz GPA, Huibers MMH, van Oudenaarden A and van Rooij E. Single-Cell Sequencing of the Healthy and Diseased Heart Reveals Cytoskeleton-Associated Protein 4 as a New Modulator of Fibroblasts Activation. *Circulation*. 2018;138:166-180.

14. Hotta K, Chen B, Behnke BJ, Ghosh P, Stabley JN, Bramy JA, Sepulveda JL, Delp MD and Muller-Delp JM. Exercise training reverses age-induced diastolic dysfunction and restores coronary microvascular function. *J Physiol*. 2017;595:3703-3719.

15. Celik M, Yalcinkaya E, Yuksel UC, Gokoglan Y, Bugan B, Kabul HK and Barcin C. The effect of age on right ventricular diastolic function in healthy subjects undergoing treadmill exercise test. *Echocardiography*. 2015;32:436-42.

16. Miyata S, Minobe W, Bristow MR and Leinwand LA. Myosin heavy chain isoform expression in the failing and nonfailing human heart. *Circ Res*. 2000;86:386-90.

17. Agah R, Frenkel PA, French BA, Michael LH, Overbeek PA and Schneider MD. Gene recombination in postmitotic cells. Targeted expression of Cre recombinase provokes cardiac-restricted, site-specific rearrangement in adult ventricular muscle in vivo. *J Clin Invest*. 1997;100:169-79.

18. Madisen L, Zwingman TA, Sunkin SM, Oh SW, Zariwala HA, Gu H, Ng LL, Palmiter RD, Hawrylycz MJ, Jones AR, Lein ES and Zeng H. A robust and high-throughput Cre reporting and characterization system for the whole mouse brain. *Nat Neurosci*. 2010;13:133-40.

19. Vigil-Garcia M, Demkes CJ, Eding JEC, Versteeg D, de Ruiter H, Perini I, Kooijman L, Gladka MM, Asselbergs FW, Vink A, Harakalova M, Bossu A, van Veen TAB, Boogerd CJ and van Rooij E. Gene expression profiling of hypertrophic cardiomyocytes identifies new players in pathological remodeling. *Cardiovasc Res*. 2020.

20. Kawasaki E, Hokari F, Sasaki M, Sakai A, Koshinaka K and Kawanaka K. Role of local muscle contractile activity in the exercise-induced increase in NR4A receptor mRNA expression. *J Appl Physiol (1985)*. 2009;106:1826-31.

21. Medzikovic L, van Roomen C, Baartscheer A, van Loenen PB, de Vos J, Bakker E, Koenis DS, Damanafshan A, Creemers EE, Arkenbout EK, de Vries CJM and de Waard V. Nur77 protects against adverse cardiac remodelling by limiting neuropeptide Y signalling in the sympathoadrenal-cardiac axis. *Cardiovasc Res*. 2018;114:1617-1628.

22. Hauck L, Grothe D and Billia F. p21(CIP1/WAF1)-dependent inhibition of cardiac hypertrophy in response to Angiotensin II involves Akt/Myc and pRb signaling. *Peptides*. 2016;83:38-48.

23. Lee SH, Lee S, Yang H, Song S, Kim K, Saunders TL, Yoon JK, Koh GY and Kim I. Notch pathway targets proangiogenic regulator Sox17 to restrict angiogenesis. *Circ Res*. 2014;115:215-26.

24. Zincarelli C, Soltys S, Rengo G and Rabinowitz JE. Analysis of AAV serotypes 1-9 mediated gene expression and tropism in mice after systemic injection. *Mol Ther*. 2008;16:1073-80.

25. Suurmeijer AJ, Clement S, Francesconi A, Bocchi L, Angelini A, Van Veldhuisen DJ, Spagnoli LG, Gabbiani G and Orlandi A. Alpha-actin isoform distribution in normal and failing human heart: a morphological, morphometric, and biochemical study. *J Pathol*. 2003;199:387-97.

26. Pugach EK, Richmond PA, Azofeifa JG, Dowell RD and Leinwand LA. Prolonged Cre expression driven by the alpha-myosin heavy chain promoter can be cardiotoxic. *J Mol Cell Cardiol*. 2015;86:54-61.

27. Boogerd CJ, Wong LY, van den Boogaard M, Bakker ML, Tessadori F, Bakkers J, t Hoen PA, Moorman AF, Christoffels VM and Barnett P. Sox4 mediates Tbx3 transcriptional regulation of the gap junction protein Cx43. *Cell Mol Life Sci*. 2011;68:3949-61.

28. Holopainen T, Rasanen M, Anisimov A, Tuomainen T, Zheng W, Tvorogov D, Hulmi JJ, Andersson LC, Cenni B, Tavi P, Mervaala E, Kivela R and Alitalo K. Endothelial Bmx tyrosine kinase activity is essential for myocardial hypertrophy and remodeling. *Proc Natl Acad Sci U S A*. 2015;112:13063-8.

29. Hathaway CK, Grant R, Hagaman JR, Hiller S, Li F, Xu L, Chang AS, Madden VJ, Bagnell CR, Rojas M, Kim HS, Wu B, Zhou B, Smithies O and Kakoki M. Endothelin-1 critically influences cardiac function via superoxide-MMP9 cascade. *Proc Natl Acad Sci U S A*. 2015;112:5141-6.

30. Min JK, Park H, Choi HJ, Kim Y, Pyun BJ, Agrawal V, Song BW, Jeon J, Maeng YS, Rho SS, Shim S, Chai JH, Koo BK, Hong HJ, Yun CO, Choi C, Kim YM, Hwang KC and Kwon YG. The WNT antagonist Dickkopf2 promotes angiogenesis in rodent and human endothelial cells. *J Clin Invest*. 2011;121:1882-93.

31. Taniike M, Yamaguchi O, Tsujimoto I, Hikoso S, Takeda T, Nakai A, Omiya S, Mizote I, Nakano Y, Higuchi Y, Matsumura Y, Nishida K, Ichijo H, Hori M and Otsu K. Apoptosis signal-regulating kinase 1/p38 signaling pathway negatively regulates physiological hypertrophy. *Circulation*. 2008;117:545-52.

32. Wu R, Wyatt E, Chawla K, Tran M, Ghanefar M, Laakso M, Epting CL and Ardehali H. Hexokinase II knockdown results in exaggerated cardiac hypertrophy via increased ROS production. *EMBO Mol Med*. 2012;4:633-46.

33. Hashimshony T, Senderovich N, Avital G, Klochendler A, de Leeuw Y, Anavy L, Gennert D, Li S, Livak KJ, Rozenblatt-Rosen O, Dor Y, Regev A and Yanai I. CEL-Seq2: sensitive highly-multiplexed single-cell RNA-Seq. *Genome Biol*. 2016;17:77.

34. Love MI, Huber W and Anders S. Moderated estimation of fold change and dispersion for RNA-seq data with DESeq2. *Genome Biol*. 2014;15:550.

35. Huang da W, Sherman BT and Lempicki RA. Systematic and integrative analysis of large gene lists using DAVID bioinformatics resources. *Nat Protoc*. 2009;4:44-57.

36. Huang da W, Sherman BT and Lempicki RA. Bioinformatics enrichment tools: paths toward the comprehensive functional analysis of large gene lists. *Nucleic Acids Res*. 2009;37:1-13.

37. Arsic N, Zentilin L, Zacchigna S, Santoro D, Stanta G, Salvi A, Sinagra G and Giacca M. Induction of functional neovascularization by combined VEGF and angiopoietin-1 gene transfer using AAV vectors. *Mol Ther*. 2003;7:450-9.

38. Heinz S, Benner C, Spann N, Bertolino E, Lin YC, Laslo P, Cheng JX, Murre C, Singh H and Glass CK. Simple combinations of lineage-determining transcription factors prime cis-regulatory elements required for macrophage and B cell identities. *Mol Cell*. 2010;38:576-89.

SUPPLEMENTARY MATERIAL

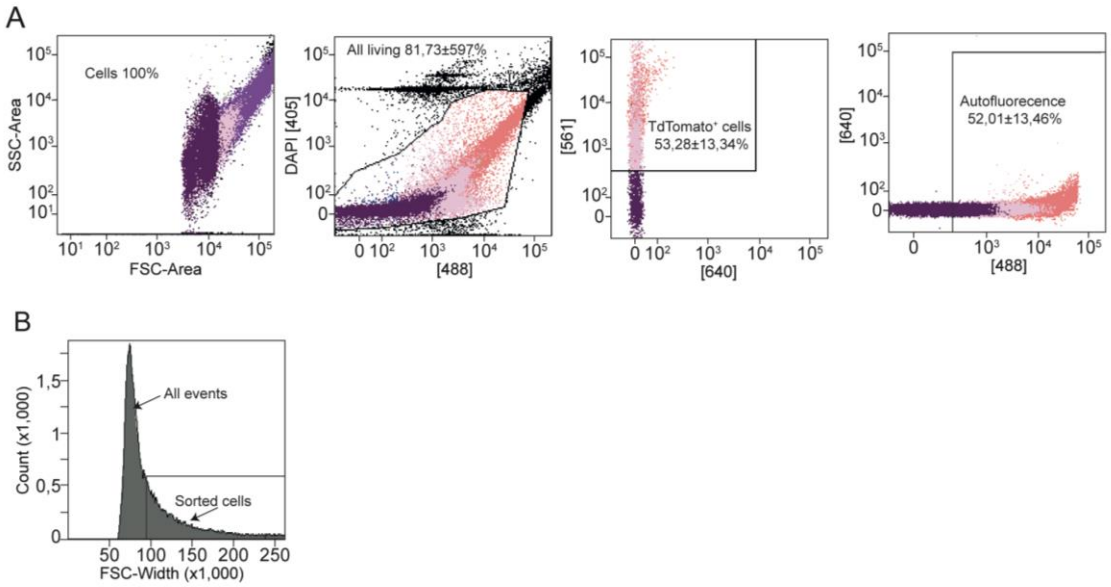

Figure S1. Representative FAC plots for sorting CMs. A, Representative FACS plots showing the gating strategy to obtain tdTomato positive CMs. Selections are based on DAPI negativity, tdTomato positivity and green auto-fluorescence. Data expressing the average ± STDEV percentage of all sorted hearts. **B**, Forward scatter (FSC)-width plot showing the fraction of sorted cells compared to all events.

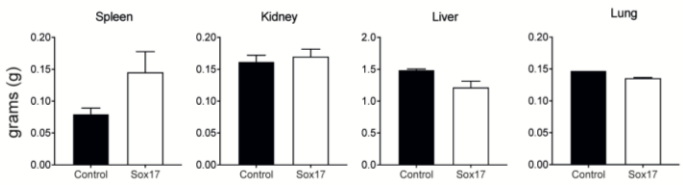

Figure S2. Morphological analysis 2 weeks after AAV9-mediated Sox17 overexpression in wildtype animals.

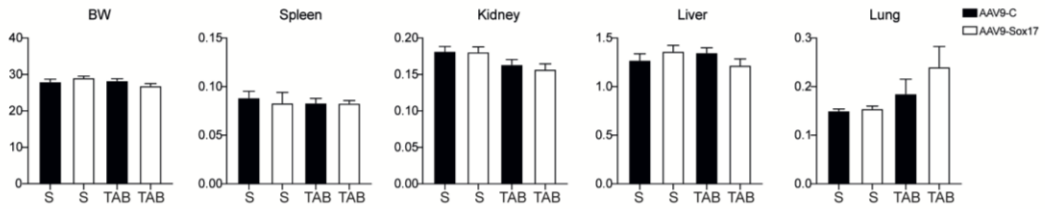

Figure S3. Morphological analysis 8 weeks after pressure overload (TAB) or sham (S) surgery.

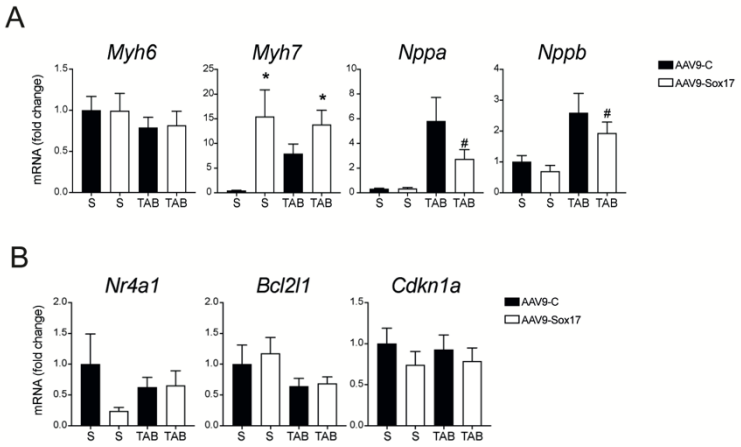

Figure S4. Sox17 overexpression during pressure overload does not induce cardioprotective factors. **A,** Real-time PCR analysis of cardiac stress markers in heart tissue after empty AAC (AAV9-C) or AAV9-Sox17 injection in sham (S) or TAB groups (n=6-8). **B,** Real-time PCR analysis of exercise-induced markers in heart tissue after AAV9-C or AAV9-Sox17 injection in S or TAB groups (n=6-8). Data expressed as mean fold change ± SEM; * indicates p<0.05 compared to AAV9-C with unpaired t-test. # indicates p<0.05 compared to S with unpaired t-test.

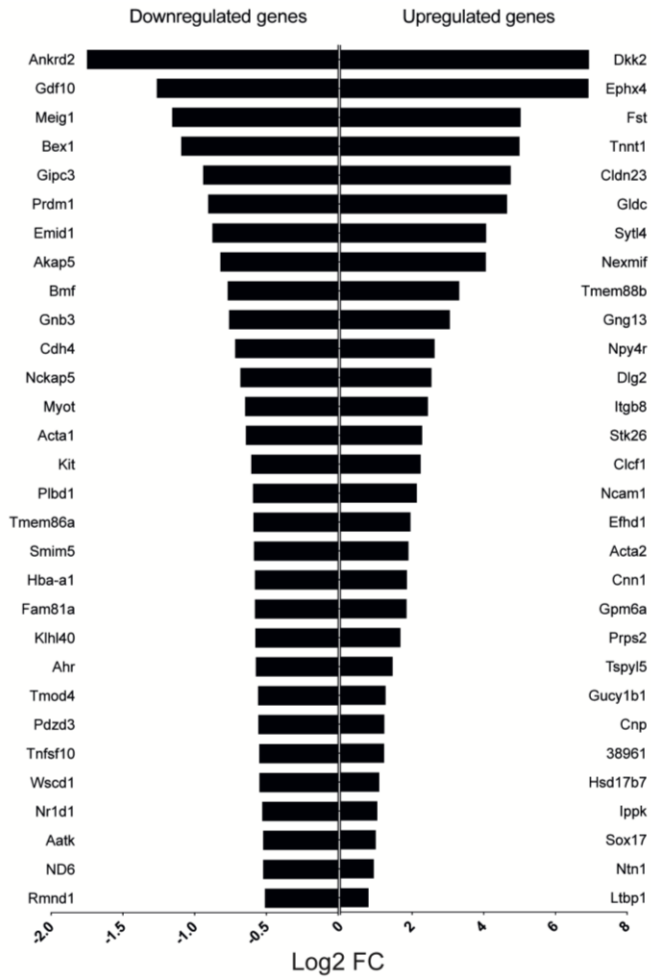

Figure S5. Top 30 regulated genes during pressure overload after Sox17 overexpression.

	Sedentary (n=6)	**Exercise** (n=7)
IVRT (ms)	17,69 ±1,47	14,13 ±1,97*
BPM	424,56 ±42,59	407,13 ±25,90
LVAW;d (mm)	0,68 ±0,11	0,70 ±0,10
LVID;d (mm)	4,14 ±0,16	4,27 ±0,29
LVPW;d (mm)	0,60 ±0,08	0,60 ±0,07
LVAW;s (mm)	1,04 ±0,14	1,09 ±0,14
LVID;s (mm)	3,01 ±0,18	3,03 ±0,24
LVPW;s (mm)	0,97 ±0,10	0,96 ±0,13
EF (%)	53,20 ±6,19	55,76 ±5,79
FS (%)	27,19 ±4,05	28,94 ±3,94

Table S1. Echocardiogram results from sedentary and exercised mice. Left ventricular anterior wall (LVAW); Left ventricular internal diameter (LVID); Left ventricular posterior wall (LVPW) are measured in both diastole (;d) and systole (;s). Ejection fraction [32] and fractional shortening [21] were calculated from short axes M-mode measurements by Vevo® LAB 1.7.1 software. Mean ± SD is shown. * indicates $p<0.05$ for exercise compared to sedentary.

Table S2. Upregulated genes with enriched Sox17 binding sites.

Gene ID(s)	Ensembl ID(s)	Chr	Gene Start	Gene End	Strand	Nearest TSS	TFBS Start	TFBS End	TFBS Rel. Start	TFBS Rel. End	TFBS Strand	Score	%Score	TFBS Sequence
Bmx	ENSMUSG00000031377	X	1,61E+08	160696125	-	1,61E+08	160696150	1,61E+08	-33	-25	+	10.760	97.1%	TTTATTGTC
Rrm2	ENSMUSG00000020649	12	25393106	25399011	+	25393617	25393575	25393583	-42	-34	+	10.459	96.1%	TGCATTGTC
Aplp1	ENSMUSG00000006651	7	31220001	31230580	-	31230580	31230652	31230660	-80	-72	-	9.869	94.2%	GCTATTGTC
Tnnt1	ENSMUSG00000064179	7	4456172	4467984	-	4466217	4466249	4466257	-40	-32	-	9.869	94.2%	GCTATTGTC
						18918961	18919014	18919022	-61	-53	-	9.768	93.9%	TGCATTGTG
Olfml2b	ENSMUSG00000038463	1	172574663	172612920	+	172574663	172574608	172574616	-55	-47	-	9.669	93.6%	TCTATTGTG
Edn1	ENSMUSG00000021367	13	42396639	42403358	+	42396639	42396560	42396568	-79	-71	-	9.581	93.3%	ATCATTGTT
Cd24a	ENSMUSG00000047139	10	43298975	43304068	+	43298975	43298925	43298933	-50	-42	+	9.178	92%	GCTATTGTG
						42396639	42396602	42396610	-37	-29	-	8.868	91%	TGTATTGTG
						51893529	51893521	51893529	-8	1	+	8.826	90.8%	CTAATTGTG
						134025657	134025569	134025577	-88	-80	+	8.188	88.8%	ATCATTGGC
Arc	ENSMUSG00000022602	15	74499513	74503000	-	74503000	74503071	74503079	-79	-71	+	8.097	88.5%	CCCATTGGC
Cenpf	ENSMUSG00000026605	1	191464478	191511965	-	191511965	191512029	191512037	-72	-64	+	8.097	88.5%	CCCATTGGC
						21903725	21903649	21903657	-76	-68	-	8.097	88.5%	CCCATTGGC
Gldc	ENSMUSG00000024827	19	30172939	30249908	-	30249908	30249992	30250000	-92	-84	-	8.097	88.5%	CCCATTGGC
Ube2c	ENSMUSG00000001403	2	164595398	164604322	+	164595398	164595338	164595346	-60	-52	+	8.097	88.5%	CCCATTGGC
						98691624	98691579	98691587	-45	-37	+	7.950	88%	TTGATTGTG
Dkk2	ENSMUSG00000028031	3	1,32E+08	131843257	+	1,32E+08	131748174	1,32E+08	-82	-74	+	7.946	88%	CTCTTTGTC
						98821002	98820952	98820960	-50	-42	-	7.946	88%	CTCTTTGTC
						4466217	4466295	4466303	-86	-78	-	7.946	88%	TTCTTTGTC
Kcna4	ENSMUSG00000042604	2	107130796	107138659	+	107131552	107131596	107131604	45	53	+	7.789	87.5%	TGTATTGTT
						112090978	112090973	112090981	-3	6	+	7.637	87%	ATCACTGTC
						129122948	129122983	129122991	-43	-35	-	7.596	86.9%	TTTATTGGC
Ephx4	ENSMUSG00000033805	5	107831755	107859054	+	107834804	107834801	107834809	-3	6	+	7.536	86.7%	TACATTGTA
Igfbp6	ENSMUSG00000023046	15	101974793	101979942	+	101974793	101974754	101974762	-39	-31	-	7.347	86.1%	CAAATTGTT
Myh7	ENSMUSG00000053093	14	55589525	55613471	-	55613471	55613562	55613570	-99	-91	-	7.347	86.1%	CCAATTGTT
Tnfaip6	ENSMUSG00000053475	2	51893529	51912206	+	51893529	51893480	51893488	-49	-41	-	7.296	85.9%	TGCATTGGC
Ckap2l	ENSMUSG00000048327	2	129093946	129122948	-	129122948	129122955	129122963	-15	-7	+	7.197	85.6%	CCTATTGGC

Enriched GO Pathway Upregulated genes	Genes
mitotic cytokinesis	CKAP2, KIF23, ZFP365, PLK1, ANLN, CEP55, STMN1, KIF20A
mitotic nuclear division	KIF23, NEK2, NUF2, TPX2, ANLN, AURKA, CEP55, KNSTRN, UBE2C, SPC25, CDCA8, NCAPH, PLK1, ZWILCH, CCNA2
cell division	KIF23, PRC1, NEK2, NUF2, TPX2, ANLN, AURKA, CEP55, KNSTRN, UBE2C, CCNE1, SPC25, CDCA8, NCAPH, PLK1, ZWILCH, CCNA2
cell cycle	CKAP2, KIF23, TRNP1, PRC1, NEK2, NUF2, TPX2, ANLN, AURKA, CEP55, KNSTRN, UBE2C, CCNE1, SPC25, CDCA8, NCAPH, PLK1, ZWILCH, CCNA2
cell surface receptor signaling pathway	NCAM1, EDN3, FCGR2B, CLCF1, GIPR, EDN1, NPY4R, CD24A, FCGR3
axonogenesis	IFIT2, IFIT1, ACTA2, IFI27L2A, STMN1, MX1
mitotic sister chromatid segregation	CDCA8, PLK1, NEK2, KNSTRN
homotypic cell-cell adhesion	NCAM1, CD24A, MEGF10
cytokinesis	KIF23, PRC1, PLK1, KIF20A
positive regulation of cell differentiation	EDN3, CCNE1, SOX17, GDNF

Enriched GO Pathway Downregulated genes	Genes
skeletal muscle fiber development	ACTA1, KLHL40, CACNA1S
positive regulation of release of cytochrome c from mitochondria	TNFSF10, GPER1, BMF
positive regulation of extrinsic apoptotic signaling pathway	TNFSF10, AGT, GPER1
positive regulation of vasodilation	AGT, GPER1, KCNMB1
negative regulation of protein ubiquitination	KLHL40, SOX4, RASD2
regulation of ion transmembrane transport	KCNJ5, SCN4B, CACNA1S, SCN4A
ion transport	KCNJ5, TMC8, SCN4B, CACNA1S, PDZD3, SCN4A, KCNMB1
muscle contraction	TMOD4, TPM2, CACNA1S
cellular oxidant detoxification	HBA-A1, HBA-A2
positive regulation of gene expression	ACTA1, AGT, GPER1, KIT, PRDM1

Table S3. Regulated genes in GO pathway analysis.

CHAPTER 4

HYDROGEL-BASED DELIVERY OF ANTIMIR-195 IMPROVES CARDIAC EFFICACY AFTER ISCHEMIC INJURY

Joep E.C. Eding[1*], **Marta Vigil-Garcia[1*],** Marit Vink[1], Charlotte J. Demkes[1,2], Danielle Versteeg[1,2], Lieneke Kooijman[1], Maarten H. Bakker[3], Maaike J.G. Schotman[3], Patricia Y.W. Dankers[3], Eva van Rooij[1,2]

[1]Hubrecht Institute, KNAW and University Medical Center Utrecht, 3584CT Utrecht, the Netherlands
[2]Department of Cardiology, University Medical Center Utrecht, 3584CT Utrecht, the Netherlands
[3]Institute for Complex Molecular Systems, Department of Biomedical Engineering, Laboratory of Chemical Biology, Eindhoven University of Technology, 5600MB Eindhoven, the Netherlands

* These authors contributed equally to this article

Submitted manuscript to Advanced Healthcare Materials

Key words: Hydrogel, antimiR, microRNA, drug delivery, cardiac regeneration

ABSTRACT

Background MicroRNAs are potent regulators of biology and disease. The *miR-15* family has been shown to regulate cardiomyocyte proliferation and antimiR-based inhibition induces a cardioprotective effect after myocardial infarction in mice. However, systemic delivery of antimiRs leads to accumulation in kidneys and liver, with relatively poor cardiac exposure. pH-responsive injectable hydrogels serve as a sustained-release drug delivery depot and could potentially be used to improve cardiac efficacy of antimiR therapeutics.

Objective Examine whether hydrogel can improve local delivery of antimiR-195 in ischemic hearts to increase cardiac efficacy and limit off-target effects.

Methods Study the effect of intramyocardial injections of hydrogel-formulated antimiR-195 under both baseline conditions and after ischemic injury.

Results Intracardiac injections of UPy-PEG induced a transient inflammatory response that was no longer present 7 days post-injection. *In vitro* experiments showed that antimiR-195 was released from the gel, and induced microRNA inhibition leading to downstream cardiomyocyte proliferation. *In vivo*, intramyocardial delivery of antimiR-195 in UPy-PEG enhanced cardiac target de-repression compared to PBS-dissolved antimiR-195, despite a low cardiac retention. After ischemic injury, this translated into a greater therapeutic effect by increasing both target de-repression and cardiomyocyte proliferation.

Conclusions UPy-PEG can be used as a cardiac delivery vehicle of antimiRs and intramyocardial injection of UPy-PEG formulated antimiR-195 is sufficient to improve cardiac efficacy of antimiR-195. Follow up experiments in large animals will enable us to assess the true added value of using UPy-PEG to increase cardiac exposure of antimiR therapies.

INTRODUCTION

Ischemic heart disease is one of the leading causes of death worldwide. Given the very limited endogenous proliferative capacity of adult human cardiomyocytes[1], the cardiomyocytes lost during myocardial infarction will not be regenerated to a meaningful extent. This loss of functional myocardium then activates maladaptive remodeling processes that put the patient at risk of developing heart failure[2]. Replacement of the lost cells by stem cell transplantation has shown promise in preclinical trials[3]. However, as it does not seem to restore cardiac function in clinical trials[4], the hope is that novel therapeutic strategies promoting the endogenous regenerative capacity of the myocardium will offer a solution.

MicroRNAs (miRs) are short, single-stranded oligonucleotides that suppress protein formation post-transcriptionally by binding to complementary sequences in the mRNA. They have been shown to have an important role in both cardiac pathophysiology, like hypertrophy[5] and fibrosis[6], as well as non-cardiac diseases like cancer[7]. Several strategies have been developed to either replace or inhibit pathologically regulated miRs[8], and are currently being tested in clinical studies[9-11].

The *miR-15* family is a group of 5 miRs (*miR-15a*, *miR-15b*, *miR-16*, *miR-195 and miR-497)* that share the same seed region, the region of the miR that governs mRNA targeting based on sequence complementarity[12]. The *miR-15* family has been shown to induce a strong inhibition of the cell cycle[13, 14]. Inhibition of the *miR-15* family with subcutaneously delivered antimiR has been shown to reduce infarct size in murine myocardial infarction (MI)[15, 16]. However, as true for most antimiRs, most of the injected compound ended up in the kidneys and liver[15], reducing cardiac exposure and increasing the chance of unwanted side effects.

Previous studies have proven the benefit of using hydrogels as an injectable vehicle to improve local delivery and reduce the risk of off-target effects by a local sustained-release drug delivery depot after intramyocardial injection. Burdick and co-workers developed an injectable hyaluronic acid based-hydrogel system[17], which provided a sustained release of miR-302 which promoted proliferation of cardiomyocytes. Another example was shown by Christman and co-workers where a hydrogel based on decellularized ECM was used to modulate the release rate of miRs and extracellular vesicles *in vitro*[18].

Koudstaal *et al*. pioneered the use of UPy-PEG hydrogel as a catheter-injectable sustained-release drug delivery depot for effective intramyocardial delivery of IGF-1/HGF in a porcine model of myocardial infarction[19]. This supramolecular hydrogel is based on the ureido-pyrimidinone moiety, which forms dimers due to the four-four hydrogen bonding moiety. Furthermore, fiber formation is induced by lateral stacking of the urea-groups present in the backbone. While no adverse effects of

UPy-PEG injection were observed, the study was not geared towards assessing safety of UPy-PEG for intramyocardial drug delivery in pigs.

Here, we investigate the use of UPy-PEG and a cationic charged UPy-PEG (UPy-Cat) for cardiac delivery of antimiR-195 to enhance cardiac repair after injury. Our data show that, despite low cardiac retention, the use of UPy-PEG for intramyocardial drug delivery is relatively safe and improves antimiR efficacy over delivery in PBS. These findings set the stage for future research in larger animal models and may aid the development of a novel therapeutic strategy to promote the endogenous regenerative capacity of the heart.

RESULTS

The *miR-15* family is induced after ischemic injury and represses pro-proliferative genes

The *miR-15* family consist of 5 members, all containing the same seed region (**Figure 1A**). To show the dynamics of cardiac expression of the *miR-15* family members in our model of ischemic injury, we subjected mice to permanent LAD ligation (MI) or LAD ligation followed by reperfusion (IR) [20] and quantified miR levels at several timepoints after injury. These data revealed *miR-16* and *miR-195* to be most abundant at baseline (**Supplemental Figure S1A**), and all *miR-15* family members showing significant and prolonged induction after injury, with the most pronounced increase seen for *miR-195* after IR (±7-fold) (**Figure 1B**, **Supplemental Figure S1B-F**). miR-15 family members have been shown to directly regulate several metabolic and cell cycle genes[21]. In analyzing the expression dynamics of several predicted *miR-15* family targets we observed an initial increase after surgery that peaked around 1-3 days after injury and declined towards baseline at later timepoints **(Figure 1C**). This suggests that miR-15 family inhibition after ischemic injury might be able to extend the induction of these proliferation related mRNA target genes leading to enhanced cardiac repair.

To start exploring whether the use of UPy-PEG hydrogel can enhance and prolong *miR-15* family inhibition in the heart, we opted to use antimiR-195 (an LNA-DNA mixmer[22]) as *miR-195* is highly expressed in the heart and showed the strongest increase in response to IR (**Figure 1B**). In addition, this antimiR is also expected to inhibit *miR-16* due to its sequence similarity with *miR-195* (**Figure 1A**). Therefore, antimiR-195 will inhibit the two *miR-15* family members that are most highly expressed at baseline and show the highest induction after injury.

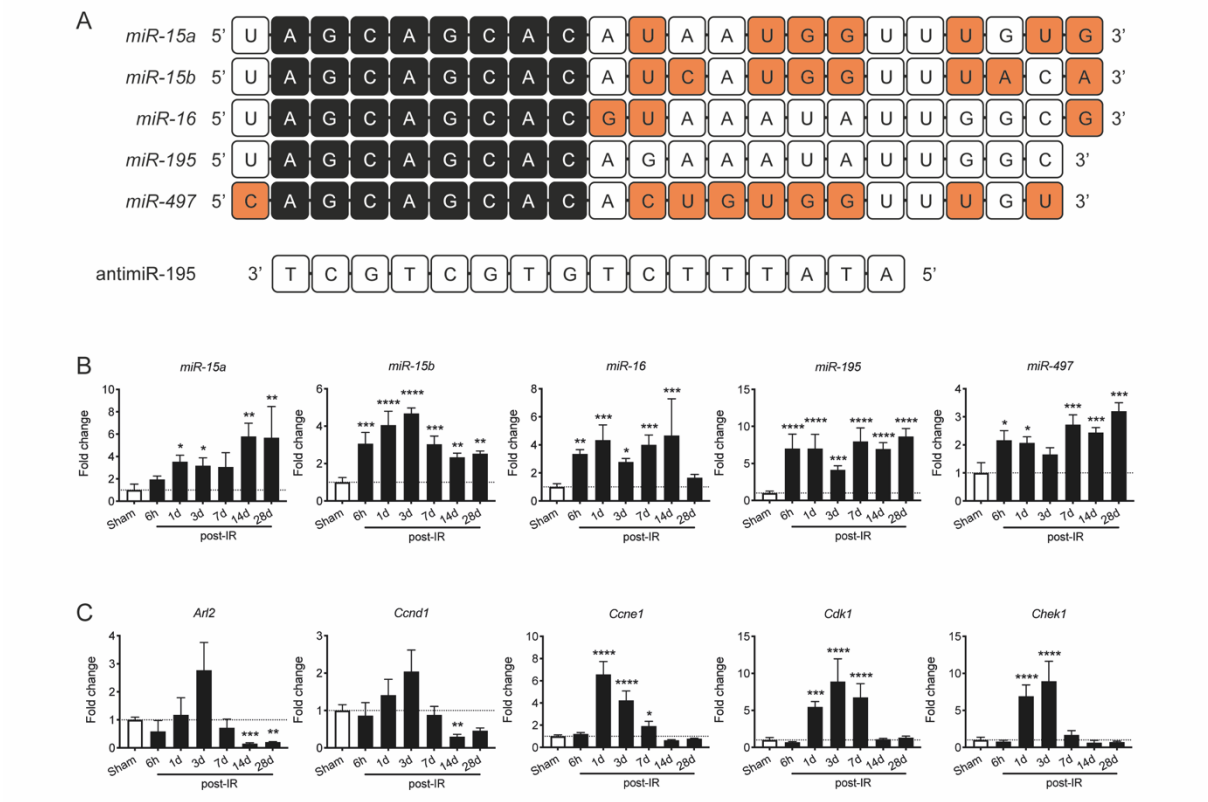

Figure 1. miR-15 family is induced in response to IR and represses pro-proliferative genes. (A) Schematic representation of the sequences of the mature miRs of the *miR-15* family. Black squares represent the seed sequence, orange squares are mismatches to *miR-195*. Below the miRs, the sequence of antimiR-195 is added. **(B)** RT-PCR quantification of *miR-15* family members in murine LV tissue at multiple timepoints after IR (n=6). **(C)** RT-PCR quantification of several predicted *miR-15* family targets in murine LV tissue at multiple timepoints after IR (n=6).

UPy-PEG-hydrogel is an injectable hydrogel that can be modified to tune drug-release properties

The hydrogel we aimed to test is based on the ureido-pyrimidinone (UPy) moiety, which is known to form dimers by four-fold hydrogen bonding. It contains urea moieties protected by an alkyl spacer that induces lateral stacking. Furthermore, it is functionalized with a poly(ethylene glycol) chain (UPy-PEG) and has been shown to have pH-responsiveness[23]. It is a viscous liquid at pH > 8.5, which facilitates drug incorporation and (catheter) injection, and gelates when pH is reduced in contact with the *in vivo* environment (**Figure 2A**). Introduction of a monofunctional UPy-moiety with a positive charge – UPy with an oligo(ethylene glycol) (OEG) functionalized with an amine (UPy-Amine) – is expected to increase the affinity with the negatively charged antimiR. Addition of the monofunctional UPy-Amine resulted in incorporation in the stacks of the network of the UPy-PEG hydrogel, creating a positively charged hydrogel network, cationic UPy-PEG hydrogel (UPy-Cat) (**Figure 2B**). *In vitro* release experiments showed that antimiR-195 release from UPy-Cat occurred over 260 hours, while UPy-PEG released >80% of the antimiR in approximately 50 hours (**Figure 2C**). The mechanical properties of UPy-PEG and UPy-Cat hydrogels showed no significant differences, nor did addition of the antimiR

influence the mechanical properties of either hydrogel. UPy-PEG and UPy-Cat showed a G' (storage modulus) of approximately 10 kPa, indicating no difference in strength with incorporation of UPy-Amine (**Figure 2D**), and in line with some of the stronger hydrogels previously tested[24]. Strain sweep experiments showed a linear course of G' and G'' (loss modulus) until a minimum of 50% deformation, where the crossover point indicated the disruption of both hydrogels (**Figure 2E**). Additionally, both hydrogels appeared to be in the gelated state over a broad range of frequencies **(Figure 2F**). Altogether, UPy-PEG and UPy-Cat showed similar mechanical properties and allowed for sustained antimiR release.

Intramyocardial injection of pristine UPy-PEG is safe

To test the *in vivo* safety of both UPy-PEG and UPy-Cat healthy mice were subjected to intramyocardial injections (2 times 10 µL) of PBS, UPy-PEG or UPy-Cat in the LAD area. At 3 and 7 days post-injection (dpi), cardiac function and dimensions were measured by echocardiography and tissue was collected for molecular analysis **(Figure 3A**). Intramyocardial injection of UPy-PEG had no significant effect on fractional shortening or thickness of the anterior or posterior left ventricular wall (LVAW or LVPW, respectively, measured in diastole) compared to intramyocardial injection of PBS (**Figure 3B**). However, UPy-Cat caused an increase in thickness of both LVAW and LVPW at 3 dpi.

As UPy-Cat also caused an increase in cardiac stress- and fibrosis markers natriuretic peptide A (*Nppa)*, β-myosin heavy chain (*Myh7)* and collagen type 1 alpha 2 (*Col1a2, non-significant)* (**Figure 3C**) we decided to continue our further investigations with UPy-PEG.

To get a more detailed view on the cardiac gene expression effects of intramyocardial injection of UPy-PEG, we submitted RNA samples from PBS- and UPy-PEG-injected hearts for RNA-sequencing (**Supplemental Figure S2A-B**). Gene ontology analysis of differentially expressed genes (>1.25 fold upregulated, $p < 0.01$) suggested the induction of inflammatory genes in response to UPy-PEG (**Figure 3D**). Realtime PCR analysis indicated the transient nature of this response (**Figure 3E**). This finding was confirmed in histological sections of murine hearts showing a more prominent infiltration of small cells in UPy-PEG-injected hearts versus those injected with PBS 3 dpi, which largely disappeared in time (**Figure 3F**). To determine cardiac retention of the UPy-PEG, we performed anti-PEG ELISA on whole-heart lysates which showed that most of the injected hydrogel is removed shortly after injection. Only 6% of the injected UPy-PEG was detected in the heart after intramyocardial injection and this declined to approximately 1% at 24 hours after injection (**Supplemental Figure S3**).

Taken together, these data show that pristine UPy-PEG does not affect cardiac function, although it induces a transient inflammatory response upon intramyocardial injection in the mouse heart despite a low cardiac retention.

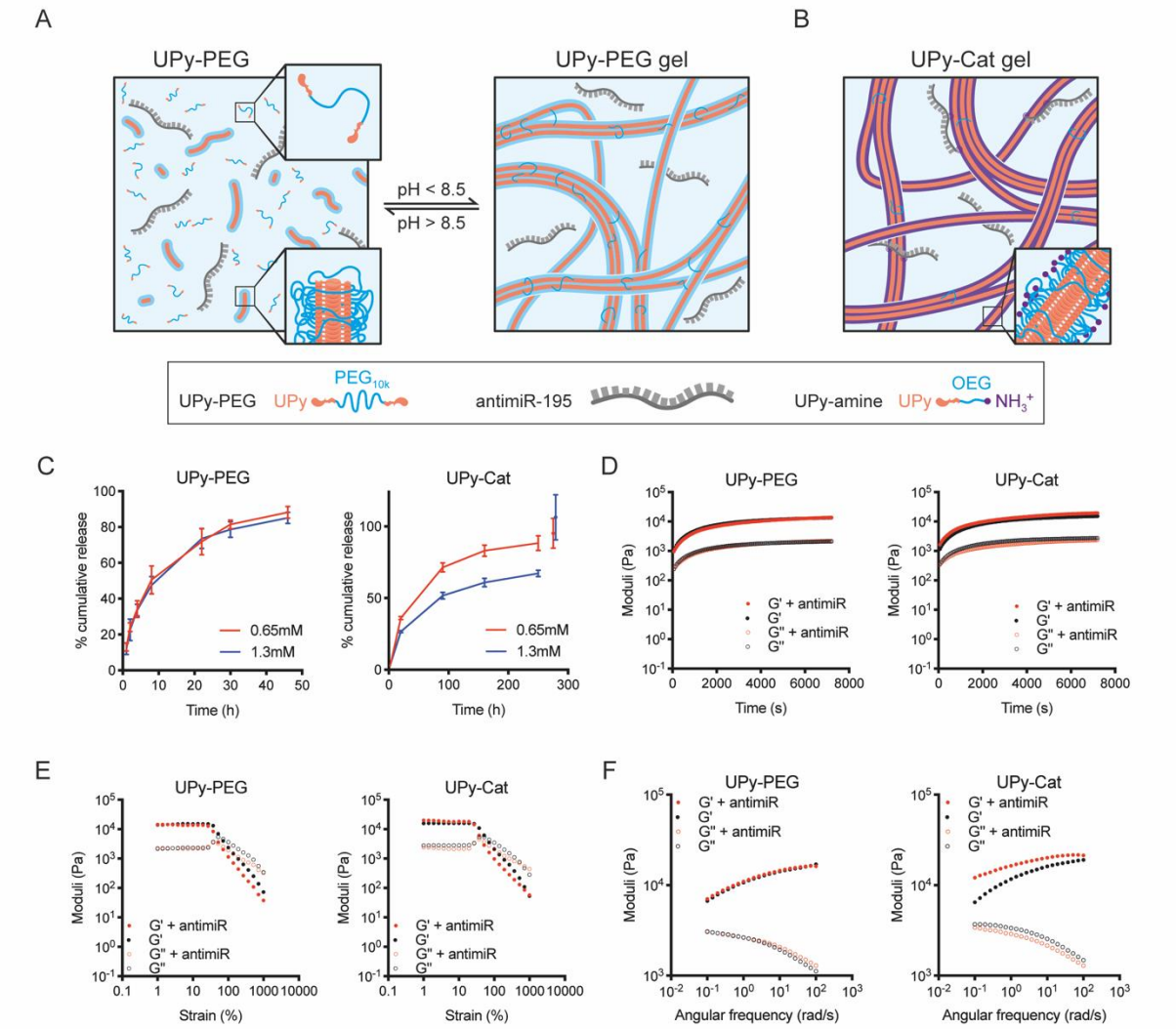

Figure 2. Schematic representation and material properties of UPy-PEG and cationic UPy-PEG. (A) Schematic overview of the gelation process of UPy-PEG. At pH>8.5 only small fibers are formed with no formation of a transient network, whereas at pH<8.5 a hydrogel network is formed. (B) Addition of monofunctional UPy-Amine results in incorporation in the stacks of the network, forming a cationic UPy-PEG network (UPy-Cat). (C) Cumulative release of antimiR-195 from UPy-PEG and UPy-Cat over time at 37 °C. (D-F) Storage modulus (G') and loss modulus (G'') of UPy-PEG and UPy-Cat at 37 °C as a function of time (D), strain (E), and over angular frequency (F).

AntimiR-195 released from UPy-PEG is functional and increases cardiomyocyte proliferation *in vitro*

To test whether antimiR-195 released from UPy-PEG is still functional *in vitro*, antimiR-195 was mixed into UPy-PEG after which we collected serial incubations of cell culture medium. Subsequently, neonatal rat ventricular myocytes (NRVM) were cultured with this medium and transcriptomic and proliferation changes were analyzed (**Figure 4A**). At all timepoints of the incubation, NRVMs cultured

with medium incubated on UPy-PEG with antimiR showed a robust decrease in both *miR-16* and *miR-195* compared to those cultured with medium incubated with pristine UPy-PEG (**Figure 4B**).

Downstream mRNA target Cyclin D1 (*Ccnd1*) showed an increase at all analyzed timepoints that peaked with the lysate coming from the UPy-PEG between D1-3 and D3-5 (**Figure 4C**). Quantification of cardiomyocyte proliferation by KI67-staining indicated a significant increase in proliferation with the medium that was incubated on UPy-PEG with antimiR between D0-1 (**Figure 4D-E**). Taken together, these data show that antimiR-195 released from UPy-PEG is still functional and able to induce proliferation in cardiomyocytes *in vitro*.

UPy-PEG-based delivery of antimiR-195 enhances cardiac target derepression

Considering previous studies targeting the *miR-15* family in the heart were done via systemic delivery of the antimiR[15, 16], we first needed to determine the required dose to see transcriptional changes with intramyocardial delivery. To establish a suitable antimiR dose, healthy mice were subjected to intramyocardial injections of UPy-PEG (2 times 10 µL), either pristine or loaded with a low dose (70 µg per mouse) or high dose (140 µg per mouse) of antimiR-195. Tissues were collected for molecular analysis at 3 and 7 dpi (**Figure 5A**). Both doses led to a robust reduction of *miR-16* and *miR-195* in the LV at both timepoints (**Figure 5B**). This resulted in an increase in mRNA targets ADP-ribosylation factor-like protein 2 (*Arl2*) and *Ccnd1* at 3 dpi, but not 7 dpi (**Figure 5C**). While miR inhibition and target derepression in the heart seemed to be comparable between the two doses, the higher dose showed stronger *miR-16* and *miR-195* inhibition in kidney and liver RNA (**Supplemental Figure S4A,C**). Only with the higher antimiR dose miR inhibition was accompanied by changes in target mRNA (**Supplemental Figure S4B,D**). Based on these findings we opted to use the lower dose for all subsequent studies.

To analyze whether UPy-PEG improved cardiac efficacy of antimiR-195 over PBS as a delivery vehicle, we subjected healthy mice to intramyocardial injections with PBS or UPy-PEG, either pristine or loaded with antimiR-195 and collected tissues for molecular analysis at 3 dpi (**Figure 5D**). With both delivery vehicles, antimiR-195 caused a strong reduction of *miR-16* and *miR-195* levels (**Figure 5E**). Pristine UPy-PEG induced a decline of *miR-16* and *miR-195* levels when compared to PBS. This was probably due to the transient stress induced upon intramyocardial injection. However, target transcripts *Arl2* and *Ccnd1* showed a stronger increase after UPy-PEG-based delivery compared to PBS-based delivery (**Figure 5F**) showing that hydrogel-based intramyocardial delivery does increase local efficacy. RNA analysis of liver and kidney tissues showed comparable inhibition of *miR-16* and *miR-195* between

delivery methods, with no significant effects on *miR-15* family target mRNAs (**Supplemental Figure 5A-D**).

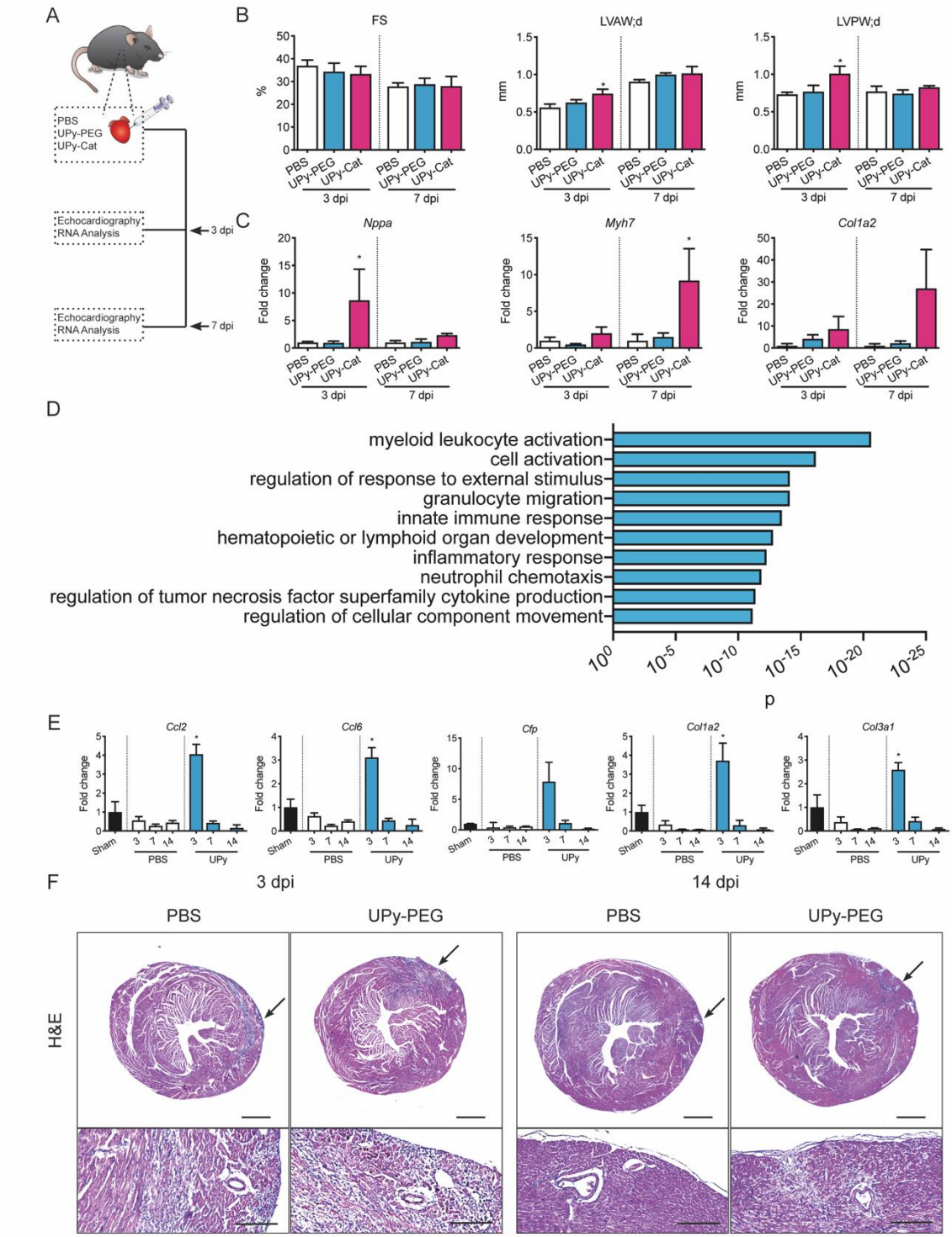

Figure 3. Injection of pristine UPy-PEG causes a transient inflammatory reaction. (A) Schematic representation of experiment. (B) Echocardiographic analysis of FS, LVAW;d, LVPW;d (n=4-5). (C) RT-PCR quantification of stress markers *Nppa*, *Myh7* and fibrosis marker *Col1a2* (n=4-5). (D) Gene ontology analysis of differentially expressed genes between mice injected with PBS and those injected with pristine UPy-PEG. (E) Hematoxylin & eosin (H&E) staining of transverse sections of murine hearts at 3 (left) and 14 (right) dpi with PBS or pristine UPy-PEG.

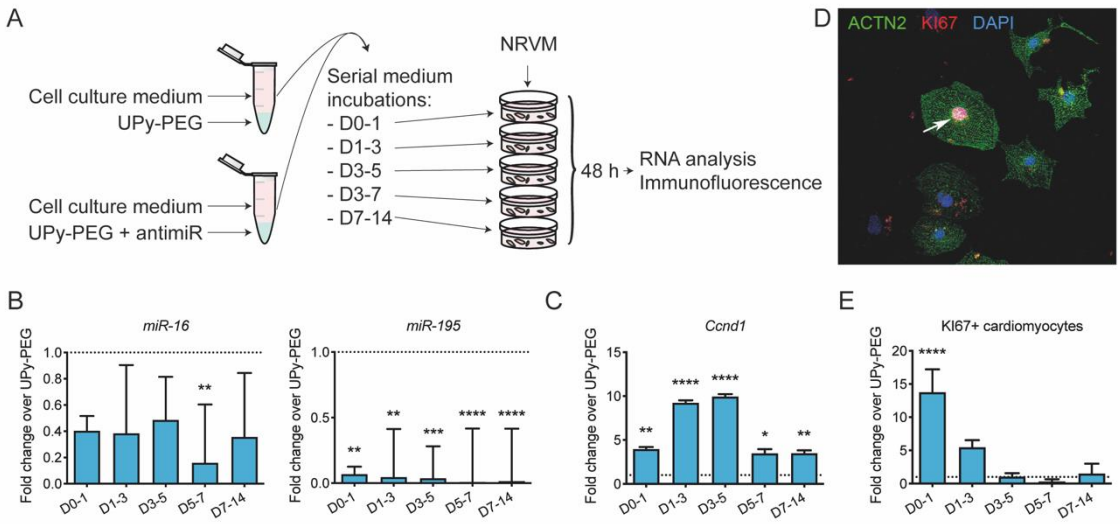

Figure 4. AntimiR-195 released from UPy-PEG activates cardiomyocyte proliferation *in vitro.* (A) Schematic overview of the *in vitro* experiment. Pristine UPy-PEG or UPy-PEG loaded with antimiR-195 was allowed to gelate in the bottom of a 2 mL Eppendorf tube. Subsequently, multiple incubations with 1.5 mL cell culture medium were performed serially. After each incubation, medium was frozen for storage. Medium was thawed for cell culture experiments, and NRVM were incubated with it for 48 hours. (B,C) RT-PCR quantification of *miR-16* and *miR-195* (B) and *Ccnd1* (C) after treatment with hydrogel-incubated medium (n=3). (D) Representative image of ACTN2 & KI67 staining on NRVM treated with medium incubated on UPy-PEG with antimiR. KI67-postive cardiomyocyte nucleus labeled with white arrow. (E) Quantification of KI67-positive cardiomyocytes. Values shown are fold change in cells exposed to medium incubated with antimiR-containing hydrogel over those exposed to medium incubated with pristine hydrogel at that same timepoint.

To investigate the transcriptomic effects of antimiR-195 delivery, RNA from LV tissue after injection with pristine UPy-PEG versus UPy-PEG with antimiR was submitted for RNA-sequencing (**Supplemental Figure S6A-B**). Gene ontology analysis of differentially regulated genes (>1.25 fold increased, $p < 0.01$) revealed mostly genes related to metabolic processes (**Figure 5G**), which could fit with a previously published effect of the *miR-15* family on mitochondrial integrity through *Arl2*[25]. Taken together, these data show that antimiR-195 released from UPy-PEG *in vivo* is still functional, that UPy-PEG-based delivery improves the efficacy of antimiR-195 over PBS-based delivery in healthy mice, and that with UPy-PEG based intramyocardial delivery there is target mRNA de-repression at a dose far lower than the dose used for systemic injection[26, 27].

UPy-PEG-based delivery of antimiR-195 induces proliferation in cardiomyocytes after ischemic injury

To determine whether the use of UPy-PEG improved cardiac efficacy of antimiR-195 after IR, mice were subjected to 60 minutes of LAD ligation and, upon reperfusion, received intramyocardial injections (2 times 10 µL) of PBS or UPy-PEG, either pristine or loaded with antimiR-195. LV-tissue was collected 3 dpi (**Figure 6A**). As expected, antimiR-195 induced a strong reduction of *miR-16* and *miR-195* levels, regardless of the vehicle used for injection (**Figure 6B**). Accordingly, antimiR therapy led to

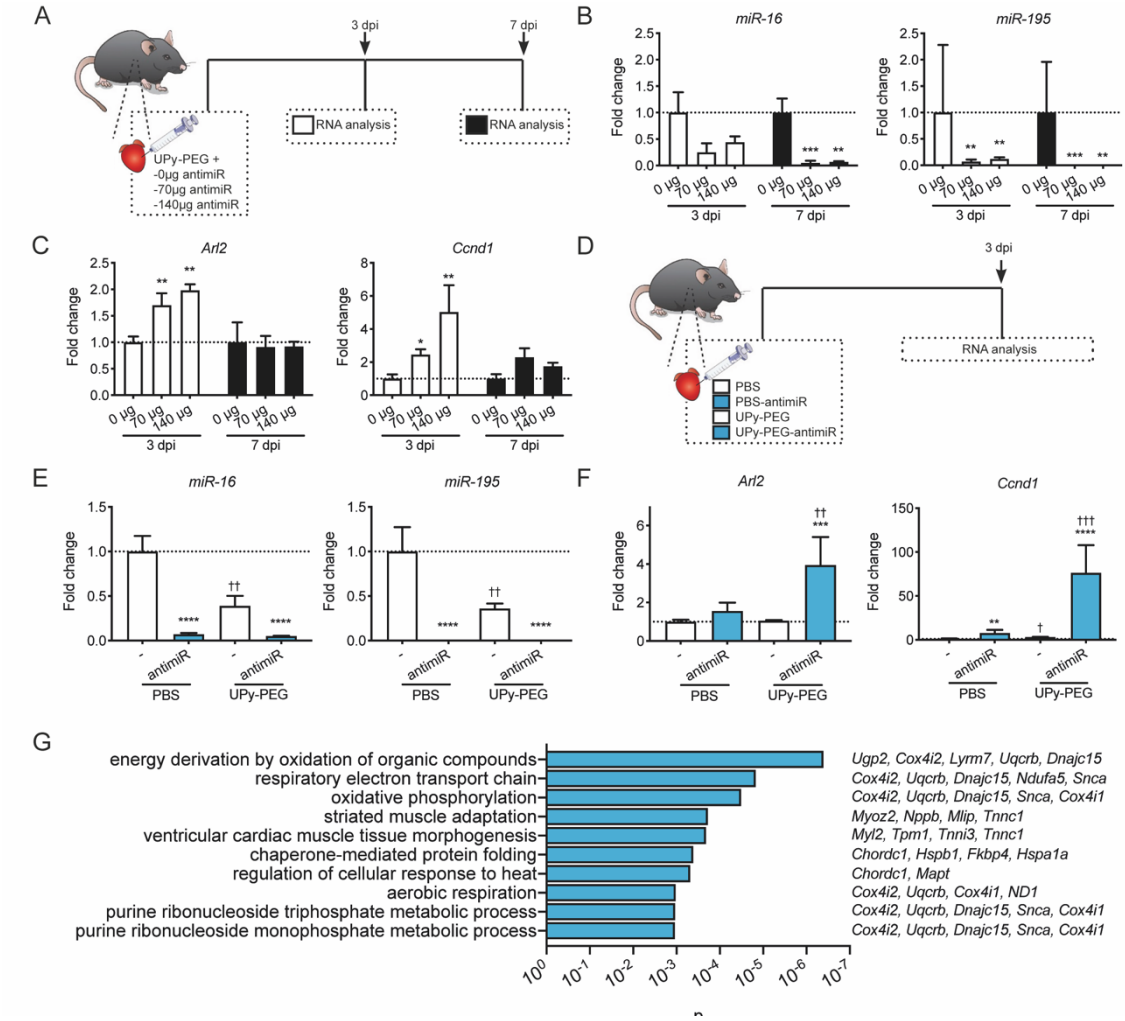

Figure 5. UPy-PEG-based intramyocardial delivery of antimiR-195 increases its efficacy over PBS-based intramyocardial delivery. (A) Schematic representation of experiment. (B) RT-PCR quantification of *miR-16* and *miR-195*. (C) RT-PCR quantification of *Arl2* and *Ccnd1* (n=5) (D) Schematic representation of experiment. (E) RT-PCR quantification of *miR-16* and *miR-195* (n=5). (F) RT-PCR quantification of *Arl2* and *Ccnd1*. (G) Gene ontology analysis of differentially expressed genes between mice injected with pristine UPy-PEG or UPy-PEG loaded with antimir with a dose of 70 µg per mouse.

upregulation of *Ccnd1* and vascular endothelial growth factor A (*Vegfa*) (**Figure 6C**). In addition to these *miR-15* family targets, there was a significant increase in *Ki67* between UPy-PEG- and PBS-based delivery of antimiR-195 (**Figure 6D**). As expected, we found a decrease of *miR-16-* and *miR-195* levels in the kidney and in the liver, with a less profound decrease of *miR-16* in livers of mice injected with antimiR-195 in UPy-PEG (**Supplemental Figure S7A,C**). *Ccnd1* was induced in the kidneys after PBS- and hydrogel-antimiR delivery, but not in the liver (**Supplemental Figure S7B,D**). To investigate the broader effect of antimiR-195 under ischemia-reperfusion stress, RNA from LV-tissue after IR treated with either pristine UPy-PEG or UPy-PEG with antimiR-195 was submitted for RNA-sequencing (**Supplemental Figure S8A-B**). Gene ontology analysis of differentially expressed genes (>1.25 fold increased, $p < 0.01$) now resulted in gene classifications linked to tissue morphogenesis and cell division (**Figure 6E**), suggesting that under stress conditions *miR-15* family repression activates the tissue morphogenesis and cell division.

Previous work from our lab showed that not only the presence or absence of stress, but also the severity of this stress influences antimiR function[28]. Based on this knowledge we extended our *in vivo* efficacy study and subjected mice to permanent LAD ligation for 28 days. Immediately after LAD ligation, the mice received intramyocardial injections (2 times 10 µL) with PBS or UPy-PEG, either pristine or loaded with antimiR-195. To track cell proliferation, mice additionally received subcutaneous EdU-injections every other day for 11 days after surgery. Twenty-eight days after surgery, tissue was collected for histological and molecular analysis (**Figure 6F**). Four weeks after antimiR-195 injections, there was still a significant reduction in *miR-16* and *miR-195* levels, with a slightly stronger inhibition after hydrogel-based delivery compared to PBS-based delivery (**Figure 6G**). UPy-PEG-formulated antimiR-195 had a stronger de-repressive effect on *Ccnd1* and *Vegfa* than PBS-formulated antimiR-195 and showed a significant induction in Pcna (**Figure 6H-I**). To quantify cardiomyocyte proliferation *in vivo* after MI we counted EdU-positive cells 28 dpi. Hydrogel-based antimiR-195 delivery caused an increase in EdU-positive cardiomyocytes compared to PBS-formulated antimiR (**Figure 6J-K**). Importantly, we saw no difference in EdU-positive non-myocytes (**Figure 6L**), indicating that antimiR-195 selectively enhances the proliferation of cardiomyocytes. However, despite the increase in cardiomyocyte proliferation we were unable to detect a beneficial effect of antimiR-195 on cardiac function by echocardiography (**Supplemental STable 1**).

RNA analysis of kidney and liver tissue from these mice revealed significant *miR-16* and *miR-195* inhibition 28 days after injection, which appeared stronger with hydrogel-based intramyocardial antimiR delivery (**Supplementary Figure S9A,C**). This could suggest a prolonged washout of antimiR-195 from the heart after hydrogel-based delivery. However, no effects on target de-repression were observed at this point (**Supplementary Figure S9B,D**).

Taken together, these data suggest that UPy-PEG-based antimiR delivery improves local cardiac efficacy and successfully activates cell cycle genes after ischemia to induce cardiomyocyte-specific proliferation.

Discussion

The current study shows that a pH-responsive hydrogel, UPy-PEG, designed for minimally invasive intramyocardial injection can be used to improve local delivery of an antimiR. Our data shows that UPy-PEG-based intramyocardial delivery of antimiR-195 enhances the effect on target derepression and stimulates cardiomyocyte proliferation after MI. While this provides support for follow up

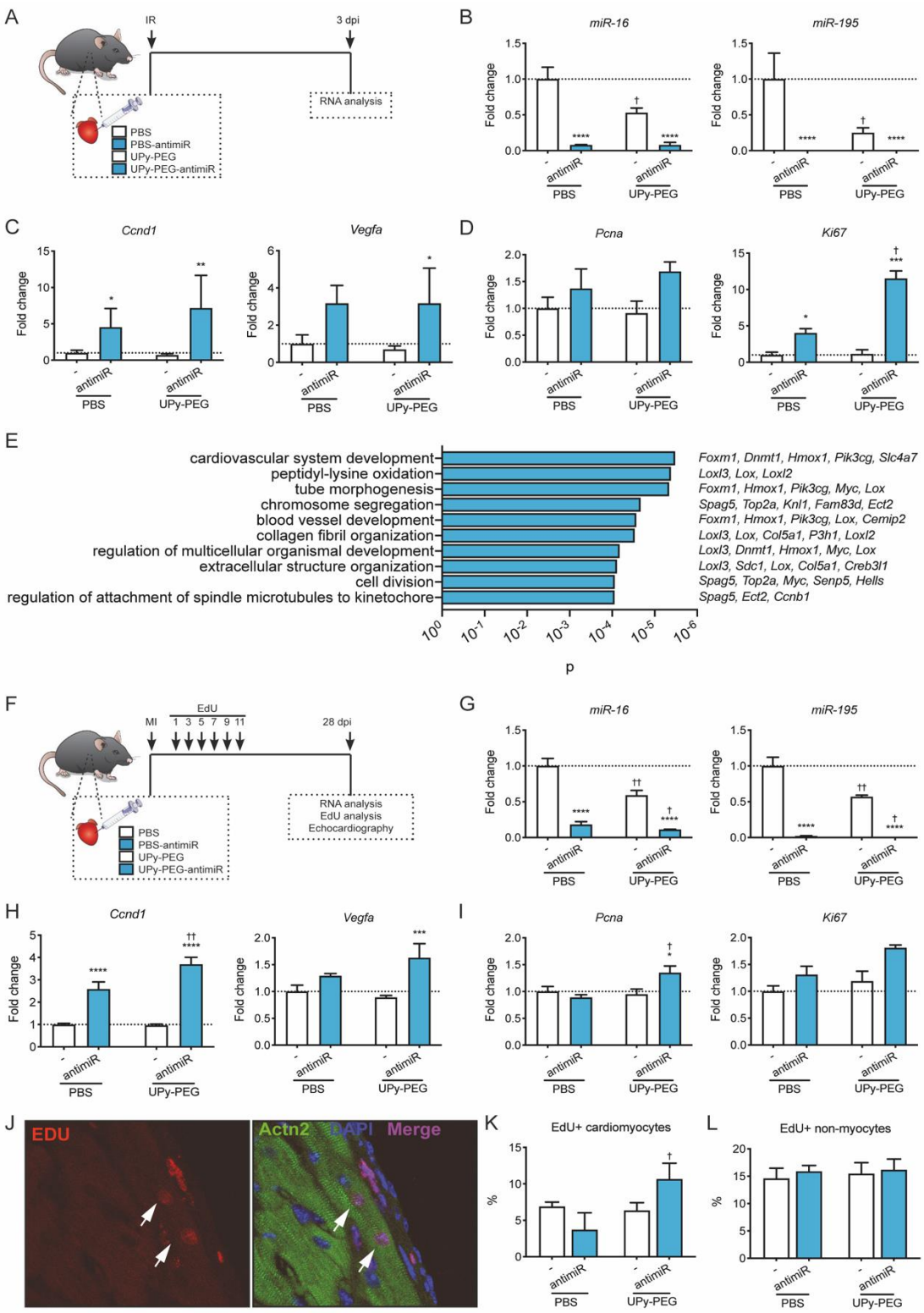

Figure 6. UPy-PEG-based intramyocardial delivery of antimiR-195 induces proliferation in cardiomyocytes after ischemic injury. (A) Schematic representation of experiment. (B) RT-PCR quantification of *miR-16* and *miR-195* (n=4-5). (C) RT-PCR quantification of *Ccnd1* and *Vegfa* (n=4-5). (D) RT-PCR quantification of *Pcna* and *Ki67* (n=4-5). (E) Gene ontology analysis of differentially expressed genes between mice injected with pristine UPy-PEG or UPy-PEG loaded with antimiR-195 after IR. (F) Schematic representation of experiment. (G) RT-PCR quantification of *miR-16* and *miR-195* (n=6-9). (H) RT-PCR quantification of *Ccnd1* and *Vegfa* (n=6-9). (I) RT-PCR quantification of *Pcna* and *Ki67*(n=6-9). (J) Representative image of EdU-detection in murine hearts treated with UPy-PEG with antimiR. White arrows mark EdU-positive cardiomyocytes. (K) Quantification of EdU-positive cardiomyocytes as a percentage of all cardiomyocytes (n=3-6). (L) Quantification of EdU-positive non-myocytes as a percentage of all non-myocytes (n=3-6).

investigation, our data also highlight some of the drawbacks and challenges to consider when using this gel.

The hydrogel used here was designed as a versatile sustained release delivery vehicle suitable for catheter-based intramyocardial injections. It has previously been shown to be easily modifiable to facilitate MRI detection[29] or modification of drug retention properties[30]. Additionally, it was used previously in a proof of concept study for the intramyocardial delivery of IGF-1/HGF in a porcine model of ischemic injury[5] which showed the UPy-PEG to enhance delivery of IGF-1/HGF to the injured myocardium. Our study adds a more thorough investigation of the hydrogel's safety and retention in mice and shows that, in addition to the delivery of proteins, the hydrogel can also be used for delivery of oligonucleotides *in vivo*.

However, our experiments investigating the safety of the hydrogel revealed that injection of pristine hydrogel into the healthy mouse heart causes a transient inflammatory reaction and seems to cause more damage than an intramyocardial injection of PBS.

Potential triggers causing this response might be inherent to the hydrogel and include the high pH of the gel when injecting and the viscosity and volume of the injections (swelling of the myocardium at the injection site is observed). Alternatively, the mouse model itself may contribute to this effect, as using mice limits us to using conventional needles and a microsurgical intercostal approach as opposed to catheter-based injections. We suspect that mice are not the optimal model to study the safety of intramyocardial injectables due to the unavailability of catheter-based delivery systems and the difficulty of manually injecting in the fast-moving heart of the mouse. Therefore, the injections may cause traumatic injury which is slightly worse in the hydrogel injections because the viscous fluid is harder to inject. We expect to observe less damage if these studies were repeated using a catheter-based delivery system in a large animal model. Furthermore, we are also unsure of the importance of these effects of intramyocardial injections of pristine hydrogel in healthy murine hearts, as the hydrogel is intended to be injected into damaged hearts as a carrier of pro-regenerative drugs. We have not investigated whether injection of the hydrogel still causes additional damage in an area already damaged by ischemia.

An additional issue we encountered when using the gel in mice was the low cardiac retention of the hydrogel at the injection site, with nearly all the UPy-PEG molecules cleared from the heart after 24 hours. Regardless, our results show that antimiR efficacy is improved with hydrogel-based delivery over PBS-based delivery, with the difference being observable at least 28 days after injection. Presumably, even a short increase in the exposure to antimiRs allows cardiomyocytes to take up more compound and subsequently, the very stable LNA-DNA mixmer antimiRs can cause a long-lasting effect. At this point we are not sure whether the short retention of the hydrogel is caused by its failure

to gelate fast enough upon injection, the lack of space in the dense cardial tissue, or whether the hydrogel is pumped out of the heart quickly in the moving and well-perfused myocardium. In the latter case, hydrogel retention may be better with injection in damaged, less contractile, less well-perfused, areas or in larger species that have a lower heart rate. Another option for improving the hydrogel retention may be to add adhesive components.

While previous research has shown high-dose systemic *miR-15* family inhibition after ischemic injury reduces infarct size and improves cardiac function[15], we could not reproduce those findings with our new delivery method even though we did see an increased efficacy on mRNA targets. Perhaps a further increase in antimiR dose could improve effect size, but the dose in the current study was picked to have no effect on off-target organs. Alternatively, the timing of the therapy could be further investigated[31], possibly antimiR-195 injection is more effective few days or weeks after the ischemic injury. However, this is unattractive in mice because it requires repeated surgery and we think that these investigations would be more suited to a large animal model where catheter delivery of the hydrogel and antimiR would be possible.

In addition to increasing local efficacy, hydrogel delivery of antimiR-195 was intended to reduce exposure of the off-target organs, like the kidney and liver. In this study we did not observe a clear difference in *miR-15* family mRNA target de-repression in liver and kidney between hydrogel- and PBS-based delivery 3 days after injection. Efforts to improve cardiac retention of the gel will inherently reduce delivery to extra-cardiac tissues and are key.

In summary, we have shown that using a hydrogel as a vehicle for intramyocardial antimiR-195 delivery in mouse improves efficacy over PBS. We showed increased target de-repression and increased cardiomyocyte proliferation. However, this did not lead to a significant improvement in cardiac function. Further research in larger animal models is needed to show whether catheter based intramyocardial injections of UPy-PEG antimiR-195 will overcome the disadvantages found in the mouse model and show an even greater benefit of using UPy-PEG as cardiac delivery vehicle of antimiR-195 in the setting of ischemic heart disease.

Materials and Methods

General

Reagents and chemicals were obtained from commercial sources with the highest purity available, used without further modification unless stated otherwise. Water used was purified on an EMD Millipore Milli-Q Integral Water Purification System.

Mice

All animal studies were performed in accordance with institutional guidelines and regulations of the Animal Welfare Committee of the Royal Netherlands Academy of Arts and Sciences. All animal

experiments were performed on adult C57Bl6J male mice from Charles River Laboratories (8-9 weeks of age).

Surgery

Mice were anesthetized with an intra-peritoneal injection of ±100µl of mixed Ketamine-Xylazine (67 mg/kg Ketamine and 8.3 mg/kg mouse weight Xylazine), intubated and ventilated using a rodent ventilator (UNO® Microventilator UMV-03). The anesthesia was maintained with 1.5%-2% isoflurane. Mice were placed in a supine position on a heated plate to maintain a body temperature between 38°C and 39°C. Hair was removed from the thorax with Veet® hair removal cream and the skin was disinfected with iodine and 70% ethanol. The skin was incised left of the midline, pectoral muscles were retracted, exposing the ribs. An incision was made between the 2nd and 3rd rib after which the left ventricle (LV) was visible. For myocardial infarction (MI) procedure a 7-0 silk suture was tied around the left anterior descending coronary artery (LAD) to permanently occlude the artery. For ischemia reperfusion (IR) injury, a 3 mm polyethylene (PE) tube was placed over the LAD. A suture was then tied around the LAD and PE tube. The PE tube was removed after one hour of ischemia and the ligature was cut to allow for reperfusion via the LAD. For sham surgeries, the surgeries were identical to MI and IR surgeries apart from that the LAD was not occluded. For the intramyocardial injections, mice were injected twice in the left ventricle (LV) at different positions on the (possible) infarct-site with 10µl PBS or UPy-gel using Hamilton syringes with 31 gauge 30° beveled needles. After injections, the ribcage was sutured (5-0 silk), the muscle layers were repositioned, and the skin was closed using a wound clip. The mice recovered on the heated plate whilst receiving oxygen supply. Once recovered, they were disconnected from the ventilator and given a single subcutaneous injection Buprenorphine (Temgesic®, 0.05-0.1mg/kg mouse weight) and were housed under standard conditions until tissue collection would take place.

EdU labeling

To assess cardiomyocyte proliferation, infarcted animals (n=4-6 per group) received ethynyl-29-deoxyuridine (EdU, Life Technologies; 350 µg per animal intraperitoneally) every other day from day 1 until day 11 after MI (6 injections total).

Synthesis of cationic UPy-Amine

1,2 CDI was used to activate the Boc-NH2-PEG11-OH, following Cbz-protected dodecyl diamine addition with DIPEA. Purification was done using C18 column chromatography. Triethylsilane was used to deprotect the Cbz-protecting group. Subsequently UPy-hexyl-isocyanate and DIPEA were added, of which the resulting product was purified using C18 column chromatography. 1H-NMR (400 MHz, CDCl3): δ – 13.10 (s, 1H), 11.84 (S, 1H), 10.08 (s, 1H), 5.84 (s, 1H), 5.04 (s, 1H), 4.87 (s, 1H), 4.68 (s, 1H), 4.45 (s, 1H), 4.20 (t, 2H), 3.6-3.7 (m, 42H), 3.53 (t, 2H), 3.1-3.35 (m, 10H), 2.23 (s, 3H), 1.15-1.7 ppm

(m, 37H); LCMS: [M] calcd 1165.47; found 533.5 [M+2H-Boc]2+, 594.3 [M+H+Na]2+. The compound was stored in the freezer and small portions were deprotected with 4M HCl in dioxane before use.

Hydrogel preparation

10 wt% UPy-PEG hydrogel was prepared by dissolving the UPy-PEG hydrogelator powder in PBS (pH 11.6) and stirring at 70 °C for 1 hour using a magnetic stirrer. For a total volume of 100 µL hydrogel, 10 mg of UPy-PEG hydrogelator powder and 90 µL PBS (pH 11.6) was used. The viscous solution was cooled to room temperature with resulting pH of 9.0. UPy-Cat hydrogels were prepared by first dissolving the precursors UPy-Amine and UPy-PEG in water/ACN (50:50) mixture, which was freeze-dried for complete molecular mixing. Subsequently, the UPy-Amine precursor powder was dissolved in PBS at 70 °C for 1 hour.

For hydrogels loaded with antimiR, the antimiR was added from a stock solution and mixed into the still-warm hydrogel before allowing it to cool. The added volume was considered when the precursor hydrogelator was prepared.

Rheology

Rheological measurements of the hydrogels were performed on an Anton Paar Physica MCR501 Rheometer. Release studies were performed using Millicell Hanging Plate inserts PIEP12R48. All rheological measurements were performed at 37 °C unless stated otherwise, in combination with a P-PTD 200 evaporation blocker preventing the sample from drying. A cone-plate geometry of 25 mm was installed with fixed distance of 0.049 mm and shear viscosity was recorded as function of shear rate (100 to 0.1 s-1, 10 points per decade). A plate-plate geometry of 25 mm was used with plate distances ranging from 0.45 to 0.6 mm. viscous liquid precursor was pipetted on the bottom plate and HCl (1 M) was pipetted on multiple places on top to initiate gelation. After curing times of 2 – 2.5 hours storage and loss moduli were recorded as function of angular frequency (100 to 0.1 rad s-1, 22 measurement points) at 1% strain and as function of strain (0.1 to 1000%, 22 measurement points) at 1 rad s-1.

AntimiR design

AntimiR-195 was designed and synthesized by miRagen®. It is an LNA/DNA mixmer: a 16-mer complementary to miR-195 and partially complementary to the remaining miR-15 family members.

Release of antimiR

For the *in vitro* antimiR release study, 100 µL of the hydrogels with antimiR were added in Millicell plate inserts. These were put in a 24-well plate and at set time points the PBS was collected, antimiR concentration was determined and fresh PBS was added to the wells. AntimiR concentration was measured with UV absorption at 261 nm. Experiments were performed in duplicate. For antimiR

release from UPy-Cat, hydrogels were dissolved before the final measurement to confirm that all antimiR was measured.

Echocardiography

Cardiac function and dimensions were evaluated by 2-dimensional echocardiography using a Vevo® 2100 Ultrasound system (Visual Sonics). Mice were sedated with 5% isoflurane and anesthesia was maintained with 1-2% isoflurane. M-mode tracings from short axis view were used to measure internal diameter, anterior and posterior wall thicknesses at end diastole and end systole. The mean value of at least 9 cardiac cycles were used to determine the measurements for each animal. LV trace measurements from short axis view in M-mode were used to calculate fractional shortening (FS) and ejection fraction (EF) and calculated by the Vevo® LAB 1.7.1 software as: FS(%) = 100* [(LVID;d – LVID;s)/ LVID;d], EF (%) = 100* [(LV Volume;d – LV Volume;s)/ LV Volume;d]. Blood flow was assessed using pulsed wave (PW)-mode, assisted by Color Doppler mode in aortic arch view.

Tissue collection

For cardiac tissue collection, mice were euthanized by cervical dislocation. The chest was opened to expose the heart. The heart was removed, washed in ice cold PBS and weighed. For RNA analysis, the atria and right ventricle were removed and the left ventricle (including the septum) was snap frozen in liquid nitrogen.

RNA extraction and real-time PCR analysis

To isolate RNA, we used TRIzol® reagent (Life Technologies) following the manufacturer's instructions. The RNA concentration was assessed by a NanoDrop Spectrophotometer. Complementary DNA (cDNA) was synthesized from a total of 500ng of RNA using the iScript cDNA Synthesis Kit (Bio-Rad, #1708891). Real-time PCR (RT-PCR) for coding genes was performed using gene specific primers according to the instructions described by the IQ™ SYBR Green Supermix (Bio-Rad, #170-8885). The real time PCR protocol was as follows: 95ºC for 15min, followed by 40 cycles at 95ºC for 15s, 60ºC for 30s and 72ºC for 30s. Gene expression was normalized to the expression of glyceraldehyde 3-phosphate dehydrogenase (*Gapdh*) or hypoxanthine-guanine phosphoribosyltransferase (*Hprt*).

For RT-PCR of microRNAs, cDNA was synthesized from 1µg total RNA using TaqMan microRNA Reverse Transcriptase kit (Applied Biosystems, #4366597). Real time PCR reactions were performed using TaqMan Universal Master Mix II (Applied Biosystems, #4440040), according to the manufacturer's instructions and using specific probes for the *miR-15* family (ThermoFisher Scientific, #4427975, product IDs: 000389, 000390, 000391, 000494, 0001346) and *U6* (ThermoFisher Scientific, #4440887, product ID 001973). Fold changes in gene expression were calculated according to the $2^{-\Delta\Delta CT}$-method and expressed as mean fold change ± SEM.

RNA sequencing

RNA integrity was analyzed using the Agilent 2100 Bioanalyzer system. RNA of each LV sample was used to prepare Illumina sequencing libraries with the TRUseq stranded mRNA kit (Illumina) and sequenced with 75bp read length with the Illumina NextSeq500 by the Utrecht Sequencing Facility. Subsequently, reads were mapped to the mouse genome (GRCm38). Differential expression was analyzed using R and the DESeq2 package. Genes with less than 1 reads per sample on average were discarded. Significantly regulated genes were defined as those with at least a 1.2-fold change over the control condition and a p-value < 0.01. For gene ontology analysis on significantly upregulated genes, all detected genes were used as a background.

Data accessibility

RNA sequencing data has been submitted to be publicly available through the NCBI Gene Expression Omnibus (GEO).

Histology

Hearts were fixed in 4% formalin at room temperature for 48h, embedded in paraffin and sectioned at 4µm. Sections were used for hematoxylin and eosin (H&E) staining using standard procedures. The short axis cross-section view and high magnification images were made using a Leica DM 4000 microscope and Leica LAS software. For immunohistochemistry, tissue sections went through a process of deparaffinization, rehydration, heat induced antigen retrieval and blocking with 1% BSA, the sections were incubated with specific primary antibodies overnight at 4°C. After washing with PBS, the sections were incubated with secondary antibodies for 1 hour at room temperature, washed and sealed with a mounting medium containing DAPI (Vector Laboratories). To reveal EdU incorporation, tissue sections were further processed using the Click-IT EdU 555 Imaging kit according to the manufacturer's instructions. Images were taken using the Leica TCS SPE confocal microscope. Antibodies used were mouse anti-α actinin (ACTN2, Sigma-Aldrich, #A7732) and the corresponding secondary fluorescent antibody anti-mouse Alexa-488 (Life Technologies).

Primary cardiomyocyte culture

Neonatal rat ventricular cardiomyocyte (NRVM) cultures were isolated by enzymatic dissociation of neonatal rat hearts, as described previously[32]. In short, hearts from 1-2-day old rat pups were collected, the atria were removed and the ventricular cells were enzymatically dissociated with trypsin (Life Technologies) in a water (37˚C) jacketed spinner flask. The single cell suspension was filtered and pre-plated to remove debris and non-myocytes respectively. Primary cardiomyocytes were initially maintained in Ham's F10 medium (Gibco) supplemented with 5% FBS (Sigma-Aldrich) and 1% penicillin/streptomycin (Life Technologies). The day after isolation, cardiomyocytes were switched to serum-free Ham's F10 medium, supplemented with 1% penicillin/streptomycin and 1µl/ml insulin-

transferrin-sodium-selenite supplement (Sigma-Aldrich, catalog number 11074547001). Pure cardiomyocytes were plated on 24-well plates with cover-slips (125,000 cells per well).

Analysis of in vitro activity of antimiR-195 released from UPy-PEG

Three-hundred µL UPy-PEG hydrogel, either pristine or with antimiR-195, was incubated with 1.5 mL cell culture medium in 2 mL Eppendorf tubes. Supernatants were collected, frozen and replaced at day 1, 3, 5, 7 and 14. NRVM were incubated for 48h with the medium incubated on UPy-PEG hydrogel. For immunofluorescence (IF) on cultured cardiomyocytes, cover-slips were incubated with blocking buffer with 1% Fish gelatin, and incubated with specific primary antibody (mouse anti-α actinin (Sigma-Aldrich, #A7732) and anti-KI67 (Abcam, ab15580)) for 25 minutes at room temperature. After washing with blocking buffer, the cover-slips were incubated with secondary antibodies (anti-mouse Alexa-488 and anti-rabbit Alexa-568 (Life Technologies)) for 25 minutes at room temperature, washed with MQ water and sealed with a mounting medium containing DAPI. The images were taken using the Leica TCS SPE confocal microscope.

Anti-PEG ELISA quantification of UPy-PEG in cardiac tissue

Total hearts were used for cardiac ELISA assays. Tissue samples were homogenized in 1 mL PBS in lysing matrix tubes (FastPrep®) using the Fastprep®-24 sample preparation system. The standard curve was prepared by post-mortem injection of 20 µL UPy-PEG in a control heart, adding 1 mL of PBS and homogenizing it in the same manner as the other samples. This sample was diluted with homogenized cardiac tissue without added hydrogel in 10-fold steps to create a standard curve. Coating buffer (5.3 g Na_2CO3 + 4.2 g $NaHCO_3$/Liter, pH = 8, adjusted pH with 1N HCl) and phosphate-citrate buffer (17.4 g K2HPO4 + 21 g citric acid/Liter) were prepared. The ELISA plates (Nunc MaxiSorp C96, ThermoFisher Scientific, #430341) were coated with 50 µL (5 µg/mL diluted in coating buffer) AGP4 capture antibody per well and incubated overnight at room temperature. Plates were washed with PBS after which 200 µL blocking solution (5% BSA in PBS) was added for two hours at room temperature. Plates were washed 5 times. Tissue samples and standard curve samples were diluted (1:1) in dilution buffer (2% BSA in PBS) and 50 µL of diluted sample was added in three replicates to the plates. Plates were incubated for two hours at room temperature and were then washed one time with PBS-C (0.05% CHAPS in PBS) and two times with PBS for five minutes each, shaking gently on an analog shaker (VWR). The detection antibody, 6.3-biotin, was diluted in dilution buffer (0.05 µl/mL) and 50 µl was added to the plate. After one hour of incubation at room temperature, plates were washed one time with PBS-C and two times with PBS for five minutes each with gentle shaking. Streptavidin-HRP was diluted in dilution buffer (0.1 µg/mL) and 50 µl per well was added for one hour at room temperature. After one hour of incubation at room temperature, plates were washed three times with PBS-C (0.05% CHAPS in PBS) and two times with PBS for five minutes each with gentle

shaking. 5 mg ABTS was added to 10mL phosphate citrate buffer and kept in the dark. Following washing, 2 µl of H_2O_2 was added to the ABTS substrate solution after which 100 µL per well was added to the plate. Peroxidase activity was measured in a microplate reader at 405 nm every 5-10 minutes up until 30 minutes after the ABTS solution was added. Concentration of PEG in tissue was measured by comparison against a standard curve of tissue samples with known concentrations of PEG (tissue samples subjected to *ex vivo* injection of UPy-PEG gel) using 4-parameter logistic regression (Myassays.com). Antibodies were obtained from Steve Roffler at Academia Sinica.

Statistical analysis

Values are presented as mean ± SEM. Outliers were identified, and subsequently excluded, using Grubbs' test (GraphPad). Statistical significance was evaluated using one-way ANOVA (GraphPad) or two-way ANOVA (R), followed by post-hoc tests with correction for multiple testing according to the Benjamini-Hochberg procedure.

*, **, ***, **** indicate $p < 0.05$, 0.01, 0.001, 0.0001 compared to empty vehicle, respectively. †, ††, †††, †††† indicate $p < 0.05$, 0.01, 0.001, 0.0001 for UPy-PEG-antimiR versus PBS-antimiR, respectively.

Author contribution

Conception and design of the research: J.C.E., M.V.G., E.V.R.; acquisition of data: J.C.E, M.V.G., M.V., C.D., D.V., L.K., M.H.B., M.J.G.S; analysis and interpretation of the data: J.C.E, M.V.G., M.G.B., M.J.G.S., P.Y.W.D., E.V.R.; statistical analysis: M.V.G., C.D.; supervising the experiments: P.Y.W.D., E.V.R.; drafting the manuscript: J.C.E., M.V.G., P.Y.W.D., E.V.R.; critical revision of the manuscript for important intellectual content: P.Y.W.D., E.V.R.

Acknowledgements

We would like to thank Anko de Graaff and the Hubrecht Imaging Center for supporting the imaging. We gratefully acknowledge Jeroen Korving for help with histology. We thank Stefan van der Elst and the Hubrecht FACS facility for help with sorting cells and Judith Vivié for help with library preparation. We thank Petra van der Kraak, Joyce van Kuik and Erica Sierra-de Koning for technical support with the immunostainings of the human tissue. We thank Michal Mokry (Epigenomic facility UMC Utrecht) and the Utrecht Sequencing Facility for support in processing human RNA-seq data.

References

1. Lazar E, Sadek HA and Bergmann O. Cardiomyocyte renewal in the human heart: insights from the fall-out. *Eur Heart J*. 2017;38:2333-2342.

2. Hunter JJ and Chien KR. Signaling Pathways for Cardiac Hypertrophy and Failure. *New England Journal of Medicine*. 1999;341:1276-1283.

3. Jansen of Lorkeers SJ, Eding JEC, van der Spoel TIG, Vesterinen HM, Sena ES, Duckers HJ, Doevendans PA, Macleod MR and Chamuleau SAJ. Similar effect of autologous and allogeneic cell therapy for ischaemic heart disease: systematic review and meta-analysis of large animal studies. *European Journal of Clinical Investigation*. 2014;44:5-6.

4. Fisher SA, Zhang H, Doree C, Mathur A and Martin-Rendon E. Stem cell treatment for acute myocardial infarction. *Cochrane Database of Systematic Reviews*. 2015.

5. van Rooij E, Sutherland LB, Qi X, Richardson JA, Hill J and Olson EN. Control of stress-dependent cardiac growth and gene expression by a microRNA. *Science*. 2007;316:575-9.

6. van Rooij E, Sutherland LB, Thatcher JE, DiMaio JM, Naseem RH, Marshall WS, Hill JA and Olson EN. Dysregulation of microRNAs after myocardial infarction reveals a role of miR-29 in cardiac fibrosis. *Proc Natl Acad Sci U S A*. 2008;105:13027-32.

7. Wang Y and Lee CG. MicroRNA and cancer--focus on apoptosis. *J Cell Mol Med*. 2009;13:12-23.

8. van Rooij E and Kauppinen S. Development of microRNA therapeutics is coming of age. *EMBO Mol Med*. 2014;6:851-64.

9. Rupaimoole R and Slack FJ. MicroRNA therapeutics: towards a new era for the management of cancer and other diseases. *Nat Rev Drug Discov*. 2017;16:203-222.

10. Hanna J, Hossain GS and Kocerha J. The Potential for microRNA Therapeutics and Clinical Research. *Front Genet*. 2019;10:478.

11. Bonneau E, Neveu B, Kostantin E, Tsongalis GJ and De Guire V. How close are miRNAs from clinical practice? A perspective on the diagnostic and therapeutic market. *Ejifcc*. 2019;30:114-127.

12. Small EM, Frost RJ and Olson EN. MicroRNAs add a new dimension to cardiovascular disease. *Circulation*. 2010;121:1022-32.

13. Ofir M, Hacohen D and Ginsberg D. MiR-15 and miR-16 are direct transcriptional targets of E2F1 that limit E2F-induced proliferation by targeting cyclin E. *Mol Cancer Res*. 2011;9:440-7.

14. Porrello ER, Johnson BA, Aurora AB, Simpson E, Nam YJ, Matkovich SJ, Dorn GW, 2nd, van Rooij E and Olson EN. MiR-15 family regulates postnatal mitotic arrest of cardiomyocytes. *Circ Res*. 2011;109:670-9.

15. Hullinger TG, Montgomery RL, Seto AG, Dickinson BA, Semus HM, Lynch JM, Dalby CM, Robinson K, Stack C, Latimer PA, Hare JM, Olson EN and van Rooij E. Inhibition of miR-15 protects against cardiac ischemic injury. *Circ Res*. 2012;110:71-81.

16. Porrello ER, Mahmoud AI, Simpson E, Johnson BA, Grinsfelder D, Canseco D, Mammen PP, Rothermel BA, Olson EN and Sadek HA. Regulation of neonatal and adult mammalian heart regeneration by the miR-15 family. *Proc Natl Acad Sci U S A*. 2013;110:187-92.

17. Wang LL, Liu Y, Chung JJ, Wang T, Gaffey AC, Lu M, Cavanaugh CA, Zhou S, Kanade R, Atluri P, Morrisey EE and Burdick JA. Local and sustained miRNA delivery from an injectable hydrogel promotes cardiomyocyte proliferation and functional regeneration after ischemic injury. *Nat Biomed Eng*. 2017;1:983-992.
18. Hernandez MJ, Gaetani R, Pieters VM, Ng NW, Chang AE, Martin TR, van Ingen E, Mol EA, Sluijter JPG and Christman KL. Decellularized Extracellular Matrix Hydrogels as a Delivery Platform for MicroRNA and Extracellular Vesicle Therapeutics. *Adv Ther (Weinh)*. 2018;1.
19. Koudstaal S, Bastings MMC, Feyen DAM, Waring CD, van Slochteren FJ, Dankers PYW, Torella D, Sluijter JPG, Nadal-Ginard B, Doevendans PA, Ellison GM and Chamuleau SAJ. Sustained Delivery of Insulin-Like Growth Factor-1/Hepatocyte Growth Factor Stimulates Endogenous Cardiac Repair in the Chronic Infarcted Pig Heart. *Journal of Cardiovascular Translational Research*. 2014;7:232-241.
20. Sereti KI, Nguyen NB, Kamran P, Zhao P, Ranjbarvaziri S, Park S, Sabri S, Engel JL, Sung K, Kulkarni RP, Ding Y, Hsiai TK, Plath K, Ernst J, Sahoo D, Mikkola HKA, Iruela-Arispe ML and Ardehali R. Analysis of cardiomyocyte clonal expansion during mouse heart development and injury. *Nat Commun*. 2018;9:754.
21. Finnerty JR, Wang W-X, Hébert SS, Wilfred BR, Mao G and Nelson PT. The miR-15/107 group of microRNA genes: evolutionary biology, cellular functions, and roles in human diseases. *J Mol Biol*. 2010;402:491-509.
22. van Rooij E and Olson EN. MicroRNA therapeutics for cardiovascular disease: opportunities and obstacles. *Nat Rev Drug Discov*. 2012;11:860-72.
23. Bastings MM, Koudstaal S, Kieltyka RE, Nakano Y, Pape AC, Feyen DA, van Slochteren FJ, Doevendans PA, Sluijter JP, Meijer EW, Chamuleau SA and Dankers PY. A fast pH-switchable and self-healing supramolecular hydrogel carrier for guided, local catheter injection in the infarcted myocardium. *Adv Healthc Mater*. 2014;3:70-8.
24. Matsumura Y, Zhu Y, Jiang H, D'Amore A, Luketich SK, Charwat V, Yoshizumi T, Sato H, Yang B, Uchibori T, Healy KE and Wagner WR. Intramyocardial injection of a fully synthetic hydrogel attenuates left ventricular remodeling post myocardial infarction. *Biomaterials*. 2019;217:119289.
25. Nishi H, Ono K, Iwanaga Y, Horie T, Nagao K, Takemura G, Kinoshita M, Kuwabara Y, Mori RT, Hasegawa K, Kita T and Kimura T. MicroRNA-15b modulates cellular ATP levels and degenerates mitochondria via Arl2 in neonatal rat cardiac myocytes. *J Biol Chem*. 2010;285:4920-30.
26. Williams AL, Walton CB, MacCannell KA, Avelar A and Shohet RV. HIF-1 regulation of miR-29c impairs SERCA2 expression and cardiac contractility. *Am J Physiol Heart Circ Physiol*. 2019;316:H554-h565.

27. Rogg EM, Abplanalp WT, Bischof C, John D, Schulz MH, Krishnan J, Fischer A, Poluzzi C, Schaefer L, Bonauer A, Zeiher AM and Dimmeler S. Analysis of Cell Type-Specific Effects of MicroRNA-92a Provides Novel Insights Into Target Regulation and Mechanism of Action. *Circulation*. 2018;138:2545-2558.

28. Eding JEC, Demkes CJ, Lynch JM, Seto AG, Montgomery RL, Semus HM, Jackson AL, Isabelle M, Chimenti S and van Rooij E. The Efficacy of Cardiac Anti-miR-208a Therapy Is Stress Dependent. *Mol Ther*. 2017;25:694-704.

29. Bakker MH, Tseng CCS, Keizer HM, Seevinck PR, Janssen HM, Van Slochteren FJ, Chamuleau SAJ and Dankers PYW. MRI Visualization of Injectable Ureidopyrimidinone Hydrogelators by Supramolecular Contrast Agent Labeling. *Adv Healthc Mater*. 2018;7:e1701139.

30. Bakker MH, van Rooij E and Dankers PYW. Controlled Release of RNAi Molecules by Tunable Supramolecular Hydrogel Carriers. *Chemistry – An Asian Journal*. 2018;13:3501-3508.

31. Nguyen MM, Gianneschi NC and Christman KL. Developing injectable nanomaterials to repair the heart. *Curr Opin Biotechnol*. 2015;34:225-31.

32. van Rooij E, Fielitz J, Sutherland LB, Thijssen VL, Crijns HJ, Dimaio MJ, Shelton J, De Windt LJ, Hill JA and Olson EN. Myocyte enhancer factor 2 and class II histone deacetylases control a gender-specific pathway of cardioprotection mediated by the estrogen receptor. *Circ Res*. 2010;106:155-65.

SUPPLEMENTARY MATERIAL

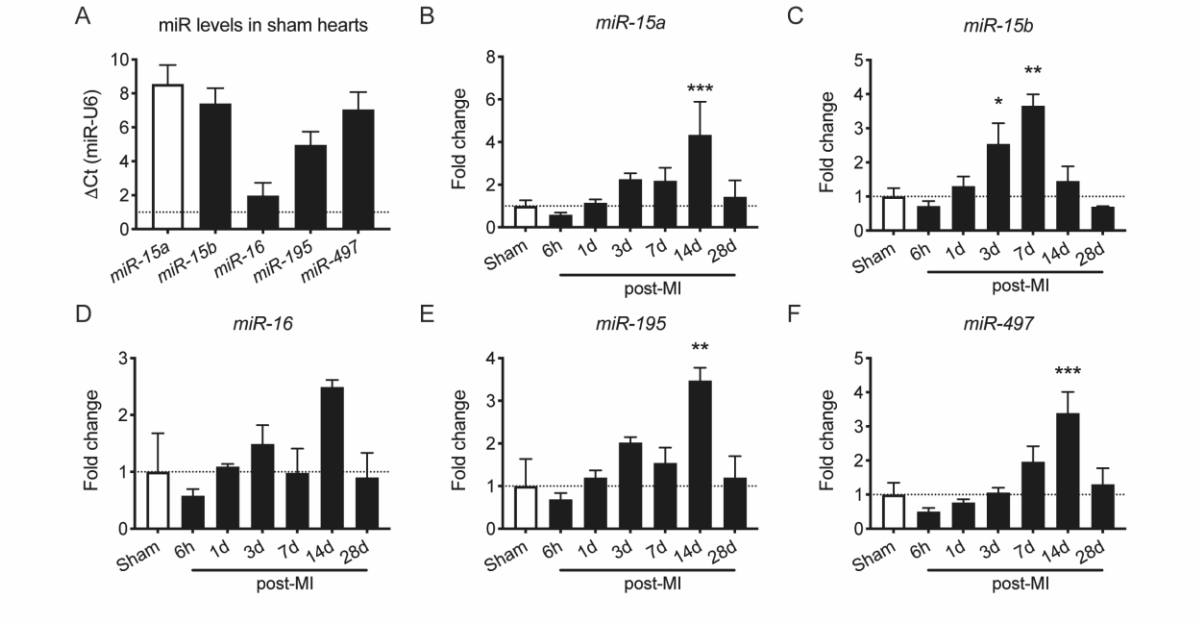

Supplemental Figure 1: RT-PCR quantification of miR-15 family members in murine LV tissue
(A) Comparison of the expression level of the *miR-15* family members in uninjured LV tissue, lower ΔCt is higher expression. **(B-F)** Changes in expression in each of the *miR-15* family members at multiple timepoints after permanent LAD ligation.

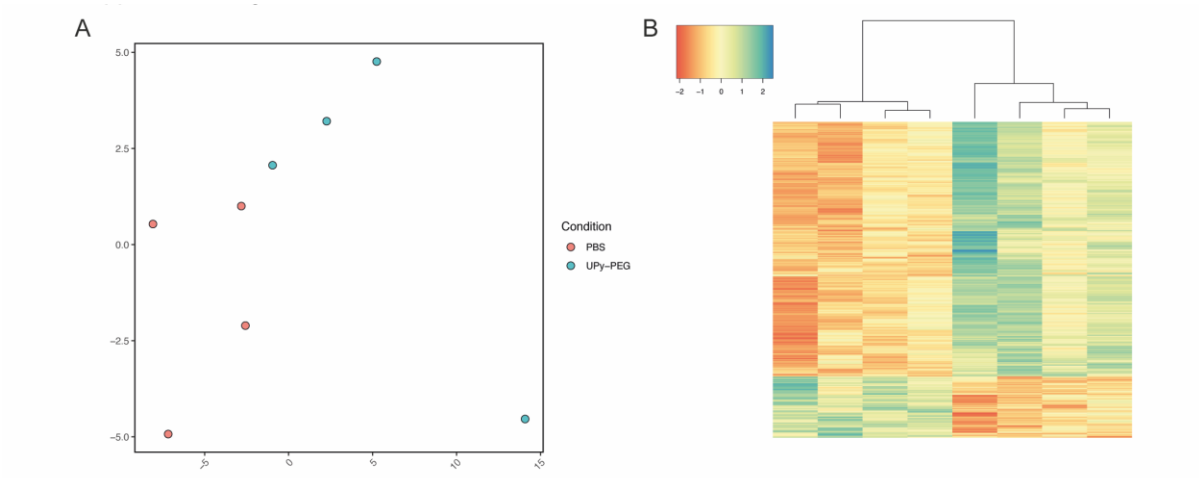

Supplemental Figure 2: Transcriptomic profiling of the effect of intramyocardial injection of pristine UPy-PEG
(A) PCA plot showing clustering of samples from mice injected with PBS or UPy-PEG. **(B)** Heatmap of differentially expressed genes between the two groups.

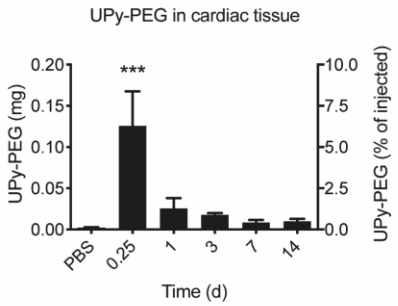

Supplemental Figure 3: Quantification of UPy-PEG retention in the heart
Anti-PEG ELISA quantification of the amount of UPy-PEG remaining in the murine heart at different times after intramyocardial injection of 2 times 10 µL UPy-PEG.

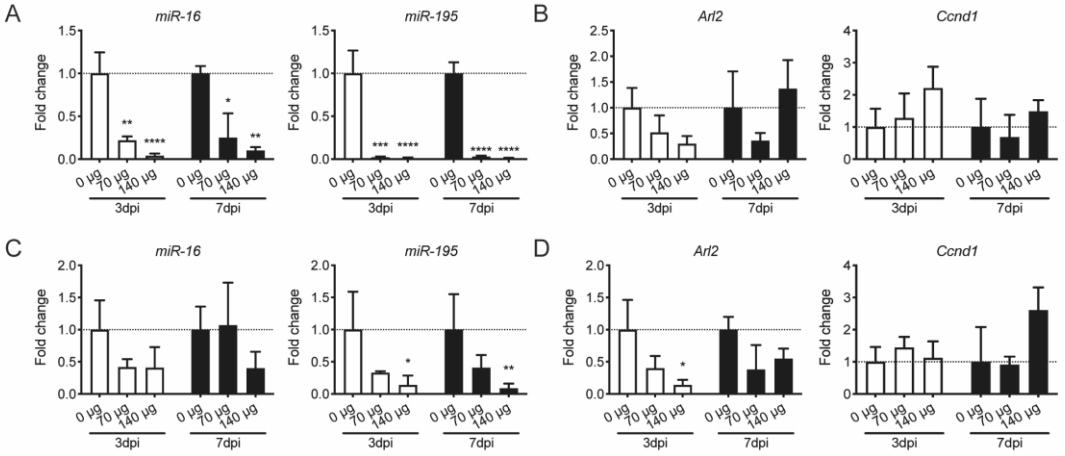

Supplemental Figure 4: Effect of intramyocardial antimiR-195 injection in off-target organs at different doses
(A,B) RT-PCR quantification of *miR-16* & *miR-195* (A) and *Arl2* & *Ccnd1* (B) in kidney tissue of mice 3 or 7 days after intramyocardial injection with UPy-PEG loaded with different concentrations of antimiR-195. **(C,D)** RT-PCR quantification of *miR-16* & *miR-195* (C) and *Arl2* & *Ccnd1* (D) in liver tissue of mice 3 or 7 days after intramyocardial injection with UPy-PEG loaded with different concentrations of antimiR-195.

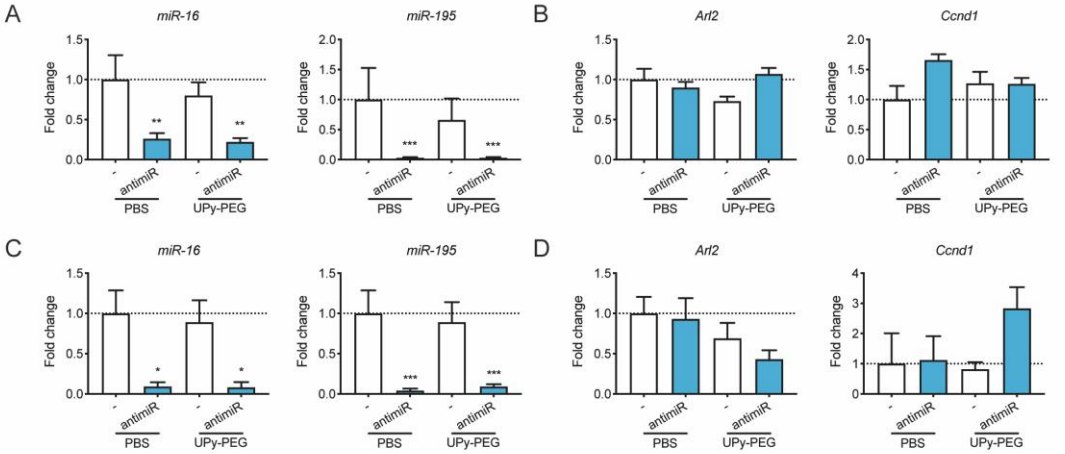

Supplemental Figure 5: Effect of intramyocardial antimiR-195 injection in off-target organs with different vehicles
(A,B) RT-PCR quantification of *miR-16* & *miR-195* (A) and *Arl2* & *Ccnd1* (B) in kidney tissue of mice 3 days after intramyocardial injection with pristine PBS, pristine UPy-PEG or those vehicles loaded with antimiR-195. **(C,D)** RT-PCR quantification of *miR-16* & *miR-195* (C) and *Arl2* & *Ccnd1* (D) in liver tissue of mice 3 days after intramyocardial injection with pristine PBS, pristine UPy-PEG or those vehicles loaded with antimiR-195.

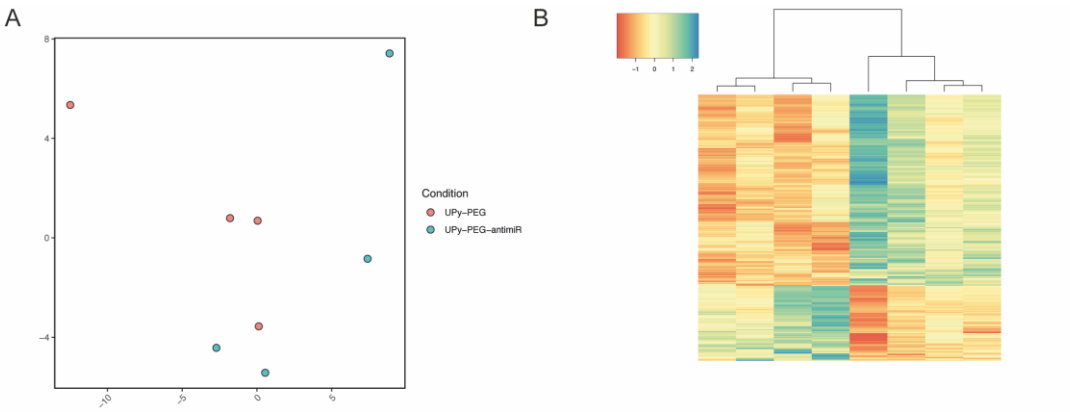

Supplemental Figure 6: Transcriptomic profiling of the effect of antimiR-195 after delivery in UPy-PEG
(A) PCA plot showing clustering of samples from mice injected with pristine UPy-PEG or UPy-PEG loaded with antimiR.
(B) Heatmap of differentially expressed genes between the two groups.

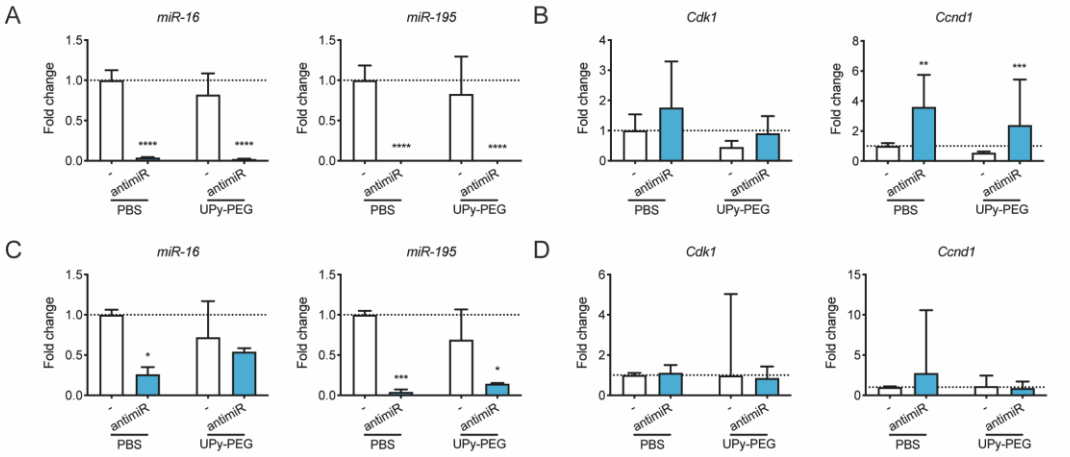

Supplemental Figure 7: Effect of intramyocardial antimiR-195 injection in off-target organs with different vehicles after IR
(A,B) RT-PCR quantification of *miR-16* & *miR-195* (A) and *Cdk1* & *Ccnd1* (B) in kidney tissue of mice 3 days after IR injury and intramyocardial injection with pristine PBS, pristine UPy-PEG or those vehicles loaded with antimiR-195. **(C,D)** RT-PCR quantification of *miR-16* & *miR-195* (C) and *Cdk1* & *Ccnd1* (D) in liver tissue of mice 3 days after IR injury and intramyocardial injection with pristine PBS, pristine UPy-PEG or those vehicles loaded with antimiR-195.

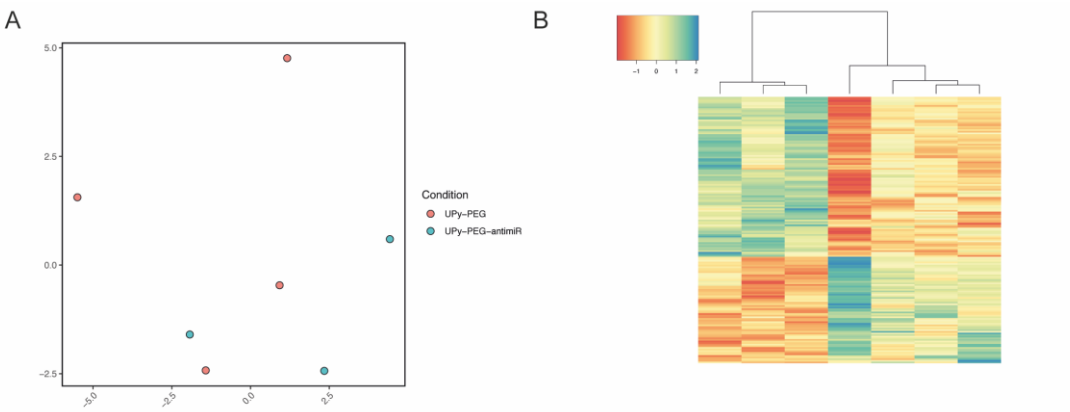

Supplemental Figure 8: Transcriptomic profiling of the effect of antimiR-195 after delivery in UPy-PEG after IR
(A) PCA plot showing clustering of samples from mice injected with pristine UPy-PEG or UPy-PEG loaded with antimiR after IR-injury. **(B)** Heatmap of differentially expressed genes between the two groups.

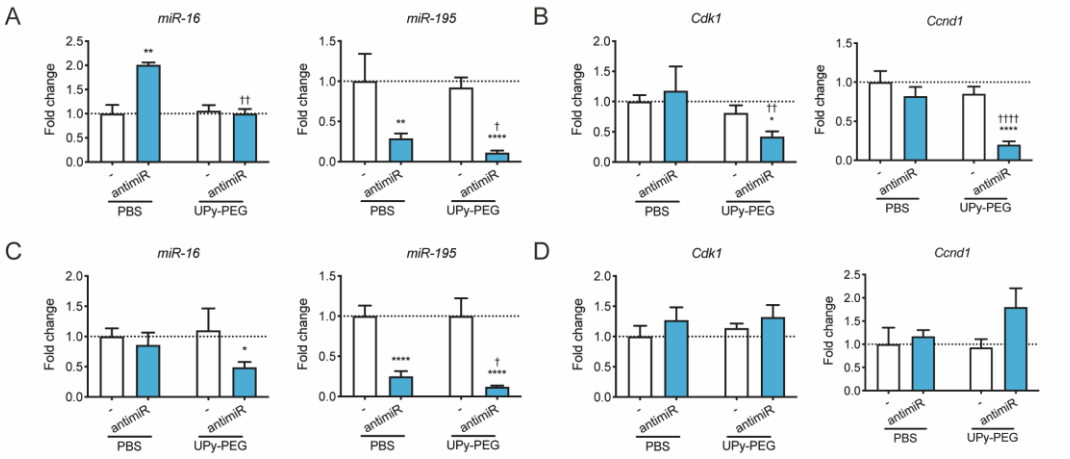

Supplemental Figure 9: Effect of intramyocardial antimiR-195 injection in off-target organs with different vehicles after MI
(A,B) RT-PCR quantification of *miR-16* & *miR-195* (A) and *Cdk1* & *Ccnd1* (B) in kidney tissue of mice 28 days after permanent LAD ligation and intramyocardial injection with pristine PBS, pristine UPy-PEG or those vehicles loaded with antimiR-195. **(C,D)** RT-PCR quantification of *miR-16* & *miR-195* (C) and *Cdk1* & *Ccnd1* (D) in liver tissue of mice 28 days after permanent LAD ligation and intramyocardial injection with pristine PBS, pristine UPy-PEG or those vehicles loaded with antimiR-195.

	Sham PBS (n=10)	MI PBS (n=14)	MI PBS antimiR (n=9)	MI UPy-PEG (n=15)	MI UPy-PEG antimiR (n=10)
IVS;d (mm)	0,83±0,11	0,91±0,17	0,96±0,15	0,88±0,22	0,96±0,17
LVID;d (mm)	3,60±0,33	4,43±0,61	4,82±1,19	4,76±1,16	4,74±1,30
LVPW;d (mm)	1,04±0,37	0,95±0,24	0,98±0,14	0,83±0,18	1,14±0,31*
IVS;s (mm)	1,12±0,24	1,15±0,25	1,09±0,27	1,03±0,38	1,16±0,31
LVID;s (mm)	2,60±0,65	3,60±0,76	4,17±1,47	4,12±1,53	4,10±1,62
LVPW;s (mm)	1,32±0,52	1,18±0,29	1,22±0,23	1,03±0,30	1,31±0,33
EF (%)	54,42±18,61	38,98±13,84	31,13±18,97	38,41±18,50	35,61±13,88
FS (%)	28,77±12,10	19,20±7,77	15,19±9,91	19,21±10,42	17,21±7,19
LV mass (mg)	98,19±21,33	136,89±36,55	152,82±42,01	125,38±28,07	155,26±43,76
CO (mL/min)	19,11±4,72	16,59±5,07	14,77±2,49	17,28±7,36	17,00±4,80

Supplemental Table 1: Echocardiography results
Interventricular septum (IVS); Left ventricular internal diameter (LVID); Left ventricular posterior wall (LVPW) are measured in both diastole (;d) and systole (;s). Ejection fraction (EF), fractional shortening (FS), left ventricular (LV) mass and cardiac output (CO) were calculated from short axis M-mode measurements by Vevo® LAB 1.7.1 software. Data are shown as mean ± SD.

CHAPTER 5

SUMMARIZING DISCUSSION

Marta Vigil-Garcia[1]

[1]Hubrecht Institute, Royal Netherlands Academy of Arts and Sciences (KNAW) and University Medical Center Utrecht (UMCU), The Netherlands.

In this thesis we studied CM-specific gene regulation associated with cardiac pathological (chapter 2) and physiological (chapter 3) remodeling. We also investigated the use of a novel hydrogel to improve therapeutic RNA regulation by improving local delivery of miRNA therapeutics (chapter 4). In this last chapter we combine the findings presented in the experimental chapters, we discuss their broader impact and context in the setting of heart disease and provide suggestions for future research.

FLOW CYTOMETRY AND DEEP SEQUENCING TO IDENTIFY RELEVANT THERAPEUTIC TARGETS

The heart consists of various cell types of which the CMs form the contractile units. In chapter 2 and 3 we used CM-specific labeling and FACS to isolate and sort CMs, followed by deep sequencing to reliably obtain gene expression that helped us get a detailed view on molecular changes during cardiac remodeling of the adult mammalian CMs. We were able to identify a genetic profile containing new genes that have not been previously linked to stressed CMs and that was conserved in mouse and human. We demonstrated that the use of deep sequencing of CM populations allows for the identification of novel and relevant targets, as PFKP.

Our results are in line with other studies using sequencing of cell populations to identify genes relevant to driving disease. The use of cell isolation and sorting methods for cell-specific RNA sequencing were recently shown to be feasible for cardiac tissue [1]. Cell-specific sequencing can obtain a higher resolution of gene expression differences and provide a better understanding of molecular changes occurring in the microenvironment of the CMs. We used similar methods and showed that by sequencing a large number of CMs, we could identify the expression of a collagen gene, which we could validate with in-situ hybridization, and which has been shown to be expressed in CMs by other studies [2-4]. Moreover, other studies performing CM sequencing of adult mammalian hearts in mouse models of ischemic injury revealed new proteins with relevant roles in cardiac remodeling. The transcription factor Zinc Finger E-Box Binding Homeobox 2 (Zeb2) was identified to have a relevant role in cardiac repair [1], and the secreted protein Beta-2-Microglobulin (B2M) was shown to be secreted by stressed CMs and to have a role in fibrosis activation after ischemia reperfusion [5]. These findings highlight the need of CM-specific sequencing to identify new target genes relevant in cardiac remodeling.

Future optimization and research to complement the results of this thesis is needed. Firstly, the adult mammalian CM is a big cell type (± 125 um long). Thus, the gating strategy used in this thesis is biased towards bigger cells, which inevitable leads to a potential loss of data coming from the smaller cell types. Cell-specific sequencing of the heart needs to be further optimized, and by optimizing the gating strategy we could improve the potential of this technique. Moreover, follow up studies to validate the presence and function of the novel targets that we identified in this thesis need to be performed. Human *in vitro* models of stressed CMs, for instance with mature human iPSC-derived CMs or cardiac

organoids, would help elucidate the human relevance of these findings. Additionally, mouse models of cardiac disease for knock-down or knock-in studies will aid in identifying the molecular mechanism behind the activation of these novel genes and help validate their therapeutic relevance *in vivo*.

METABOLIC SHIFT DURING CARDIOMYOCYTE FAILURE

In chapter 2, we exposed mice to pressure overload for eight weeks to induce pathological remodeling and CM failure and to identify genes important during the development of HF. We also used human heart samples from HF patients to identify relevant genes in a clinical setting. In both mouse and human, we showed that hearts undergoing pathological remodeling present a higher expression of the platelet isoform of PFK, which supports the switch towards glycolysis as an energy source. Additionally, we identified the downregulation of most of the mitochondrial genes in hypertrophic and pathological CMs.

In line with our findings, the failing heart has been shown to shift its source of energy towards a major reliance on glycolysis and ketone body oxidation, with a decrease in the contribution of glucose oxidation to mitochondrial oxidative metabolism [6]. This shift is accompanied by a loss in metabolic flexibility, which is the ability to respond or adapt to conditional changes in metabolic demand. There is a general consensus that metabolic flexibility is impaired in HF affecting ATP production and cardiac contractility [6]. The failing heart is characterized by a deficient energy state, as evidenced by a 30–40% reduction in ATP production and reduced phosphocreatine/ATP (PCr/ATP) ratio due to compromised mitochondrial oxidative phosphorylation [7]. As a consequence, the reliance on glycolysis increases and glucose oxidation is reduced to produce the needed energy.

There is growing evidence that suggests that enhancing glucose oxidation directly or indirectly through inhibition of fatty acid oxidation could restore metabolic flexibility and improve cardiac function and limit cardiac remodeling [7]. Restoring the rates of metabolism is dependent on changing the expression and function of mitochondria and metabolic enzymes, and peroxisome proliferator-activated receptor gamma (PPAR-γ) coactivator-1 (PGC-1)-α is an important regulator of these adaptations [7].

Drugs that affect fatty acid oxidation, including PPAR agonists [8] and acetyl-CoA carboxylase (ACC) inhibitors [9], have been developed to affect the metabolism in obesity, diabetes and heart disease. Notable recent examples of this has been the documented use of Meldonium to inhibit fatty acid oxidation through decreases in carnitine palmitoyl transferase (CPT), in order to treat cardiac dysfunction and impaired cardiac metabolism [10]. Moreover, improving glucose oxidation to mitigate cardiac dysfunction in HF was shown to be a second potential strategy. Studies using dichloroacetate (DCA), a pyruvate dehydrogenase kinase (PDK) inhibitor, reversed insulin resistance and improved cardiac function [8].

Investigating the role of PFKP in cancer, Jong-Ho Lee et al. showed that PFKP translocation and phosphorylation promotes PI3K and AKT signaling leading to glucose transporter 1 (GLUT1) expression [11]. Consequently, PFKP activation feeds a positive loop leading to increased glucose uptake. PFK(P) is the second regulatory enzyme after hexokinase to control glycolysis. Over-activation of PFKP during stress might lead to increased glucose uptake and lactate production, while emphasizing the uncoupling with glucose oxidation, which leads to detrimental effects by promoting contractile dysfunction and thus enhancing pathological remodeling [6]. To investigate the potential protective effects of reducing glycolysis, a transgenic mouse model overexpressing kinase-deficient Phosphofructokinase 2 (Pfk2) in CMs was generated [12]. Pfk2 is an enzyme that regulates glycolysis by phosphorylation of fructose 6-phosphate and producing fructose 2,6-biphosphate (BP), and Pfk-1 activity is tightly controlled by fructose 2,6-BP [12]. This mouse model showed that permanent reduction of glycolysis, attributed to a low level of fructose 2,6-BP, led to a more-profound hypertrophy, elevated fibrosis, and cardiac dysfunction.

Future research to perform specific PFKP isoform inhibition in a transient manner in *in vitro* and *in vivo* models of HF could elucidate the relevance of this enzyme in disease development and its potential as a therapeutic target. PFKP-specific inhibitors could provide insights in the therapeutic relevance of PFKP. By transiently inhibiting PFKP function, reduced lactate accumulation and milder uncoupling of glucose oxidation might reduce the stress in failing CMs. Additionally, for future targeted therapies, it is also relevant to identify the molecular mechanisms behind *PFKP* overexpression in failing CMs and the downstream effects of *PFKP* inhibition.

Comparing CM-specific gene regulation during physiological and pathological hypertrophy

In chapter 2 and 3 we compared the molecular differences between different stages of CM remodeling: 1) CM adaptive hypertrophy upon pathological stress, 2) CM failure and 3) CM hypertrophy upon exercise. To facilitate this comparison, we used R26-LSL-tdTomatoxMyh6-Cre mice and subjected them to pressure overload or exercise. We performed RNA sequencing on the different CM populations, and compared the transcriptional expression, along with validation experiments. We compared the genes that were differentially regulated in the compensatory and failing state. To identify potential cardioprotective factors to tackle maladaptive remodeling in the early stages and to provide promising therapeutic strategies to prevent HF, we looked at the genes that were upregulated during compensatory hypertrophy and downregulated during failure.

We found different genetic programs activated in the different phases. For instance, *Nppb* overexpression was specifically linked to the failing status, while *Nppa* was expressed in both hypertrophic and pathologic stages. This also occurs to the beneficial pathways that are activated

during physiological remodeling. As mentioned previously, AKT activation is a compensatory effect with beneficial effects in short term, while long term activation triggers pathological hypertrophy and cardiomyopathy [13]. Consequently, the pathways activated are not exclusive to either state. These findings provide a view of the complex mechanisms and maybe overlapping signaling pathways that lead to pathological and/or physiological remodeling and could indicate that the duration of the stimulus is a (major) determinant for the development of pathological remodeling.

These complex results highlight the relevance of validation studies *in vivo*. Follow up analysis focusing on knockout experiments and overexpression experiments should be performed to validate the functionality of the identified gene programs. Subsequently, downstream analysis would be required to quantify effects on hypertrophy and to determine the regulation of downstream targets to identify relevant cardiac stress markers. Also, apoptosis, contractility and calcium handling analysis can further elucidate the function of these proteins in CMs.

Molecular effects of exercise

In chapter 3, we exposed mice to a swimming exercise protocol to develop physiological hypertrophy. After 2 weeks of training, mice presented cardiac hypertrophy and improved cardiac function compared to mice that did not train. To identify CM-specific exercise-induced transcriptomic changes, we isolated and sorted control and hypertrophic CMs and perform RNA sequencing. Hypertrophic CMs after exercise showed an upregulation of known exercise-induced genes, but also, we revealed new markers with a potential role in adaptive hypertrophy and cardiac-protection.

It has been 60 years since the findings proposing that an increased level of physical activity provides protection from cardiovascular events [14]. Since then, exercise has been recognized as a therapeutic option for improving functional capacity in HF subjects. Clinical trials of exercise training in patients suffering from HF show improvements in exercise duration, functional capacity, and peak oxygen consumption. Moreover, exercise training seems to be safe and well tolerated [15]. To investigate the cardioprotective effects of exercise, mouse models undergoing swimming or running exercises are used. Swimming and running are a type of exercise with moderate-static power demand and high endurance demand [16]. Endurance exercise has been shown to decrease glycolysis after ischemia, improve contractility, enhance angiogenesis and decrease inflammatory mediators in mice [17-20]. Our study showed that CMs express genes involved in these pathways.

Our model of swimming involved training mice for 21 hours per week for 4 weeks. Our findings correlate to the cardiac changes that athletes present, including increase in heart weight and decreased IVRT [21]. Having validated the cardioprotective effects of exercise in our model, we provide a resource for a CM-specific exercise genetic program to investigate the molecular changes and

mechanism that could potentially serve for therapy development. By regulating the identified pathways, treatment could be provided to patients suffering from ischemia or HF could be prevented.

MiRNA THERAPEUTICS FOR CARDIAC DISEASE

MiRNAs are post-transcriptional regulators of gene expression. Many studies have shown the involvement of miRNAs in controlling the onset of cardiac disease; however, the use of miRNA as therapeutic targets remains open to investigation. In chapter 4, we aimed to investigate and assess the significance of miRNA regulation during heart disease, by injecting antimiR-195 in mouse models of IR and MI. To enhance cardiac uptake, we used a novel hydrogel-based delivery method. This resulted in a stronger de-repression of target genes of miR-195, when compared to naked delivery of antimiR-195. Injections of antimir-195 with hydrogel-based delivery led to increased CM proliferation. Nevertheless, the inhibition of miR-195 did not reduce cardiac dysfunction after ischemic events.

In general, miRNA-based treatments have shown positive results in *in vivo* models. In a mouse model of MI, inhibition of the *miR-15* family with subcutaneously delivered antimiR showed to reduce infarct size after MI [22]. In an adult porcine model of re-perfused MI, a single intracoronary administration of encapsulated antimiR-92a prevented left ventricular remodeling without adverse effects; also, delivery of locked nucleic acid-modified antimiR-92a reduced infarct size and post-ischemic loss of function in a model of percutaneous IR, and similarly, systemic delivery of antimiR-15 effectively rendered CMs resistant to hypoxia-induced CM cell death [22-24]. Combined, these studies suggest that miRNA-based therapies using modified oligonucleotides are promising therapeutic agents to affect cardiac remodeling and preserve cardiac function after ischemic injury.

Although promising, there are limitations of miRNA-based therapies for cardiovascular diseases and there needs to be a better understanding of the mechanism of any miRNA-based therapy for cardiac disease before they can enter the clinic. For example, our study did not reduce cardiac dysfunction 28 days post MI. In line with this, a study that administered antimiR-34a, targeting *miR-34a*, a miRNA usually elevated in settings of cardiac stress and aging, showed different effects depending on severity of the pathology and sex. In a setting of moderate dilated cardiomyopathy, it was more effective in females than in males. However, in a setting of more severe dilated cardiomyopathy, it showed little benefit for either sex [25]. This suggests disease conditions should be considered, since the expression levels of miRNAs and their targets can significantly change under disease conditions [26]. Moreover, as true for most antimiRs, most of the injected compound ends up in the kidneys and liver, reducing cardiac exposure and increasing the chance of unwanted side effects [25, 27, 28]. Key points to investigate for efficacy of miRNA therapeutics are bioavailability and biodistribution, mechanism of cellular uptake, the sequence of the miRNA, as well as the specific sequence of the inhibitor itself.

HYDROGEL-BASED DELIVERY TO DECREASE OFF-TARGET EFFECTS AND TO INCREASE EFFICIENCY OF MIRNA THERAPEUTICS IN THE HEART

In chapter 4, we investigated the use of UPy-PEG and a cationic charged UPy-PEG (UPy-Cat) for cardiac delivery of antimiR-195. We showed that UPy-PEG for intramyocardial drug delivery is safe and improves antimiR efficacy, by enhancing target de-repression. UPy-PEG hydrogel is pH-responsive and designed for minimally invasive intramyocardial injection. However, we encountered low cardiac retention of the hydrogel at the injection site, with nearly all the UPy-PEG molecules cleared after 24 hours.

Hydrogels are a porous and hydratable structure that induces their gelation and swelling in a biological microenvironment, enabling their local administration and controlled delivery of RNA molecules while enhancing local delivery and limiting undesired targets. Over the past years, UPy-hydrogels have been investigated as a controlled release system for different applications, including for growth factors and miRNA delivery. Successful examples of hydrogel-based delivery exist. For instance, injection of ACE-shRNA plasmid-loaded hydrogel into impaired myocardium was shown to obtain more cardioprotective effects than delivered alone in rat with MI [29]. Injectable hyaluronic acid based-hydrogel system provided a sustained release of *miR-302* which promoted proliferation of CMs, and the delivery of miR-29b mimics with hydrogel improved functional recovery after MI [30].

However, limitations considering safety and low cardiac retention are common, and off-target events, cardiac toxicity, conduction abnormalities and alteration of action potential propagation may occur. In our study we observed that the intra-cardiac injection with hydrogel caused a transient inflammatory reaction, which could have been triggered by the hydrogel's high pH, the viscosity and/or the volume of the injections. We hypothesized that the use of a mouse model itself limited us to using conventional needles and a microsurgical intercostal approach as opposed to catheter-based injections. Moreover, we observed poor cardiac retention upon injection**.** The fast heart rate of mice could make mice an unsuitable model to test the delivery efficiency.

Another important concern is that different hydrogels demonstrate varying degrees of interstitial spread, 1) with low spread the gel is confined in a localized region resulting in myocardium being pushed to the perimeter of the hydrogel structure, or 2) high spread hydrogels occupy the interstitial space between neighboring CMs resulting in the presence of myocardial fibers throughout the hydrogel structure. The amount of integration with the native myocardium may therefore influence how the hydrogel impacts the electrophysiological properties of the underlying tissue. To overcome these barriers, supra-molecularly crosslinked, shear-thinning hydrogels could promote self-healing,. However, these hydrogels are softer and have low mechanical properties. Moreover, thermal transitions can be used for gelation when injected. Some of the most common functionalities

introduced for siRNA delivery are poly(organophosphazene)s and chitosan/β-glycerophosphates. These can undergo transitions at 37°C from small molecules to solid materials (sol-gel transitions) [31]. Lastly, translatability of these findings requires an improved understanding of different methods of cellular trafficking which can help design novel polymeric methods towards *in vivo* application. To promote the application of hydrogel RNAi therapeutics, cellular trafficking methods should be explored by cell type, assessing how hydrogels either become incorporated or are degraded. This can provide fundamental understanding of release and uptake from hydrogels.

CONCLUDING REMARKS

In this thesis we showed the diverse genetic profiles of CMs at various stages of cardiac remodeling and their potentially relevant role in regulating heart remodeling, from metabolic switch to transcription factors to miRNAs. At therapeutic level, we show that we can intervene using RNA therapeutics and hydrogel-based delivery. Because cardiovascular disease is the major cause of mortality worldwide, the identification of new components provides a better understanding of the complex regulatory mechanisms that occur during cardiac remodeling and their effect on disease, relevant for the complex therapeutic development pathway towards clinical use.

References

1. Gladka MM, Molenaar B, de Ruiter H, van der Elst S, Tsui H, Versteeg D, Lacraz GPA, Huibers MMH, van Oudenaarden A and van Rooij E. Single-Cell Sequencing of the Healthy and Diseased Heart Reveals Cytoskeleton-Associated Protein 4 as a New Modulator of Fibroblasts Activation. *Circulation*. 2018;138:166-180.
2. DeLaughter DM, Bick AG, Wakimoto H, McKean D, Gorham JM, Kathiriya IS, Hinson JT, Homsy J, Gray J, Pu W, Bruneau BG, Seidman JG and Seidman CE. Single-Cell Resolution of Temporal Gene Expression during Heart Development. *Dev Cell*. 2016;39:480-490.
3. Cui Y, Zheng Y, Liu X, Yan L, Fan X, Yong J, Hu Y, Dong J, Li Q, Wu X, Gao S, Li J, Wen L, Qiao J and Tang F. Single-Cell Transcriptome Analysis Maps the Developmental Track of the Human Heart. *Cell Rep*. 2019;26:1934-1950 e5.
4. Heras-Bautista CO, Mikhael N, Lam J, Shinde V, Katsen-Globa A, Dieluweit S, Molcanyi M, Uvarov V, Jutten P, Sahito RGA, Mederos-Henry F, Piechot A, Brockmeier K, Hescheler J, Sachinidis A and Pfannkuche K. Cardiomyocytes facing fibrotic conditions re-express extracellular matrix transcripts. *Acta Biomater*. 2019;89:180-192.
5. Molenaar B, Timmer LT, Droog M, Perini I, Versteeg D, Kooijman L, Monshouwer-Kloots J, de Ruiter H, Gladka MM and van Rooij E. Single-cell transcriptomics following ischemic injury identifies a role for B2M in cardiac repair. *Commun Biol*. 2021;4:146.
6. Tran DH and Wang ZV. Glucose Metabolism in Cardiac Hypertrophy and Heart Failure. *J Am Heart Assoc*. 2019;8:e012673.
7. Karwi QG, Uddin GM, Ho KL and Lopaschuk GD. Loss of Metabolic Flexibility in the Failing Heart. *Front Cardiovasc Med*. 2018;5:68.
8. Sahebkar A, Chew GT and Watts GF. New peroxisome proliferator-activated receptor agonists: potential treatments for atherogenic dyslipidemia and non-alcoholic fatty liver disease. *Expert Opin Pharmacother*. 2014;15:493-503.
9. Bourbeau MP and Bartberger MD. Recent advances in the development of acetyl-CoA carboxylase (ACC) inhibitors for the treatment of metabolic disease. *J Med Chem*. 2015;58:525-36.
10. Arduini A and Zammit VA. A tennis lesson: sharp practice in the science behind the Sharapova case. *Postgrad Med J*. 2016;92:429-30.
11. Lee JH, Liu R, Li J, Wang Y, Tan L, Li XJ, Qian X, Zhang C, Xia Y, Xu D, Guo W, Ding Z, Du L, Zheng Y, Chen Q, Lorenzi PL, Mills GB, Jiang T and Lu Z. EGFR-Phosphorylated Platelet Isoform of Phosphofructokinase 1 Promotes PI3K Activation. *Mol Cell*. 2018;70:197-210 e7.
12. Donthi RV, Ye G, Wu C, McClain DA, Lange AJ and Epstein PN. Cardiac expression of kinase-deficient 6-phosphofructo-2-kinase/fructose-2,6-bisphosphatase inhibits glycolysis, promotes

hypertrophy, impairs myocyte function, and reduces insulin sensitivity. *J Biol Chem*. 2004;279:48085-90.

13. Chaanine AH and Hajjar RJ. AKT signalling in the failing heart. *Eur J Heart Fail*. 2011;13:825-9.

14. Morris JN and Crawford MD. Coronary heart disease and physical activity of work; evidence of a national necropsy survey. *Br Med J*. 1958;2:1485-96.

15. Davies EJ, Moxham T, Rees K, Singh S, Coats AJ, Ebrahim S, Lough F and Taylor RS. Exercise training for systolic heart failure: Cochrane systematic review and meta-analysis. *Eur J Heart Fail*. 2010;12:706-15.

16. Morici G, Gruttad'Auria CI, Baiamonte P, Mazzuca E, Castrogiovanni A and Bonsignore MR. Endurance training: is it bad for you? *Breathe (Sheff)*. 2016;12:140-7.

17. Shephard RJ and Balady GJ. Exercise as cardiovascular therapy. *Circulation*. 1999;99:963-72.

18. Ellison GM, Waring CD, Vicinanza C and Torella D. Physiological cardiac remodelling in response to endurance exercise training: cellular and molecular mechanisms. *Heart*. 2012;98:5-10.

19. Burelle Y, Wambolt RB, Grist M, Parsons HL, Chow JC, Antler C, Bonen A, Keller A, Dunaway GA, Popov KM, Hochachka PW and Allard MF. Regular exercise is associated with a protective metabolic phenotype in the rat heart. *Am J Physiol Heart Circ Physiol*. 2004;287:H1055-63.

20. Bjornstad HH, Bruvik J, Bjornstad AB, Hjellestad BL, Damas JK and Aukrust P. Exercise training decreases plasma levels of soluble CD40 ligand and P-selectin in patients with chronic heart failure. *Eur J Cardiovasc Prev Rehabil*. 2008;15:43-8.

21. Claessens PJ, Claessens CW, Claessens MM, Claessens MC and Claessens JE. Supernormal left ventricular diastolic function in triathletes. *Tex Heart Inst J*. 2001;28:102-10.

22. Hullinger TG, Montgomery RL, Seto AG, Dickinson BA, Semus HM, Lynch JM, Dalby CM, Robinson K, Stack C, Latimer PA, Hare JM, Olson EN and van Rooij E. Inhibition of miR-15 protects against cardiac ischemic injury. *Circ Res*. 2012;110:71-81.

23. Bellera N, Barba I, Rodriguez-Sinovas A, Ferret E, Asin MA, Gonzalez-Alujas MT, Perez-Rodon J, Esteves M, Fonseca C, Toran N, Garcia Del Blanco B, Perez A and Garcia-Dorado D. Single intracoronary injection of encapsulated antagomir-92a promotes angiogenesis and prevents adverse infarct remodeling. *J Am Heart Assoc*. 2014;3:e000946.

24. Hinkel R, Penzkofer D, Zuhlke S, Fischer A, Husada W, Xu QF, Baloch E, van Rooij E, Zeiher AM, Kupatt C and Dimmeler S. Inhibition of microRNA-92a protects against ischemia/reperfusion injury in a large-animal model. *Circulation*. 2013;128:1066-75.

25. Bernardo BC, Ooi JY, Matsumoto A, Tham YK, Singla S, Kiriazis H, Patterson NL, Sadoshima J, Obad S, Lin RC and McMullen JR. Sex differences in response to miRNA-34a therapy in mouse

models of cardiac disease: identification of sex-, disease- and treatment-regulated miRNAs. *J Physiol*. 2016;594:5959-5974.

26. Eding JE, Demkes CJ, Lynch JM, Seto AG, Montgomery RL, Semus HM, Jackson AL, Isabelle M, Chimenti S and van Rooij E. The Efficacy of Cardiac Anti-miR-208a Therapy Is Stress Dependent. *Mol Ther*. 2017;25:694-704.

27. Bernardo BC, Gao XM, Tham YK, Kiriazis H, Winbanks CE, Ooi JY, Boey EJ, Obad S, Kauppinen S, Gregorevic P, Du XJ, Lin RC and McMullen JR. Silencing of miR-34a attenuates cardiac dysfunction in a setting of moderate, but not severe, hypertrophic cardiomyopathy. *PLoS One*. 2014;9:e90337.

28. Lucas T, Bonauer A and Dimmeler S. RNA Therapeutics in Cardiovascular Disease. *Circ Res*. 2018;123:205-220.

29. Wan WG, Jiang XJ, Li XY, Zhang C, Yi X, Ren S and Zhang XZ. Enhanced cardioprotective effects mediated by plasmid containing the short-hairpin RNA of angiotensin converting enzyme with a biodegradable hydrogel after myocardial infarction. *J Biomed Mater Res A*. 2014;102:3452-8.

30. Monaghan MG, Holeiter M, Brauchle E, Layland SL, Lu Y, Deb A, Pandit A, Nsair A and Schenke-Layland K. Exogenous miR-29B Delivery Through a Hyaluronan-Based Injectable System Yields Functional Maintenance of the Infarcted Myocardium. *Tissue Eng Part A*. 2018;24:57-67.

31. Wang LL and Burdick JA. Engineered Hydrogels for Local and Sustained Delivery of RNA-Interference Therapies. *Adv Healthc Mater*. 2017;6.

ADDENDUM

ENGLISH SUMMARY
NEDERLANDSE SAMENVATTING
ACKNOWLEDGEMENTS
LIST OF PUBLICATIONS
CURRICULUM VITAE

Marta Vigil-Garcia[1]

[1]Hubrecht Institute, Royal Netherlands Academy of Arts and Sciences (KNAW) and University Medical Center Utrecht (UMCU), The Netherlands.

ENGLISH SUMMARY

Cardiovascular diseases (CVDs) are diseases that affect the heart and blood vessels and to date, there is no cure. The only available clinical practices to manage CVDs are suggesting lifestyle changes, exercise-based cardiac rehabilitation, symptom management with medication, surgical intervention to prevent sudden cardiac arrest, or heart transplantation in case of end-stage heart failure. In this thesis we performed studies to extend our knowledge on 1) cardiac-specific gene regulation pathways relevant during CVDs and 2) new therapeutic approach to deliver pharmacological agents in the heart cells to treat ischemic heart disease. To do so, we sequenced the RNA of cardiomyocytes isolated from mouse models of cardiac pathological and physiological hypertrophy, we used *in vitro* cardiac models to identify and investigate the role of novel gene targets. Additionally, we studied the safety and efficacy of a hydrogel-based delivery method to increase local delivery of miRNA therapeutics to cardiomyocytes in a mouse model of ischemic heart disease. Our results showed that cardiomyocytes at various stages of cardiac remodeling present remarkably diverse genetic profiles and that these genetic profiles have a potentially relevant role in regulating heart remodeling, from metabolic switch to transcription factors to miRNAs. At therapeutic level, we show that we can intervene using RNA therapeutics and hydrogel-based delivery.

Thesis outline

The studies described in this thesis were aimed to extend our insights on cardiomyocyte (CM)-specific gene regulation relevant for cardiac remodeling and to study a novel therapeutic approach for CM-specific delivery.

In **chapter 2** we investigate CM-specific gene programs in pathological remodeling. Using a model of pressure overload, we identified a failure-induced gene program, which is conserved between mouse and human. Here, we identified phosphofructokinase-platelet isoform (*PFKP)* to play a role in CM remodeling during HF.

In **chapter 3** we investigate CM-specific gene programs driving physiological hypertrophy. Using a model of swimming, we identified the exercise-induced gene program in CMs. By focusing on transcription factors, we identified high expression of Sox17 in hypertrophic CMs. We investigated the potential cardioprotective role of Sox17 in a model of pressure overload by using adenoviral delivery which failed to preserve cardiac function during pathology.

In **chapter 4** we investigate the efficacy and safety of a new hydrogel-based delivery system in a model of ischemic injury. Hydrogel-based delivery of antimir-195 improved CM local delivery and enhanced target de-repression and CM proliferation.

Finally, in **chapter 5** we discuss all findings in a broader context together with future perspectives.

NEDERLANDSE SAMENVATTING

Hart- en vaatziekten zijn aandoeningen aan het hart en/of de bloedvaten. Tot op heden zijn er vaak geen remedies beschikbaar voor deze aandoeningen. Mogelijke aanpakken om hart- en vaatziekten te behandelen zijn het suggereren van aanpassingen in levensstijl, hartrevalidatie op basis van fysieke inspanning, symptoombestrijding door middel van medicatie, en chirurgische ingrepen ter voorkoming van plotselinge hartstilstand, of, in het geval van hartfalen in het eindstadium, harttransplantatie. Om onze kennis verder uit te breiden over dit onderwerp, komen de volgende studies in dit proefschrift aan bod; 1) Hart specifieke genregulatieroutes bij hart- en vaatziekten, en 2) Het ontrafelen van nieuwe afgifteroutes om farmacologische middelen specifiek in de hartcellen te krijgen bij de behandeling van ischemische hartziekte. Om deze twee vraagstukken te behandelen, hebben we de sequentie bepaald van het ribonucleïnezuur (RNA) van hartspiercellen geïsoleerd van muizen met pathologische en fysiologische hypertrofie in het hart. Met het gebruik van *in vitro* modellen hebben wij de rol van nieuwe genen bestudeerd. Vervolgens hebben we de veiligheid en werkzaamheid van een op hydrogel gebaseerde leveringsmethode getest voor de levering van microRNA-therapeutica lokaal en specifiek aan hartspiercellen te doseren in een muismodel van ischemische hartziekte. Onze resultaten toonden aan dat hartspiercellen zeer diverse genetische profielen vertonen in verschillende stadia van hartremodellering en dat deze genetische profielen potentieel van invloed kunnen zijn bij de regulatie van hartremodellering; van metabole switch, tot transcriptiefactoren, tot miRNA's. Op therapeutisch vlak laten we zien dat we kunnen ingrijpen met behulp van RNA-therapeutica en op hydrogel gebaseerde toediening.

Proefschrift overzicht

De studies beschreven in dit proefschrift waren bedoeld om onze inzichten in cardiomyocyten (CM)-specifieke genregulatie die relevant is voor cardiale remodellering uit te breiden en om een nieuwe therapeutische benadering voor CM-specifieke afgifte te bestuderen. We hebben CM's geïsoleerd en gesequenced uit muismodellen van pathologische en fysiologische hermodellering en *in vitro* CM's gebruikt modellen om nieuwe kandidaat-gendoelen te identificeren en te onderzoeken. Daarnaast hebben we de veiligheid en werkzaamheid bestudeerd van een op hydrogel gebaseerde toedieningsmethode om de CM-lokale levering van miRNA-therapieën te vergroten en de bescherming van het hart na MI te verbeteren.

In **hoofdstuk 2** onderzochten we CM-specifieke genprogramma's in pathologische remodellering. Met behulp van een muismodel waarin de hydrostatische druk in het hart wordt verhoogd, en het specifiek isoleren van CMs identificeerden we een genprogramma, wat wordt geactiveerd tijdens HF. Dit programma is vergelijkbaar tussen muis en mens. We identificeerden fosfofructokinase-bloedplaatjes isovorm (*PFKP)* als een belangrijke speler in CM-remodellering tijdens HF.

In **hoofdstuk 3** onderzochten we CM-specifieke genprogramma's die fysiologische hypertrofie aansturen. Door middel van een zwemmodel als model voor sporten identificeerden we het genprogramma in CM's wat wordt geactiveerd tijdens langdurige fysieke inspanning. Door ons te concentreren op transcriptiefactoren, identificeerden we een hoge expressie van Sox17 in hypertrofische CM's. We onderzochten de potentiële cardioprotectieve rol van Sox17 in een model van drukoverbelasting door gebruik te maken van adenovirale afgifte die de hartfunctie niet kon behouden tijdens pathologie.

In **hoofdstuk 4** onderzochten we de werkzaamheid en veiligheid van een op hydrogel gebaseerd toedieningssysteem in een model van ischemisch letsel. Op hydrogel gebaseerde levering van antimir-195 verbeterde lokale CM-afgifte en verbeterde doelwitdepressie en CM-proliferatie.

Tot slot bespreken we in **hoofdstuk 5** alle bevindingen in een bredere context samen met toekomstperspectieven.

Acknowledgements

It's been a while since I finished my time at the Hubrecht Institute in December 2019. Therefore, I will keep it short and sweet.

First, thank you Eva for giving me the opportunity to pursue this PhD, for your guidance, for being an example of strength and for helping me become the professional I am now.

I would also like to give special thanks to the van Rooij lab and all Hubrecht colleagues who enjoyed with me long gezellig borrels, PhD retreats, congresses… without you it wouldn't have been so fun! Thank you for the amazing support and teamwork. Special thanks to Maya, Anne, Arwa, and Corina who made this journey easier and better.

Por último, gracias a la familia por vuestro apoyo incondicional, sobre todo a mi hermana melliza Ariana y mi madre Isabel. Mama, gracias por enseñarme a tener una visión positiva de la vida que me ha ayudado a lograr todo lo que me propongo y llegar a este momento. Es todo gracias a ti.

LIST OF PUBLICATIONS

Publications:

Lacraz GPA, Junker JP, Gladka MM, Molenaar B, Scholman KT, **Vigil-Garcia M**, Versteeg D, de Ruiter H, Vermunt MW, Creyghton MP, Huibers MMH, de Jonge N, van Oudenaarden A, van Rooij E. Tomo-Seq identifies SOX9 as a key regulator of cardiac fibrosis during ischemic injury. Circulation 2017;136:1396–1409.

Vigil-Garcia M*, Demkes CJ*, Eding JEC, Versteeg D, de Ruiter H, Perini I, Kooijman L, Gladka MM, Asselbergs FW, Vink A, Harakalova M, Bossu A, van Veen TAB, Boogerd CJ and van Rooij E. Gene expression profiling of hypertrophic cardiomyocytes identifies new players in pathological remodeling. *Cardiovasc Res*. 2020.

Manuscripts in preparation:

Vigil-Garcia M*, Eding JEC*, Vink M, Demkes CJ, Versteeg D, Kooijman L, Bakker MH, Schotman MJG, Dankers PYW, van Rooij E. Hydrogel-based delivery of antiR-195 improves cardiac efficacy after ischemic injury. *Submitted*

Vigil-García M, Demkes CJ, Eding JEC, Wright Clark M, Peterse C, de Ruiter H, Kooijman L, Versteeg D, Giacca M, Boogerd CJ, van Rooij E. Gene expression profile of cardiomyocytes after exercise. *In prep.*

Curriculum Vitae

Marta Vigil García was born the 15th of April 1989 in Porlamar, Isla Margarita, Venezuela. In 2008 she received her high school diploma from Instituto La Marina, in Santa Cruz de Bezana, Cantabria, Spain. In that same year she started her bachelor + master's degree in Biology with a focus on Molecular Biology and Genetics at University of Oviedo in Asturias. Owing to her interest in scientific research and biology, she performed a summer internship under the supervision of Prof. dr. Fernando de la Cruz, in the department of Molecular Genetics at the University of Cantabria in 2011. In 2013 she received an Erasmus scholarship to study abroad and moved to The Netherlands where she successfully finished a semester in Biomedical Science at Leiden University, and an internship under the supervision of Prof. dr. Paul Hooykaas (Molecular and Developmental Genetics, Institute of Biology at Leiden University). Subsequently, she had an interest and curiosity for biopharma, so she pursued an internship in preclinical research and biotechnology at Hall Allergy, Leiden in 2014. After completing the internship and receiving her bachelor + master's degree in Biology in 2014, she started working in the department of Biochemistry and Protein Characterization (Hal Allergy) as a research assistant. In 2015 she selected a PhD position with Prof. dr. Eva van Rooij in the department of Molecular Cardiology (Hubrecht Institute), where she focused on identifying factors relevant to cardiac pathology and physiology. The results of this work are published in this thesis.